Developing novel heat treatments for automotive spring steels
Phase transformations, microstructure and performance

Goulas, Konstantinos

DOI
10.4233/uuid:ce01998a-0830-494e-a403-9f0696aa0dce

Publication date
2018

Document Version
Final published version

Citation (APA)
Goulas, K. (2018). *Developing novel heat treatments for automotive spring steels: Phase transformations, microstructure and performance*. [Dissertation (TU Delft), Delft University of Technology]. https://doi.org/10.4233/uuid:ce01998a-0830-494e-a403-9f0696aa0dce

Developing Novel Heat Treatments for Automotive Spring Steels

Phase Transformations, Microstructure and Performance

Constantinos GOULAS

Developing Novel Heat Treatments for Automotive Spring Steels

Phase Transformations, Microstructure and Performance

Proefschrift

ter verkrijging van de graad van doctor
aan de Technische Universiteit Delft,
op gezag van de Rector Magnificus prof. dr. ir. T.H.J.J. van der Hagen,
voorzitter van het College voor Promoties,
in het openbaar te verdedigen op Mondag 22 Januari 2018 om 12:30 uur

door

Constantinos GOULAS

Ingenieur in Metaalkunde en Mijnbouw
National Technical University of Athens geboren te Marousi, Griekenland

This dissertation has been approved by the

promotor: Prof. dr. ir. J. Sietsma

Composition of the doctoral committee:

Rector Magnificus,	voorzitter
Promotor:	
Prof. dr. ir. J. Sietsma,	Technische Universiteit Delft
Independent Members:	
Dr. C. Capdevila,	CENIM, Spain
Dr. M.H.F. Sluiter,	Technische Universiteit Delft
Prof. dr. I.M. Richardson,	Technische Universiteit Delft
Prof. dr. P. Rivera Diaz Del Castillo,	Lancaster University, UK
Other Members:	
Dr. M.G. Mecozzi,	Technische Universiteit Delft
Prof. dr. K.O. Findley,	Colorado School of Mines, USA
Reserve Member:	
Prof. dr. J. Dik,	Technische Universiteit Delft

The research described in this thesis was carried out in the Department of Materials Science and Engineering, of Delft University of Technology, in the Netherlands.

Dr. M.G. Mecozzi has contributed greatly to this dissertation as daily supervisor.

This research was carried out under project number M22.5.12476 in the framework of the research program of the Materials innovation institute (M2i) in the Netherlands (www.m2i.nl).

Printed by: ProefschriftMaken || www.proefschriftmaken.nl

Front & Back: Ir. N. Mavrikakis and Ir. C. Jiménez-Peña

ISBN 978-94-91909-49-8

An electronic version of this dissertation is available at
http://repository.tudelft.nl/.

Contents

Summary

This Ph.D. thesis investigates the substitution of quenching and tempering treatments by isothermal bainitic treatments in automotive spring production. An isothermal bainitic treatment has benefits mainly in terms of energy savings, but it can also prevent quench cracking, distortion and residual stresses, commonly found in quenched and tempered components. A medium carbon low alloy spring steel commonly employed in automotive spring production is used for this research. The study focuses on the microstructure formation and its effect on the performance of a spring steel component. In the first part of the thesis, bainite formation is investigated by dilatometry and microscopy. It is found that the chemical heterogeneity of the industrially produced material has a significant influence on the microstructure formation. The analysis of the microstructure at different stages of the transformation shows that chemical segregation of substitutional alloying elements, resulting from casting, strongly affects the bainite formation by retarding the transformation kinetics and limiting the maximum bainite fraction. During holding at temperatures slightly above the martensite start temperature, a homogeneous lower bainitic microstructure is obtained, whereas at higher temperatures, an incomplete bainitic reaction is evident. It is also found that at the early stages of the transformation, differences in the bainite formation kinetics, due to local inhomogeneity in Cr and Mn concentration, result in retardation of the growth of bainite in the high Mn and Cr concentration regions. The research activity on bainite formation continues with in-depth characterization work on specimens, which are isothermally treated at different temperatures within the bainitic temperature range. Three different morphologies are identified based on Transmission Electron Microscopy (TEM) analysis: upper, lower and inverse bainite. Lower bainite contains cementite precipitates, which show no partitioning of substitutional elements, as detected by Atom Probe Tomography (APT). Carbon in the bainitic ferrite is found to segregate at dislocations and to form Cottrell atmospheres, while the microstructure also shows a relatively high carbon concentration remaining in solution. Upper bainite contains cementite as well, but limited partitioning of Cr is evident. As the conventional bainite, inverse bainite is a ferrite-plus-cementite phase mixture formed in hypereutectoid steels; the segregation of alloying elements in the investigated steel lowers the eutectoid carbon concentration and allows inverse bainite to be formed, even in a nominally hypo-

eutectoid steel. Inverse bainite forms at high isothermal holding temperatures and it consists of Widmanstätten carbide needles surrounded by ferrite. Site-specific APT analysis of the inverse bainite reveals significant partitioning of Mn and Cr both at the carbides and at the ferrite/martensite interfaces. An essential treatment applied to automotive springs is shot peening, an efficient method to induce compressive stresses to the component in order to prevent fatigue crack initiation. By applying a bainitic treatment instead of a quenching and tempering treatment, the obtained microstructure can potentially respond differently to the shot peening treatment, which can result in non-optimised properties. Therefore, effect of the microstructure on the mechanical properties and its relation to the response to the shot peening treatment is investigated. We observe that the resulting roughness for the bainitic specimens is consistently higher than the one measured for the tempered martensitic specimens, which can be explained by the higher degree of work hardening of the bainite compared to the tempered martensite. Using Electron Back Scatter Diffraction (EBSD) and Finite Element Modelling (FEM), we explore in detail the deformation behaviour of the two microstructures. We observe that the two microstructures accommodate strain differently, due to their different microstructural features such as platelet size and carbide distribution. FEM simulations show that shot peening of a bainitic microstructure results in higher compressive stresses below the dimple of the shot and limited surrounding tensile stresses compared to a tempered martensitic microstructure. This difference in strain accommodation can influence the shot peening parameters to obtain full coverage of the shot peened surface, which is an important prerequisite for improving the fatigue life of components. Additionally, the possibly increased roughness of the bainitic specimens needs to be considered for shot peening parameter selection. Furthermore, the influence of heat treatment on the fatigue properties of 51CrV4 spring steel with bainitic and tempered martensitic microstructures is investigated. The microstructure characterisation shows that lower bainite and tempered martensite exhibit differences in microstructural features, which are the martensite block size / bainite plate size, dislocation structure and density, and the size and distribution of carbide precipitates. Static mechanical properties are investigated by standard tensile tests. The results show higher tensile strength for bainite than for tempered martensite. Kocks-Mecking analysis is employed to determine the yield stresses of the two microstructures. The yield stresses are found to be similar. A physically based model is used for characterizing the dislocation structure and provides valuable insight into the mechanical response of the two microstructures. Rotating bending fatigue tests are carried out to evaluate the fatigue performance of the two microstructures. The fatigue performance of bainite is found to be superior to that of tempered martensite. Fracture analysis of the

fatigue specimens by stereo-microscopy and SEM reveals different morphologies for bainite and tempered martensite. On the fracture surfaces of tempered martensite, multiple damage-initiation sites and ratchet marks are evident, while fracture of bainite initiates mostly at a single point at a surface inclusion. This is attributed to competing fatigue-crack initiation mechanisms between plasticity-induced failure and inclusion-controlled failure. Final fracture zones of tempered martensite are dominated by micro-void coalescence. In contrast, the same zone in bainite mainly consists of cleavage-like features, indicating lower fracture toughness for bainite. The last chapter of this thesis investigates an alternative heat treatment method based on ultra-fast induction heating, the Ultra-Fast Heat Treatment (UFHT). With the motivation of preventing decarburization, alternative methods to heat the steel bars are investigated. It results that via induction heating, ultrafast heating can be achieved, which leads to complex microstructures. This is possible because the short stay at austenitisation temperature results in carbon gradients in the austenitic microstructure, which yield different austenite decomposition products upon cooling. A comparative study on the microstructure after conventional (20 °C/s) and ultrafast (300 °C/s) heating is performed on a medium carbon steel in the soft annealed condition (ferrite plus spheroidised cementite microstructure). Continuous-heating dilatometry experiments are carried out and the volume phase fraction of austenite is evaluated throughout the heat treatment. The microstructure is analysed via Optical Microscopy (OM), SEM and TEM. The analysis shows that ultrafast heating leads to the formation of compositional gradients within austenite as also confirmed by diffusion simulations performed with the software Dictra. A thorough investigation of the initial microstructure by TEM shows that the initial chromium-rich carbides dissolve only partially during the rapid heat treatment. The product microstructure after UFHT is thus a mixture of undissolved carbides embedded in a very fine combination of martensite and bainite. It is shown that the phase distribution after the UFHT is related to carbon gradients in the microstructure. This research has shown that the implementation of a bainitic treatment in automotive spring production can lead to improved properties. Industrial trials carried out by VDL Weweler verified reduced energy consumption during the isothermal bainitic treatment when compared to quenching and tempering. Further cost reduction can be achieved by optimizing the alloy composition. The findings of the present study suggest that the composition of the alloy 51CrV4, specifically designed for quenching and tempering treatment, is not optimal for applying a bainitic treatment, due to slow bainite formation kinetics and the consequences of the presence of segregation of alloy elements, especially Cr. The microstructural characterization and especially the APT compositional analysis of the bainitic carbides has shown that

vanadium is not forming carbides during a bainitic treatment and therefore the micro-alloying element composition would need to be revised. The last chapter of the thesis discusses the findings of the research and presents suggestions for industrial implementation and further development.

Samenvatting

In dit proefschrift wordt de vervanging van afschrik- en ontlaatbehandelingen met isotherme bainitische behandelingen voor de productie van verenstaal voor de autoindustrie onderzocht. Een isotherme bainitische behandeling heeft voordelen, voornamelijk op het gebied van energiebesparing, maar het kan ook afschrikscheurvorming verhinderen, alsmede vervormingen en restspanningen, welke vaak gevonden worden in onderdelen die afgeschrikt en ontlaten zijn. In dit onderzoek wordt het vaak in de auto-industrie toegepaste laaggelegeerd koolstof-verenstaal gebruikt. Het onderzoek richt zich op de vorming van microstructuren en het effect daarvan op de eigenschappen van een verenstaal onderdeel. In het eerste deel van het proefschrift wordt bainiet-vorming onderzocht door middel van microscopie en dilatometrie. Er wordt gevonden dat de chemische heterogeniteit van de industrieel geproduceerde materiaal een significante invloed heeft op de vorming microstructuur. De analyse van de microstructuur in verschillende stadia tijdens de transformatie toont chemische segregatie van legeringselementen, als gevolg van het gieten, die een grote invloed heeft op de vorming van bainiet door middel van het vertragen van de transformatiekinetiek en het beperken van de maximale fractie bainiet. Tijdens gloeien bij temperaturen iets boven de martensiet-starttemperatuur wordt een homogene laag-bainitische microstructuur verkregen, terwijl bij hogere temperaturen de bainitische reactie onvolledig is. Ook blijkt dat in de vroege stadia van de transformatie verschillen in de vormingskinetiek van bainiet vanwege plaatselijke inhomogeniteit van de Cr en Mn concentratie resulteert in vertraging van de groei van bainiet in de gebieden met een hoge Mn en Cr concentratie. De bainiet-vorming is onderzocht door middel van gedetailleerde karakterisering op isotherm behandelde monsters die bij diverse temperaturen in het bainitische temperatuurbereik zijn gegloeid. Drie verschillende morfologieën worden geïdentificeerd op basis van Transmission Electron Microscopy analyse (TEM): hoog, laag en geïnverteerd bainiet. Laag bainiet bevat cementiet precipitaten, welke geen herverdeling van substitutionele legeringselementen vertonen, hetgeen is aangetoond met Atom Probe Tomography (APT). Koolstof in de bainitische ferriet blijkt te segregeren op dislocaties en een Cottrell atmosfeer te vormen, terwijl een relatief hoge koolstofconcentratie in oplossing is gebleven. Hoog-bainiet bevat ook cementiet, maar er is ook een beperkte herverdeling van Cr. Geïnverteerd bainiet is een ferriet plus cementiet twee-fasen-

mengsel, gevormd in hyper-eutectoidische staalsoorten, dat toch is gevonden in het onderzochte hypo-eutectoidische staal vanwege de segregatie van legeringselementen. Het vormt tijdens het isotherm gloeien op hoge temperaturen en bestaat uit Widmanstätten carbide-naalden omgeven door ferriet. Plaats-specifieke analyse van de APT waarnemingen aan geïnverteerd bainiet laat significante herverdeling van Mn en Cr zien, zowel in de carbiden als in de ferriet/martensiet-grensvlakken. Een essentiële behandeling bij de productie van verenstaal voor de auto-industrie is kogelstraalharding, een efficiënte werkwijze om drukspanningen in de onderdelen te induceren teneinde de initiatie van vermoeiingsscheuren te voorkomen. Door het toepassen van een bainiet-behandeling in plaats van een afschrik- en ontlaatbehandeling, kan de verkregen microstructuur potentieel verschillend reageren op de het kogelstralen, hetgeen kan resulteren in suboptimale eigenschappen. Derhalve wordt het effect van de microstructuur op de mechanische eigenschappen en de relatie met de reactie op het kogelstralen onderzocht. We zien dat de resulterende ruwheid van de bainitische monsters consequent hoger ligt dan die gemeten voor de monsters van ontlaten martensiet, hetgeen verklaard kan worden door de hogere werkversteviging van het bainiet in vergelijking met het ontlaten martensiet. Met behulp van Electron Back Scatter Diffraction (EBSD) en eindige elementen modelleren, Finite Element Modelling (FEM), verkennen we in detail het deformatiegedrag van de twee microstructuren. Wij zien dat de twee microstructuren verschillend vervormen, vanwege de verschillen in de microstructuren, zoals de korrelgrootte en de carbide-verdeling. FEM simulaties laten zien dat kogelstraalharden van een bainitische microstructuur resulteert in hogere drukspanningen onder de impact van het schot en beperkte trekspanningen in de omgeving vergeleken met een ontlaten martensitische microstructuur. Dit verschil in vervormingsgedrag kan de optimale parameters voor het kogelstralen beïnvloeden, met name om een volledige dekking van het kogelgestraalde oppervlak te verkrijgen, hetgeen een belangrijke voorwaarde is voor de verbetering van de levensduur van onderdelen. Daarnaast dient de mogelijk verhoogde ruwheid van de bainitische monsters te worden overwogen bij de selectie van de parameters van de kogelstraalbehandeling. Ook de invloed van de warmtebehandeling op de vermoeiingseigenschappen van 51CrV4 verenstaal met bainitische en ontlaten martensitische microstructuren is onderzocht. De karakterisering van de microstructuur toont dat laag bainiet en ontlaten martensiet verschillen vertonen in de microstructuur, zoals de blokgrootte van de martensiet- en bainietplaten, de dislocatiedichtheid en -structuur, en de grootte en verdeling van carbideprecipitaten. Statische mechanische eigenschappen zijn onderzocht met standaard trekproeven. De resultaten tonen een hogere treksterkte voor bainiet dan voor ontlaten martensiet. Kocks-Mecking-analyse is toegepast om

de vloeispanning van beide microstructuren te bepalen. De vloeispanning blijken vergelijkbaar te zijn. Een fysisch gebaseerd model wordt gebruikt om de dislocatiestructuur te karakteriseren en verschaft waardevolle inzichten in het mechanische gedrag van de twee microstructuren. Roterende buigvermoeidheidstesten zijn uitgevoerd om de vermoeiingseigenschappen van de twee microstructuren te evalueren. De vermoeiingseigenschappen van bainiet zijn superieur aan die van ontlaten martensiet. Breukanalyse van de vermoeiingsmonsters met stereomicroscopie en SEM onthult verschillende morfologieën bij bainiet en bij ontlaten martensiet. Op de breukvlakken van ontlaten martensiet zijn meervoudige initiatieplaatsen voor de vermoeiingsschade en ratchet sporen te vinden, terwijl breuk van bainiet meestal initieert op één punt op een oppervlakte-insluitsel. Dit wordt toegeschreven aan concurrerende vormingsmechanismen voor vermoeiingsscheuren, tussen plasticiteitgeïnduceerd falen en insluitsel-gecontroleerde breuk. Breukzones van ontlaten martensiet worden gedomineerd door samenvoeging van microholten. Dezelfde zone voor bainiet daarentegen, bestaat hoofdzakelijk uit karaktersiteiken voor brosse breuk, hetgeen de lagere breuktaaiheid van bainiet weergeeft. Het laatste hoofdstuk van dit proefschrift onderzoekt een alternatieve warmtebehandeling methode op basis van ultra-snelle inductie-verwarming. Om ontkoling te voorkomen zijn ook alternatieve methoden om de staven te verwarmen onderzocht. Via inductieverwarming kunnen ultrasnelle verwerkingssnelheden worden bereikt, hetgeen leidt tot complexe microstructuren. Dit is mogelijk omdat het korte verblijf in het austenietgebied resulteert in koolstofgradiënten in het austeniet, hegeen verschillende decompositie-producten van de austenite zal opleveren bij het afkoelen. Vergelijkend onderzoek naar de microstructuur na de gebruikelijke verwarmingssnelheid (20 °C/s) en ultrasnelle verwarming (300 °C/s) wordt uitgevoerd op een medium koolstofstaal in de zacht-gegloeide toestand (een microstructuur van ferriet plus globulair cementiet). Dilatometrie-experimenten met continue verwarming zijn uitgevoerd en de volumefractie van austeniet is geëvalueerd tijdens de gehele warmtebehandeling. De microstructuur is geanalyseerd met behulp van optische microscopie (OM), SEM en TEM. De analyse laat zien dat ultrasnelle verhitting leidt tot de vorming van samenstellingsgradiënten binnen het austeniet, hetgeen ook is bevestigd door diffusieberekeningen uitgevoerd met de Dictra software. Uit een grondig onderzoek van de oorspronkelijke microstructuur met TEM blijkt dat de aanvankelijk chroomrijke carbiden slechts gedeeltelijk oplossen tijdens de snelle warmtebehandeling. De microstructuur na ultra-fast induction heating (UFHT) is dus een mengsel van onopgeloste carbiden ingebed in een zeer fijne combinatie van martensiet en bainiet. Er wordt aangetoond dat de fasenverdeling na UFHT gerelateerd is aan koolstof-gradiënten in de microstructuur. Dit onderzoek heeft aan-

getoond dat de uitvoering van een bainiet-behandeling in auto-industrie veerstaal productie kan leiden tot verbeterde eigenschappen. Industriële proeven, uitgevoerd door VDL Weweler laten een verminderd energieverbruik zien tijdens de isothermische bainitische behandeling in vergelijking met afschrikken en ontlaten. Verdere kostenbesparing kan worden bereikt door het optimaliseren van de samenstelling van de legering. De bevindingen van deze studie suggereren dat de samenstelling van de legering 51CrV4, speciaal ontworpen voor afschrik- en ontlaatbehandeling, niet optimaal is voor het aanbrengen van bainitische behandeling, vanwege de langzame kinetiek van de bainietvorming en de gevolgen van de segregatie van legeringselementen, met name Cr. De microstructurele karakterisering en voornamelijk APT samenstellingsanalyse van de bainitische carbiden heeft aangetoond dat vanadium geen carbides vormt tijdens de bainitische behandeling. Daarom zouden de concentraties van micro-legeringselementen moeten worden herzien. Het laatste hoofdstuk van het proefschrift bespreekt de bevindingen van het onderzoek en er worden voorstellen gedaan voor industriële uitvoering en verdere ontwikkeling.

Περίληψη

Η παρούσα διδακτορική διατριβή διερευνά την πιθανή υποκατάσταση της θερμικής κατεργασίας με βαφή και επαναφορά με ισοθερμοκρασιακές μπαινιτικές βαφές. Η ισοθερμοκρασιακή μπαινιτική βαφή προσφέρει πλεονεκτήματα ως προς την κατανάλωση ενέργειας, αλλά μπορεί να αποφευχθούν και άλλα ελαττώματα όπως η ρηγμάτωση κατά τη βαφή, η παραμόρφωση και οι παραμένουσες τάσεις, τα οποία εμφανίζονται συχνά σε προϊόντα στα οποία εφαρμόζεται βαφή και επαναφορά. Για την παρούσα μελέτη χρησιμοποιείται ένας ελαφρά κραματωμένος χάλυβας ελατηρίων, μεσαίου άνθρακα. Η μελέτη επικεντρώνεται στο σχηματισμό της μικροδομής και στην επίδρασής της στην απόδοση ενός προϊόντος κατασκευασμένου από χάλυβα ελατηρίων.

Στο πρώτο μέρος της διατριβής μελετάται ο σχηματισμός του μπαινίτη μέσω διαστολομετρίας και μικροσκοπίας. Η χημική ετερογένεια του υλικού όπως παρήχθη από τη βιομηχανία βρέθηκε να έχει σημαντική επίδραση στο σχηματισμό της μικροδομής. Η ανάλυση της μικροδομής σε διαφορετικά χρονικά διαστήματα κατά τον μετασχηματισμό δείχνει ότι ο μακροδιαφορισμός κραματικών στοιχείων αντικατάστασης, ο οποίος λαμβάνει χώρα κατά τη χύτευση, επηρεάζει καθοριστικά το σχηματισμό του μπαινίτη επιβραδύνοντας την κινητική και περιορίζοντας το μέγιστο δυνατό ποσοστό σχηματισμού μπαινίτη. Κατά την ισοθερμοκρασιακή βαφή σε θερμοκρασίες λίγο πάνω από τη θερμοκρασία έναρξης του μαρτενσιτικού μετασχηματισμού, παράγεται μια ομοιόμορφη μικροδομή αποτελούμενη εξολοκλήρου από κατώτερο μπαινίτη, ενώ σε ανώτερες θερμοκρασίες ισοθερμοκρασιακής βαφής, ο σχηματισμός του μπαινίτη είναι ημιτελής. Κατά τα πρώτα στάδια του μετασχηματισμού, λόγω της τοπικής χημικής ανομοιογένειας σε Μαγγάνιο (Mn) και Χρώμιο (Cr) παρατηρείται καθυστέρηση στην κινητική της ανάπτυξης του μπαινιτικού φερρίτη στις περιοχές στις οποίες η συγκέντρωση του Mn και του Cr είναι υψηλή. Η έρευνα στο σχηματισμό του μπαινίτη συνεχίζεται με ενδελεχή χαρακτηρισμό της μικροδομής των δοκιμίων, τα οποία υποβλήθηκαν σε ισοθερμοκρασιακή βαφή σε διαφορετικές θερμοκρασίες εντός των θερμοκρασιακών ορίων στα οποία αναμένεται σχηματισμός μπαινίτη. Μετα από ανάλυση μέσω ηλεκτρονικής μικροσκοπίας διερχόμενης δέσμης (TEM), ταυτοποιήθηκαν τρεις διαφορετικές μορφολογίες: Κατώτερος, ανώτερος και ανάστροφος μπαινίτης. Οι μετρήσεις που πραγματοποιήθηκαν μέσω Atom Probe Tomography (APT) δείχνουν ότι ο κατώτερος μπαινίτης περιέχει κατακρημνίσματα σεμεντίτη, στα οποία δεν παρατηρείται αναδιάταξη των κραματικών στοιχείων (σε σχέση με τη φερριτική μήτρα). Ο άνθρακας συγκεντρώνεται στις διαταραχές σχη-

ματίζοντας ατμόσφαιρες Cottrel, παραμένοντας παράλληλα εν μέρει σε στερεό διάλυμα στον μπαινιτικό φερρίτη, εμφανίζοντας υψηλή συγκέντρωση. Ο ανώτερος μπαινίτης περιέχει επίσης κατακρημνίσματα σεμεντίτη, αλλά εντώς τον κατακρημνισμάτων παρατηρείται ελαφρά αναδιάταξη του Cr. Ο ανάστροφος μπαινίτης είναι ένα μίγμα φάσεων επίσης αποτελούμενο από φερρίτη και σεμεντίτη, το οποίο σχηματίζεται σε υπερευτηκτοειδείς χάλυβες, ο οποίος όμως βρέθηκε να σχηματίζεται στον υποευτηκτοειδή χάλυβα της παρούσας μελέτης λόγω της ύπαρξης του διαφορισμού. Σχηματίζεται σε υψηλές θερμοκρασίες ισοθερμοκρασιακής βαφής και αποτελείται από βελονοειδή σεμεντίτη (Widmanstätten) περιβαλλόμενο από φερρίτη. Η ανάλυση συγκεκριμένων περιοχών μέσω APT αποκαλύπτει ότι το Mn και το Cr αναδιατάσσονται έντονα τόσο εντός των βελονών του σεμεντίτη, όσο και στις διεπιφάνειες μεταξύ φερρίτη και μαρτενσίτη.

Μία σημαντική και αναπόσπαστη κατεργασία η οποία εφαρμόζεται κατά την παραγωγή ελατηρίων αυτοκινητοβιομηχανίας είναι η σφαιριδιοβολή (shot peening). Η σφαιριδιοβολή είναι μια αποδοτική μέθοδος κατά την οποία εισάγονται στο προιόν θλιπτικές παραμένουσες τασεις προκειμένου να αποφευχθεί η έναρξη ρηγματώσεων κόπωσης. Εφαρμόζοντας μία ισοθερμοκρασιακή μπαινιτική βαφή αντί της βαφής και επαναφοράς, σχηματίζονται διαφορετικές μικροδομές οι οποίες μπορεί να ανταποκριθούν διαφορετικά στη σφαιριδιοβολή, με πιθανό αποτέλεσμα να μην επιτευχθούν οι βέλτιστες επιθυμητές ιδιότητες. Για αυτόν το λόγο ερευνάται η επίδραση της μικροδομής στις μηχανικές ιδιότητες και η σχέση τους με την τελική απόδοση της σφαιριδιοβολής. Παρατηρείται ότι η τραχύτητα των μπαινιτικών δοκιμίων παραμένει συστηματικά υψηλότερη σε σχέση με την αντίστοιχη των επαναφερμένων μαρτενσιτικών δοκιμίων, το οποίο μπορεί να εξηγηθεί λόγω του υψηλότερου βαθμού εργοσκλήρυνσης που επιτυγχάνουν τα μπαινιτικά δοκίμια. Με τη χρήση περιθλασιμετρίας οπισθοσκεδαζόμενων ηλεκτρονίων (EBSD) και προσομοιώσεων μέσω της μεθόδου των πεπερασμένων στοιχείων (FEM), αναλύεται η συμπεριφορά των δύο μικροδομών κατά την παραμόρφωση. Παρατηρείται ότι οι δύο μικροδομές συμπεριφέρονται διαφορετικά, λόγω της ύπαρξης διαφορετικών μικρογραφικών συστατικών όπως το μέγεθος των πλακιδίων, και το μέγεθος και η κατανομή των καρβιδίων. Οι προσομοιώσεις πεπερασμένων στοιχείων δείχνουν ότι η σφαιριδιοβολή σε μια μπαινιτική μικροδομή οδηγεί σε υψηλότερες παραμένουσες τάσεις κάτω από το σημείο της πρόσκρουσης του σφαιριδίου, σε σύγκριση με μία επαναφερμένη μαρτενσιτική μικροδομή. Αυτή η διαφορά στη συμπεριφορά κατά την παραμόρφωση μπορεί να επηρεάσει τις παραμέτρους της σφαιριδιοβολής, προκειμένου να επιτευχθεί πλήρης κάλυψη της επιφάνειας του προιόντος. Η πλήρης κάλυψη είναι αναγκαία συνθήκη για την βελτίωση της αντοχής σε κόπωση. Επιπρόσθετα, η πιθανή αυξημένη τραχύτητα των μπαινιτικών δοκιμίων πρέπει να ληφθεί υπόψη κατά το σχεδιασμό μιας κατεργασίας σφαιριδιοβολής.

Στη συνέχεια μελετάται η επίδραση της θερμικής κατεργασίας στην αντοχή σε κό-

πωση στον χάλυβα 51CrV4 με μπαινιτική και επαναφερμένη μαρτενσιτική μικροδομή. Ο χαρακτηρισμός της μικροδομής δείχνει ότι οι δύο μικροδομές έχουν διαφορές ως προς τα μικρογραφικά χαρακτηριστικά, τη διάταξη και την πυκνότητα των διαταραχών, και το μέγεθος και την διασπορά των καρβιδίων. Οι μηχανικές ιδιότητες υπό στατική καταπόνηση μελετήθηκαν μέσω πρότυπων δοκιμών εφελκυσμού. Τα αποτελέσματα δείχνουν ότι η αντοχή των μπαινιτικών δοκιμίων είναι υψηλότερη σε σχέση με αυτή των επαναφερμένων μαρτενσιτικών. Πραγματοποιείται ανάλυση Kocks-Mecking προκειμένου να υπολογιστούν με ακρίβεια τα όρια διαρροής των δύο μικροδομών. Τα όρια διαρροής υπολογίζονται να είναι παρόμοια και στις δύο περιπτώσεις. Ένα φυσικό μοντέλο χρησιμοποιείται για το χαρακτηρισμό της διάταξης των διαταραχών και παρέχει σημαντικές πληροφορίες που βοηθούν στην εξήγηση της μηχανικής συμπεριφοράς των δύο μικροδομών. Πραγματοποιούνται δοκιμές κόπωσης υπό ταυτόχρονη στρέψη και κάμψη προκειμένου να αξιολογηθεί η απόδοση των δύο μικροδομών. Η απόδοση των μπαινιτικών δοκιμίων διαπιστώνεται υψηλότερη. Η θραυστογραφία στα δοκίμια της κόπωσης με χρήση στερεοσκοπίου και ηλεκτρονικού μικροσκοπίου σάρωσης (SEM) αποκαλύπτει διαφορές στη μορφολογία των επιφανειών θραύσης μεταξύ των δύο μικροδομών. Στις επιφάνειες θραύσης των επαναφερμένων μαρτενσιτικών δειγμάτων εμφανίζουν πολλαπλά σημεία έναρξης ρωγμών, καθώς επίσης και ratchet marks, ενώ στα μπαινιτικά δείγματα οι ρωγμές ξεκινούν κυρίως από ένα σημείο, σε εγκλείσματα που βρίσκονται στην επιφάνεια του δοκιμίου. Αυτό μπορεί να είναι αποτέλεσμα ανταγωνιστικών μηχανισμών έναρξης ρωγμών κόπωσης, μεταξύ του μηχανισμού έναρξης λόγω πλαστικής παραμόρφωσης και της αστοχίας ελεγχόμενης από τα εγκλείσματα. Οι περιοχές τελικής αστοχίας του επαναφερμένου μαρτενσίτη έχουν κυρίως χαρακτηριστικά όλκιμης θραύσης, ενώ του μπαινίτη είναι κυρίως ψαθυρές. Αυτό μπορεί να είναι ένδειξη χαμηλής δυσθραυστότητας για τον μπαινίτη.

Το τελευταίο κεφάλαιο ασχολείται με μια εναλλακτική θερμική κατεργασία βασισμένη στην ταχεία επαγωγική θέρμανση. Με πρωταρχικό κίνητρο να αποφευχθεί η απανθράκωση κατά την αναθέρμανση, ερευνώνται εναλλακτικοί τρόποι θέρμανσης των χαλύβων. Προκύπτει ότι μεσω επαγωγικής θέρμανσης μπορούν να επιτευχθούν πολύ υψηλοί ρυθμοί αναθέρμανσης, οι οποίοι μπορεί να προκαλέσουν το σχηματισμό πολύπλοκων μικροδομών. Αυτό είναι εφικτό διότι η σύντομη παραμονή στην περιοχή του ωστενίτη καταλήγει σε ανομοιογενή κατανομή του άνθρακα στην ωστενιτική μικροδομή, η οποία κατά την ψύξη θα μετασχηματιστεί σε διαφορετικές μικροδομές. Πραγματοποιείται μια συγκριτική μελέτη στη μικροδομή ενός μικροκραματωμένου χάλυβα μεσαίου άνθρακα με αρχική μικροδομή φερρίτη και σφαιροποιημένου σεμεντίτη, μετά από αναθέρμανση με ρυθμό 20ºC/s και ρυθμό 300ºC/s. Πραγματοποιούνται δοκιμές διαστολομετρίας διαρκούς θέρμανσης και καταγράφεται το ποσοστό του ωστενίτη κατά την εξέλιξη της θερμικής κατεργασίας. Η διεξοδική ανάλυση της μικροδομής μετά από ταχεία αναθέρμανση

μέσω ηλεκτρονικής μικροσκοπίας διερχόμενης δέσμης (TEM) δείχνει ότι υπάρχουν διαφορές στην τοπική χημική σύσταση του ωστενίτη, κατι που επεβαιώνεται και από υπολογισμούς διάχυσης με το λογισμικό Dictra. τα καρβίδια της αρχικής μικροδομής, τα οποία είναι πλούσια σε χρώμιο, διαλυτοποιούνται μερικώς κατά την ταχεία αναθέρμανση. Η παραγόμενη μικροδομή μετά την ταχεία αναθέρμανση είναι μια μίξη από μερικώς διαλυτοποιημένα καρβίδια, σε μια λεπτομερή μήτρα αποτελούμενη από μαρτενσίτη και μπαινίτη. Προκύπτει ότι η κατανομή των φάσεων μετά την ταχεία αναθερμανση είναι αποτέλεσμα της χημικής ανομοιογένειας της μικροδομής.

Η παρούσα μελέτη δείχνει ότι η εφαρμογή μίας ισοθερμοκρασιακής μπαινιτικής θερμικής κατεργασίας στην παραγωγή ελατηρίων για την αυτοκινητοβιομηχανία μπορεί να οδηγήσει σε βελτιωμένες ιδιότητες. Διεξάγονται βιομηχανικές δοκιμές από την VDL Weweler, τα αποτελέσματα των οποίων δείχνουν μειωμένη κατανάλωση ενέργειας κατά την ισοθερμοκρασιακή μπαινιτική κατεργασία σε σύγκριση με την βαφή και επαναφορά. Επιπλέον μείωση του κόστους μπορεί να επιτευχθεί με τη βελτιστοποίηση της χημικής σύστασης του κράματος για τη συγκεκριμένη εφαρμογή. Με βάση τα ευρήματα της μελέτης διαπιστώνεται ότι η χημική σύσταση του 51CrV4, το οποίο έχει σχεδιαστεί για βαφή και επαναφορά, δεν είναι βέλτιστη για μπαινιτικές θερμικές κατεργασίες, διότι η κινητική του μπαινιτικού μετασχηματισμού είναι αργή και υπάρχουν περιπλοκές λόγω του διαφορισμού του Χρωμίου και των λοιπών κραματικών στοιχείων. Ο χαρακτηρισμός της μικροδομής, ιδίως η ανάλυση της χημικής σύστασης των καρβιδίων στον μπαινίτη μέσω APT, δείχνει ότι το Βανάδιο δεν σχηματίζει καρβίδια κατά την διάρκεια της μπαινιτικής βαφής, και επομένως θα πρέπει να αναθεωρηθεί η χημική σύσταση μικροκραματικών στοιχείων. Το τελευταίο κεφάλαιο της διατριβής περιλαμβάνει μια γενική συζήτηση των αποτελεσμάτων της έρευνας και παρουσιάζει ορισμένες κατευθυντήριες γραμμές για περεταίρω έρευνα.

1

Introduction

1.1. Introduction

In the past decades, continuous market demand for improving vehicle performance and rising awareness about CO_2 emission and energy consumption have created the need to develop new, more energy efficient steel production processes. The greatest achievement of the steel research was the creation of the family of Advanced High Strength steels (AHSS) for automotive applications. AHSS are flat steel products with a strength-ductility combination superior to conventional steel grades. Members of the AHSS family are Dual Phase steel (DP), Complex Phase steel (CP), Transformation Induced Plasticity steel (TRIP) and Twinning Induced Plasticity steel (TWIP). AHSS obtain their superior properties through a multiphase microstructure, which is a carefully designed combination of phases with different properties.

Although much has been achieved for the Body-In-White of cars with the successful development of the different grades of AHSS, other mechanical components not constructed from thin sheet steel are still produced by using conventional steels and heat treatments. One category of these components is that of flat springs, a type of spring often used in the suspension system of trucks. Flat springs are heavy components manufactured from conventional hot rolled bar medium- or high-carbon steel. They obtain the required strength level after a Quenching and Tempering (Q&T) heat treatment, **Figure 1.1**.

Quenched and tempered components have a tempered martensitic microstruc-

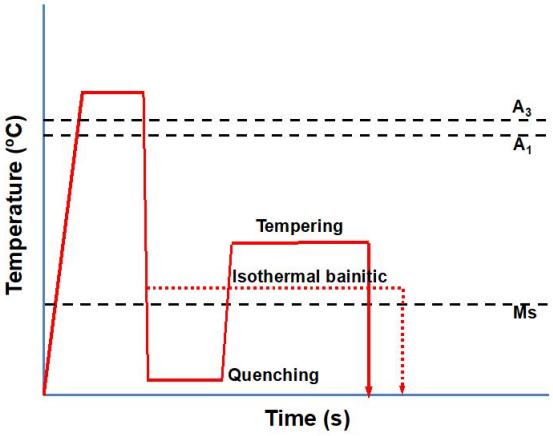

Figure 1.1: Schematic overview of Quenching and Tempering (solid line) and isothermal bainitic treatments (dashed line).

ture, which gives the material a good combination of strength, ductility and fatigue resistance and a performance that is sufficient for the most demanding automotive applications. Nevertheless, during a Q+T heat treatment, the component is likely to distort, because of the temperature gradient during quenching, and also quench cracking is likely to appear, both phenomena leading to rejection of the produced component.

Recently, research on spring steels has started to concentrate on springs with bainitic microstructures, instead of the commonly used tempered martensitic microstructures. When bainite is formed isothermally, a treatment also called austempering, the complete austenite transformation occurs after many minutes or hours at a typical temperature of 400 °C, which is above the martensite start temperature Ms, thus avoiding non-uniform transformation, which can cause distortions and quench cracks.

Bainite is, from a mechanical point of view, a very promising microstructural feature that can form in rapidly cooled steels. It combines high strength with good ductility, while production of components with bainitic microstructure by heat treatment can be cost and energy efficient compared to Q+T treatments. In a bainitic treatment, there is no need for a tempering step, so the entire treatment can be completed in one heat, **Figure 1.1**. Without tempering, an indispensable, energy-intensive and costly step of the heat treatment is avoided. If one considers not only the cost of the heat treatment, but also the additional cost inspecting for cracking and correcting distortion, the potential benefit of industrial adaptation of isothermal heat treatments can be significant. It is known that bainite also offers increased

fatigue life; therefore, it can be an optimal choice for components that are subjected to cyclic loading.

Spring production, apart from the heat treatment, includes surface treatments in order to meet the component fatigue requirements. A typical surface treatment used is shot peening. In shot peening, spherical particles are accelerated towards the surface of an engineering component, causing plastic deformation. This deformation results in compressive residual stresses, which are beneficial for increasing fatigue resistance. Changing the microstructure of the spring can also influence the result of the shot peening, so shot peening parameters might need to be changed if the heat treatment is altered.

Following a completely different heat treatment scheme and with the use of the induction heating method instead of salt baths, interesting microstructures can be created in short times, which can be proven beneficial to the industry since the required time for heat treatment can be shortened. In the framework of this research, these possibilities will be investigated as well.

Although bainite and its advantages have been known for decades, the high demands for process control and the incomplete understanding of the influence of chemical composition and process parameters on the resulting properties of bainite limit the industrial development of bainitic steels. For almost a century, a large body of research has been accumulated on the bainite reaction and two conflicting ideas about the mechanism of formation of bainite have been developed, neither of which can falsify the other. Even though no scientific consensus on the formation mechanism has been reached yet, bainitic steels do find their way to the market, as new technologies allow precise process control and monitoring.

1.2. Aim of this Thesis

This aim of the present thesis is to define alternative heat treatments to produce flat automotive springs. The most promising heat treatment is the isothermal bainitic (austempering), which is the one on which the research mainly focuses. By gaining fundamental understanding of the mechanism of bainite formation, we address the challenges that keep bainitic treatments from being industrially applied.

We investigate bainite formation in a conventional, industrially produced medium carbon spring steel alloy. Based on in-depth characterisation, thermodynamic, and kinetic analysis, we provide an explanation of the underlying mechanism of the microstructure formation, which helps to identify the possible challenges for large scale application. Finally, we link the resulting mechanical properties and fatigue performance with the microstructural features.

1.3. Outline

Chapter 2 contains our approach to explaining bainite formation in materials that contain chemical segregation from the casting. We see that the chemical heterogeneities in substitutional alloying elements like manganese and chromium affect the formation kinetics of bainite. The study consists of experimental work and thermodynamic analysis.

In Chapter 3 we examine at the atomic scale the different morphologies of bainite, which were found to form at different isothermal holding temperatures. The focus of this chapter is mainly on characterization of bainite, which aims to elucidate the fundamental mechanisms that lead to its morphological diversity. For the characterization work, we used high resolution electron microscopy and Atom Probe Tomography.

Chapter 4 focuses on a different topic than the previous ones. In order to enhance fatigue performance, springs are usually shot-peened, a treatment that modifies the surface microstructure. In this chapter, the effect of shot peening treatments on the microstructure is discussed. Using Electron Back Scatter Diffraction as well as Finite Element Modelling, we characterise the strain accommodation caused by the shot impacts during shot peening, when the microstructure of the peened component is either bainitic or tempered martensitic. It is shown that distinct differences in strain accommodation between the bainitic and the tempered martensitic microstructure result in different optimum shot peening parameters in terms of coverage and resulting residual stresses.

Based on microstructure and mechanical properties discussussed in Chapter 2-4, we chose the most promising heat treatment scheme to produce bainitic specimens with the aim of evaluating the fatigue properties of the designed microstructure. Chapter 5 focuses particularly on the fatigue properties of lower bainite in comparison with high-temperature tempered martensite, which is the current state of the art and serves as our benchmark. The study includes mechanical tests, high resolution electron microscopy, fatigue tests and fractography of the failed specimens. The fatigue behaviour is explained in terms of microstructure, which determines the crack initiation mechanism.

Chapter 6 is an independent study of alternative heat treatments, which could produce similar mechanical properties as the ones studied in the previous chapters, but in a small fraction of the time. We experimented with ultrafast heating via induction, instead of the conventional gas furnace, followed by rapid water quenching instead of the timely isothermal salt bath quenching. The short austenitisation times result in carbon gradients within the material, which enable the formation of multiple

phases.

Chapter 7 discusses the challenges of industrial upscaling of the bainitic treatment. Since industrial implementation of the project is already ongoing, input from the industry is used as a proof of concept. The chapter concludes with a general discussion of the outcome of this research, recommendations to the industry and suggestions for future work.

2

Bainite Formation in Medium Carbon Spring Steels Accounting for Chemical Segregation*

In this chapter, isothermal bainite formation is investigated in the 51CrV4 spring steel by dilatometry and microscopy. As the material studied is an industrially produced steel grade, it was found to contain alloying element segregation. Thus, the effect of chemical alloying element segregation on bainite formation is particularly highlighted as a challenge for industrial adaptation of bainitic treatments. The analysis of the microstructure at different times during transformation shows that chemical segregation of substitutional alloying elements strongly affects the bainite formation by retarding the transformation kinetics and limiting the maximum achievable bainite fraction. During holding at temperatures close to and above the martensite start temperature, at the early stage of isothermal holding, the bainite transformation occurs preferentially in regions of low alloy concentration; as the heat treatment proceeds, a homogeneous lower bainitic microstructure is obtained. On the contrary

* This chapter is based on the article: Bainite formation in medium carbon spring steels accounting for chemical segregation, by C. Goulas, M.G. Mecozzi and J. Sietsma, Metall. Mater. Trans 47A (2016) 3077-3087.

at higher temperatures, incomplete bainitic reaction is evident. It was also found that at the early stages of the transformation, differences in the bainite formation kinetics, due to local inhomogeneities in Cr and Mn concentration, result in retardation of the growth of bainite in the high Mn and Cr concentration regions. The calculated difference in driving force for nucleation between the enriched and the depleted areas is not by itself sufficient to explain the microstructures obtained and thus significant influence of growth on bainite formation is observed.

2.1. Introduction

In the past decades, the continuous market demand for improving vehicle performance and the rising awareness about CO_2 emission and energy consumption created the need to develop new, more energy efficient production processes that include commonly used heat treatments. To reduce the overall weight of vehicles, the automotive industry needs to focus on each individual component. This research is related to the definition of alternative heat treatments to produce automotive springs. Low-alloyed, medium or high carbon steels are the most commonly used materials for automotive spring production. Recently, research on spring steels started to concentrate on springs with bainitic microstructures, instead of the commonly used tempered martensitic microstructures. Bainitic microstructure offers in principle significant advantages over the most commonly used tempered martensite. First of all, it offers a fine microstructure with high strength and acceptable ductility. The fully bainitic microstructure has a lower crack growth rate than tempered martensite. Tomita and Okabayashi showed that lower bainite exhibits increased fracture ductility and notch toughness, because micro-crack propagation is effectively inhibited by the fine bainitic ferrite plate morphology [1]. The bainitic microstructure, containing fine and evenly dispersed hard cementite precipitates, can be expected to effectively retard the fatigue crack growth by crack interlocking [2]. Additionally, during processing, the tempering treatment can be avoided, which is an indispensable and costly step of the tempered martensite production. In this way temper embrittlement is avoided as well and a less energy is needed for the heat treatment.

Although bainite and its advantages have been known for decades, the incomplete understanding of the influence of chemical composition and process parameters on the resulting bainite fraction and morphology limits the industrial development of bainitic steels. For almost a century, a large body of research has been done on the bainite reaction and two conflicting ideas about mechanism of formation of bainite have been developed. When formed at low temperatures, bainite looks like martensite and it is sometimes even impossible to distinguish them mi-

croscopically. This experimental finding suggests that the mechanism of formation of bainite is similar to that of martensite and therefore is diffusionless in nature. On the other hand, an increasing number of experimental and theoretical studies support the similarity between bainitic ferrite and proeutectoid ferrite with Widmanstätten morphology and the idea that bainite growth is strongly influenced by carbon diffusion.

Hultgren first proposed in 1947 that upper bainite could form by initial Widmanstätten ferrite formation, with subsequent formation of cementite on its sides [3]. The concept was further analysed by Hillert, who has shown that there is no reason to treat Widmanstätten ferrite and bainitic ferrite as different products, as there is no kinetic discontinuity [4]. According to this approach, the bainitic ferrite nucleates at austenite grain boundaries and grows at a rate determined by the diffusivity of carbon. Aaronson et al., supporting the above described theory, have considered the effect of alloying elements on the bainitic transformation, and the potential segregation of substitutional elements at the growing phase interface [5]. The incomplete reaction phenomenon, described as the premature cessation of bainite formation before the equilibrium fraction of this phase is attained, is explained by the solute drag effect that significantly retards the growth of the bainitic ferrite [6-8].

The diffusionless approach was introduced by Zener in 1946 [9], further developed by Ko and Cottrell [10], and more recently supported by Bhadeshia [11]. According to this approach, a sub-unit of bainitic ferrite, supersaturated in carbon, nucleates on an austenite grain boundary. The growth is practically instantaneous and displacive and stops because of the plastic deformation of the adjacent austenite. After growth stops, carbon is rejected from the supersaturated ferrite by diffusion into the residual austenite, in which it can form carbides with para-equilibrium composition. Carbon can also precipitate within the bainitic ferrite sub-unit in the form of carbides, if insufficient diffusion can take place due to the transformation temperature being low. Once bainitic sub-units have formed, the bainite formation can continue by the autocatalytic nucleation and displacive growth of new sub-units on the tip of previously formed sub-units. Bainitic transformation can be incomplete if carbide precipitation is inhibited. This implies that the austenite is gradually enriched in carbon and is eventually stabilized at the given temperature. In this case, according to Zener, diffusionless growth would cease when the carbon content of the residual austenite reaches the value for which, at the given temperature, ferrite and austenite have the same Gibbs free energies. These values at different temperatures form a curve in the phase diagram, which was later named "T_0 curve" [12]. It has also been proposed that the line of equal Gibbs free energy of austenite and ferrite should be calculated with an additional term for bainitic ferrite due to the

strain energy in the untransformed austenite. Therefore, the maximum carbon content for diffusionless growth should differ from the value predicted by the T_0 curve. Bhadeshia estimated the driving force for diffusionless growth at experimental bainite start temperature equal to 400 J/mol [12]. The calculated curve with 400 J/mol of additional energy in ferrite was denoted with "T_0'" curve.

The role of carbon and substitutional alloy elements in the bainite formation is described differently within the two different schools of thought. This makes the design of bainitic treatments on industrial scale a very challenging task, especially in presence of compositional inhomogeneity in the industrial steel product. One source of compositional inhomogeneity in steel is the micro-segregation of alloying elements during the solidification process. Micro-segregation occurs when the liquid metal present in the inter-dendritic spaces becomes enriched in alloying elements (like manganese, chromium, silicon, molybdenum and phosphorous) and the dendrite cores become depleted of these solute elements. After solidification, there are regions with low and high solute element concentrations in austenite. Hot rolling transforms these regions into parallel layers in which austenite exhibits different transformation kinetics to allotriomorphic and Widmanstätten ferrite, pearlite, bainite or martensite. This can determine the formation of a laminated microstructure, called banding.

In the present study, we will explore the microstructure evolution of hot rolled 51CrV4, in case a subsequent isothermal bainitic treatment is applied. The effect of compositional inhomogeneity on the bainite formation kinetics is analysed. Interrupted dilatometry tests, microscopy and thermodynamic calculations help to monitor and explain the segregation-induced differences in the formation of bainite at different temperatures.

2.2. Experimental procedure

Samples of 51CrV4 steel with chemical composition shown in **Table 2.1** were received in as rolled condition. The samples were cut out of hot rolled bars with dimensions 95 x 49 x 5500 mm^3. The chemical analysis was performed on 30 x 30 mm^2 cross-sections of the bars, transverse to the rolling direction, by means of Optical Emission Spectroscopy (OES). Dilatometric cylindrical specimens were machined using Wire Electro-Discharge Machining (EDM) with dimensions Φ 4 x 10 mm^2. EDM was used to assure that the dimensions have low tolerance and at the same time the initial microstructure remains intact.

The dilatometric tests were performed in a Bähr 805A Quench dilatometer. This instrument uses an induction coil to heat the sample and detects the length change

of the sample with a Linear Variable Displacement Transducer (LVDT). The specimens were placed in the dilatometer with a thermocouple spot welded at the middle in order to control the temperature. Experiments with two thermocouples were also performed, one at the edge and the second at the centre, in order to check the temperature gradient and whether the transformations occur evenly throughout the sample. In all experiments, the temperature differences recorded by the two thermocouples were within 10 °C.

All samples were heated within 60 s to the austenitisation temperature (900 °C) under vacuum and then quenched to an isothermal holding temperature in the range 300 °C-510 °C using helium gas. The quenching rate was high enough to avoid austenite-ferrite transformation according to CCT diagrams for the specific chemical composition, which was confirmed by the dilatometric observations. This rate was chosen to be 30 °C/s. After the isothermal holding, the samples were quenched to room temperature. Interrupted treatments were performed on the basis of time intervals allowing the same volume fraction of bainite to be transformed for the different temperatures, as reported in **Table 2.2**. The holding for 125 s at 420 °C produces equivalent bainite fraction as the holding for 250 s at 300 °C. For 510 °C, the transformation kinetics is slower and the times chosen allow for an observation of the products of the isothermal transformation. 500 s was the minimum time of isothermal holding for which transformation products could be observed under the optical microscope and 3600 s was sufficient to allow for the microstructrural products of the isothermal transformation to develop. After 3600 s of isothermal holding at 510°C, the treatment was interrupted.

Dilatometric curves were analysed in order to evaluate the bainite formation at the different temperatures. For microstructural characterization, the dilatometric samples were mounted on a specially designed sample holder, then ground, polished and etched with Nital 2% for 6 s. The specimens were examined by means of light optical microscopy for phase identification. An Olympus BX60M optical mi-

Table 2.1: Chemical composition of the 51CrV4 grade as measured by Optical Emission Spectroscopy.

Elements	C	Mn	Si	Cr	V
Wt. %	0.51	1.02	0.33	1.15	0.12

Table 2.2: Time and temperature conditions for the 51CrV4 dilatometric tests.

Temperature (^oC)	Time (s)
300	250, 3600
420	125, 2500
510	500, 3600

croscope was used for the analysis.

For Scanning Electron Microscopy (SEM) and Scanning Transmission Electron Microscopy - Energy Dispersive Spectroscopy (STEM-EDS) analysis, specimens were prepared from the dilatometry samples. Even though the temperature differences within the dilatometric specimen during the heat treatment was found to be within 10 °C, in order to ensure that the microstructure observations were consistent with the dilatometry measurements, the sample discs were cut from the middle zone of the dilatometric specimen. For SEM, the specimen was prepared following standard metallographic polishing procedure and for STEM the discs were manually ground down to 60 μm, and then Ar-ion polished to final thickness using GATAN 691 PIPS system. For the SEM observation, a Field Emission Gun (FEG)-SEM JEOL 6500F operated at 15 kV was employed, while for the STEM EDS analysis, a JEM 2100 electron microscope operated at 200 kV was used.

Finally, Electron Probe Micro Analysis (EPMA) was performed to evaluate alloying element segregation. The measurements were performed with a JEOL JXA 8900R microprobe using an electron beam with energy of 10 keV and beam current of nominal 1000 nA employing Wavelength Dispersive Spectrometry (WDS). The points of analysis were located along a 500 μm line with increments of 5 μm and involved the elements Mn, Cr, Si and V.

2.3. Results

Figure 2.1 shows the dilatometric curves obtained for treatments at different isothermal holding temperatures.

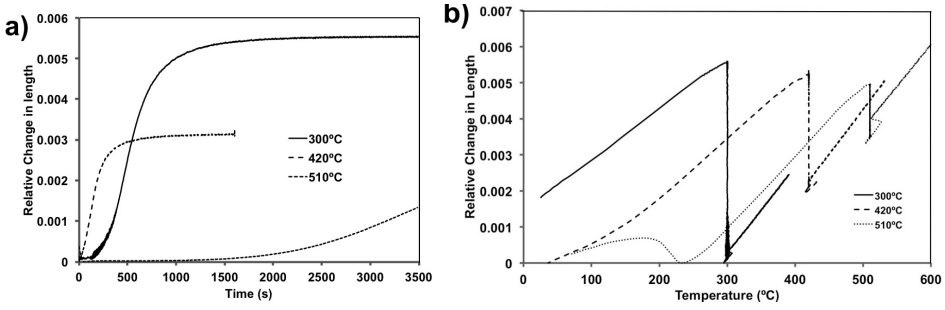

Figure 2.1: Graphs of the cooling and isothermal holding segments of the dilatometric tests. a) Relative change in length vs. temperature, during the cooling part of the heat treatment. b) Relative change in length vs. time, for isothermal holding at different temperatures.

It can be noticed in **Figure 2.1a** that as the isothermal holding temperature becomes higher, the relative dilatation during holding decreases. After the isothermal

holding at 420 °C and 510 °C, fresh martensite forms during the final quench, as shown by the deviation from the linearity of the dilatation curve. After isothermal holding at the lowest temperature, the dilatometric signal is linear during the final quench, indicating absence of transformation in that segment. The artefact at the onset of the isothermal holding observed in the temperature monitoring of the treatments is caused by the shifting from the quenching stage to the isothermal stage, and was found to have no implication on the subsequent isothermal phase transformation. No ferrite was found to form at the prior austenite grain boundaries. In **Figure 2.1b** it can be seen that the bainite formation goes to completion within one hour for the lower two temperatures. During the isothermal holding at 510 °C the dilatation is still increasing at the end of the experiment, but this change in length is attributed to a transformation product different than normal bainite/bainitic ferrite, as will be shown later.

From the samples used for the curves of **Figure 2.1**, only information about the final microstructure can be obtained. Interrupted heat treatment experiments were performed in order to follow the microstructure evolution. The samples that were heat treated in the dilatometer have been analysed by means of optical microscopy. Representative examples of the morphologies formed are presented in **Figure 2.2**. In order to show the scale at which the segregation occurs, low magnification micrographs are shown.

Bainite was found to form during all heat treatments. The temperature of the isothermal holding determines the microstructure and the final fraction of bainite obtained. It can be observed that bainitic ferrite plates do not nucleate homogeneously at all temperatures; instead, a banded structure forms at early stages of the transformation. The microstructure becomes more homogeneous at the scales of **Figure 2.2** after 1 h of isothermal annealing at 300°C. For the higher temperatures, untransformed regions (appearing white in the micrograph) are identified after the transformation ceases (see **Figure 2.2d** and **Figure 2.2f**). It is of particular interest to mention that the sample quenched after 500 s at 510 °C exhibited very strong surface relief, which results in the distortion of the polished surface, which appears as grey in **Figure 2.2e**. The differences in the appearance of the bands among the samples can be attributed to the initial position of the dilatometer sample in the hot rolled bar, from which they were taken. The samples that were extracted from a point closer to the surface, where a higher reduction ratio is expected, exhibit distinct linear bands. On the other hand, samples in which the bands show dendritic characteristics, are likely to have been extracted from a position closer to the centre of the hot-rolled bar.

The banded structure observed indicates chemical segregation of substitutional

alloying elements in the examined steel. Electron Probe Micro Analysis was employed to measure the segregation of Mn, Cr, Si and V. The results are illustrated in **Figure 2.3**. Since both Mn and Cr lower the activity of C, Mn- and Cr-rich regions tend to attract C. Therefore, the carbon segregation occurs in the same regions and at the same time of the segregation of substitutional alloy elements. Nevertheless, thermodynamic calculations show that the difference in C cincentration between the regions with different Mn and Cr concentrations is very small. The obtained values of the C concentration in C-rich and C-poor regions are 0.54 wt% and 0.50 wt% respectively, with the average composition being 0.51 wt%, as reported in **Table 2.1**.

It is evident that all measured alloying elements segregate simultaneously in alternating bands with average width of 150 μm. From the data obtained by the linear scan presented, Mn, Cr and Si can reach concentrations that are up to 60% higher than the nominal or average composition measured by Optical Emission Spectroscopy. It is found that the difference in chemical composition is at similar levels in all the samples measured.

For characterization at a smaller scale, SEM was applied on the same samples. The micrographs are shown in **Figure 2.4**. After isothermal treatment for 250 s at 300 °C, the microstructure consists of bainitic ferrite in plate morphology and cementite particles precipitated within the bainitic ferrite with orientation 55° - 60° to the growth direction of the plate [13]. This microstructure typically represents lower bainite. Fresh martensite/retained austenite was also present around the lower bainite. After isothermal treatment for 125 s at 420 °C, the structure of bainite is different. The microstructure consists of sheaves of bainitic ferrite with boundaries indicating edgewise growth, with coarse cementite precipitates located at the bainitic ferrite/martensite boundaries. The precipitates do not have a specific orientation to the growth orientation of the bainitic ferrite sheaf. Cementite occasionally is found to form a central lamella, towards the growth direction of the bainitic ferrite sheaf, as also reported in [14] in a Cr-rich, high carbon steel. Fresh martensite and/or retained austenite islands are also identified, which indicates that the bainite reaction was incomplete within the time limit of the experiment, as can be also seen in **Figure 2.1b**.

After isothermal treatment for 3500 s at 510 °C, the microstructure is banded, with fresh martensite being the dominant phase. In this case, at the very early stages of the transformation, a small fraction of bainitic ferrite forms at the prior austenite grain boundaries in absence of any carbide precipitation. The morphology of this ferrite is different from the ones found at lower temperatures. The ferrite formed at this temperature is formed at the early stages of the isothermal holding

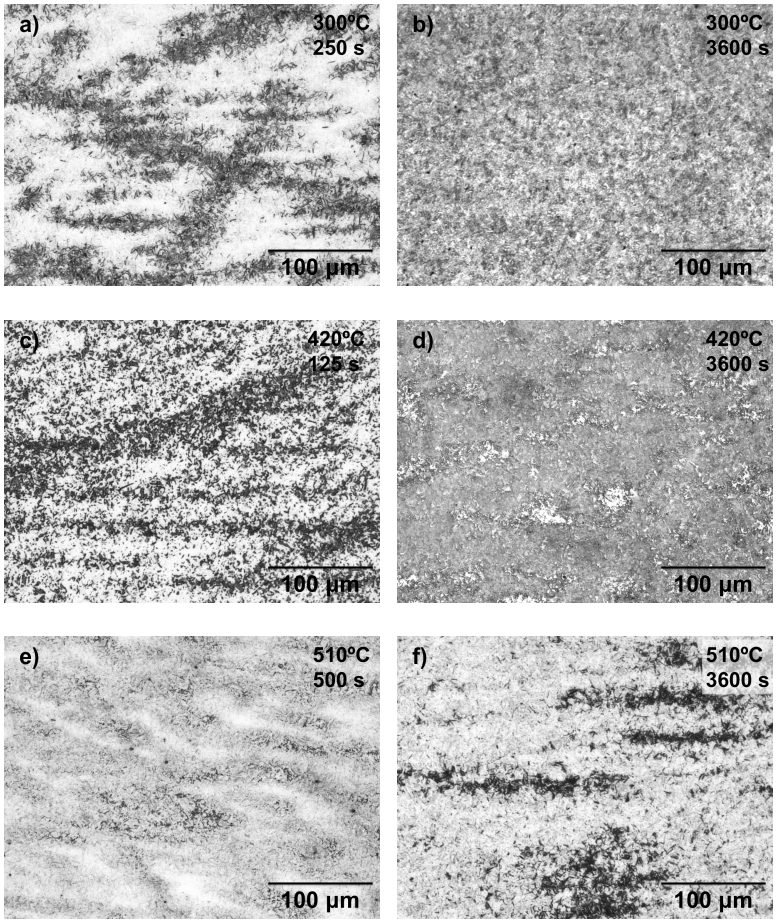

Figure 2.2: Low magnification micrographs showing the microstructure obtained after interrupted isothermal treatments, with the time and temperature indicated in the top right corner of each micrograph. In all cases, dark-etching phase is bainite and white-etching phase is fresh martensite and/or retained austenite. The samples were etched with Nital 2%.

(up to 500 s), but the fraction produces macroscopic change in length that is below the analytical resolution of the dilatometer, as observed in **Figure 2.1b**. After ferrite has formed, a dark-etching austenite decomposition product begins to form. In the SEM, **Figure 2.4**, it was possible to identify that this product has a needle like morphology with its constituents being ferrite and cementite, as will be further analysed in Chapter 3, using higher magnification techniques. The cementite is found in the middle of the needle with ferrite around it, along the needle's growth direction. The needles also form branches, often perpendicular to the growth direction of the main

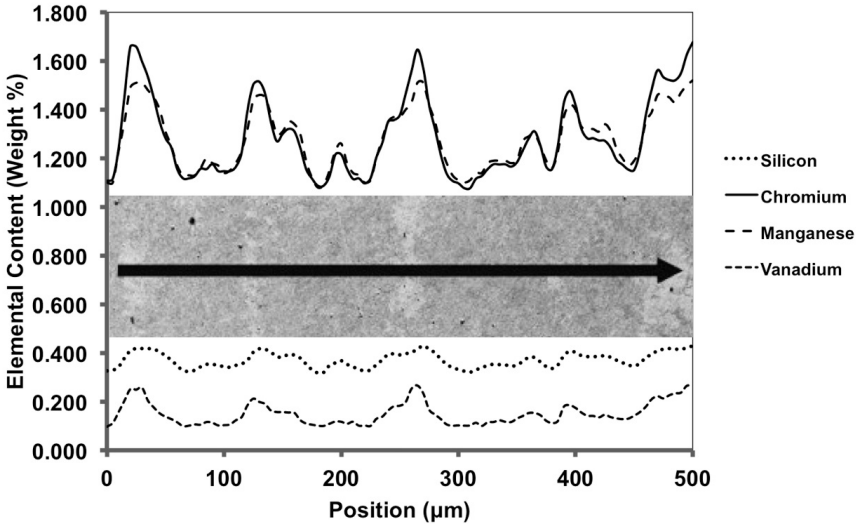

Figure 2.3: Electron Probe Micro analysis results of an as received sample. Mn, Cr, Si, and V are found to form segregated bands. The segregation of these elements follows the same trend and the high segregation areas can be matched with the martensite/austenite regions (white in SEM).

needle. The carbides are also found to have a curved shape, which is attributed to the possible local stacking fault variation, as described in [15].

Presence of retained austenite is difficult to be verified with the optical microscopy or even SEM analysis. In order to verify the presence of retained austenite in the final microstructure, samples of the isothermal treatments were analysed by means of X-Ray Diffraction. The results of the measurements show that in all cases (300 °C, 420 °C and 510 °C) a limited volume fraction of approximately 2% austenite is present. These results indicate that most remaining austenite transforms into martensite during the final quench after the isothermal treatment but there is a limited fraction of austenite that is stable enough to be retained at room temperature.

2.4. Discussion

The microstructural evidence of banded structures found at short isothermal holding times that become (more) homogeneous as the isothermal holding time increases, needs further discussion. The experimentally produced microstructures raise questions about the formation mechanism and the nature of bainite transformation. The chemical inhomogeneity will be used as a tool to interpret the evolution of the bainitic transformation in 51CrV4 steel.

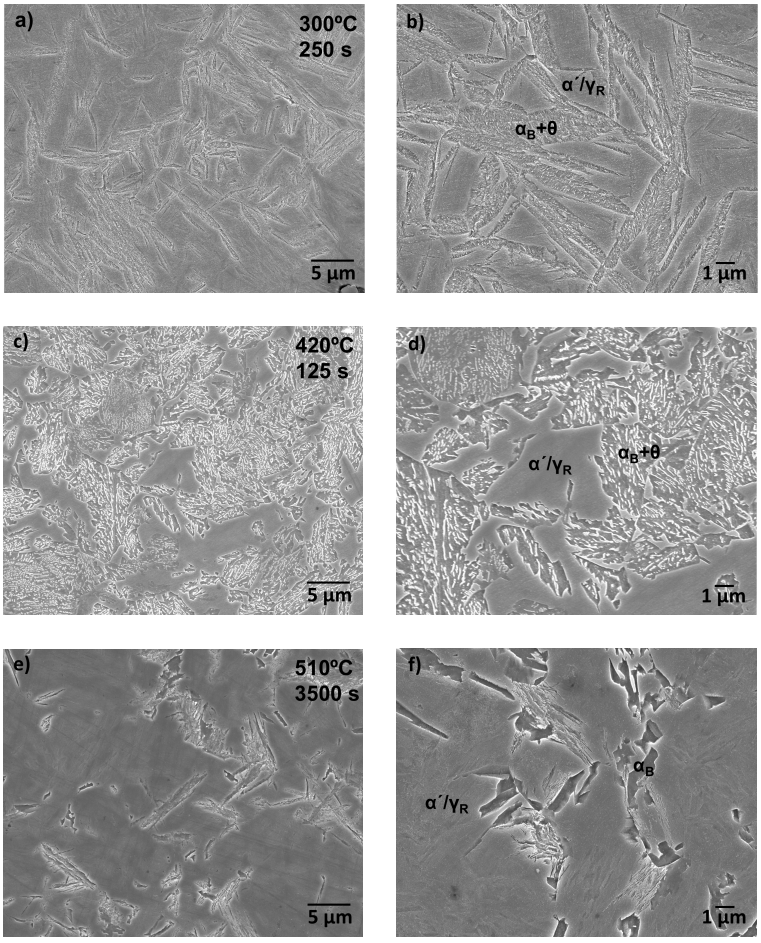

Figure 2.4: Scanning electron micrographs showing the different bainite morphology obtained after isothermal holding at different temperatures. The samples were etched with Nital 2 %.

2.4.1. Diffusionless assumption - Driving force for nucleation and nucleation rate

Assuming that bainite forms by a diffusionless mechanism, the formation kinetics is determined by the nucleation rate of bainitic ferrite. In the present case, the microstructure analysis for the interrupted samples after short isothermal holding times shows that bainitic ferrite is detected only in the Mn-Cr-poor regions. In the Mn-Cr-rich regions, no evidence of bainitic ferrite formation is found. At longer times, especially at lower temperatures (300 °C), the bainitic ferrite forms in the entire sample. This change in the microstructure can be attributed to a difference in the formation

kinetics of bainitic ferrite between the different regions. Following the diffusionless assumption, this difference in the formation kinetics can only be attributed to the difference in the local nucleation conditions of bainitic ferrite plates according to the local chemical composition. One would expect that the nucleation conditions be fulfilled only for the compositions at which bainitic ferrite is found to form experimentally. In order to validate this assumption, the theoretical nucleation conditions for the extreme values of the local composition were calculated.

According to the diffusionless approach, bainite is expected to form when two conditions are fulfilled simultaneously. First, the maximum driving force for nucleation ΔG_m must be higher than the value given by the general nucleation function, G_N. Additionally, the driving force for transformation of austenite into ferrite must exceed the energy barrier for bainite, so diffusionless growth can be sustained. The above conditions are summarized as:

$$\Delta G_m < G_N \tag{2.1}$$

$$\Delta G^{\gamma \rightarrow \alpha} < G_{SB} \tag{2.2}$$

where both ΔG_m and $\Delta G^{\gamma \rightarrow \gamma}$ are negative; G_{SB} is the stored energy of bainite, equal to 400 J/mol, and G_N is a universal nucleation function, as described in detail in [12]. The first of these conditions ensures that nucleation takes place and the second that the chemical free energy change exceeds the stored energy of bainite. The driving force for nucleation of bainitic ferrite was calculated for different temperatures for both the high and low Mn, Cr concentrations, as derived from the segregation curve in **Figure 2.3** using Thermo-Calc software. The calculations performed are illustrated in **Figure 2.5**.

In the temperature range of bainite formation in 51CrV4, it is evident that the both chemical compositions fulfil both nucleation conditions at low temperatures, while at high temperature, the T_0' limitation (indicated in **Figure 2.5**) for highly segregated chemical composition could explain the incomplete reaction observed. This means that the local chemical composition would allow the formation of bainitic ferrite nuclei at 300 °C both in the Mn-Cr-rich regions and in the Mn-Cr-poor regions. Thus, we would expect to have a generally homogeneous microstructure at low temperatures. Additionally, the formed nuclei are expected to be evenly distributed in the microstructure. Neither of these expectations could be verified at the scale detectable by the techniques used.

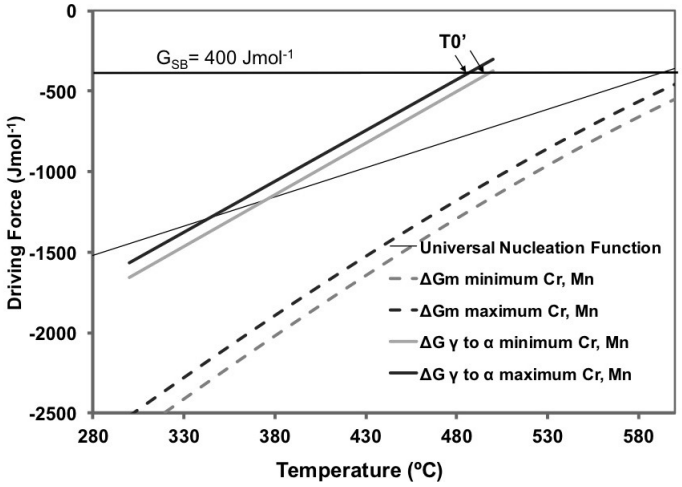

Figure 2.5: Composition dependent driving force versus temperature for diffusionless nucleation and diffusionless growth conditions. G_N is a universal nucleation function.

2.4.2. Thermodynamic calculations - Similarities with high C steels

Figure 2.6 shows the calculated Fe-C phase diagram of 51CrV4 alloy with constant concentrations of Cr, Mn, Si. For the calculations of **Figure 2.6a**, the minimum values of concentrations of **Figure 2.3** were used, while **Figure 2.6b** was constructed based on the maximum values. The calculations were performed with Thermo-Calc software. The 51CrV4 alloy can actually behave like a hyper-eutectoid steel in regions containing high concentrations of Cr and Mn, even though the overall composition is hypo-eutectoid (or near eutectoid), **Figure 2.6**. The fact that 51CrV4 can behave like a hyper-eutectoid steel explains morphological similarities between this medium carbon steel and findings reported for bainite in higher carbon steels.

The isopleths of **Figure 2.6** also show that the austenite decomposition under equilibrium in the high and the low concentration regions will be different. In the case of the low Mn and Cr concentrations, the austenite will decompose into ferrite and cementite first and at lower temperatures, below 580 °C, also precipitation of M_7C_3 is expected. In the case of high Cr and Mn concentrations, the austenite is expected to decompose first into M_7C_3 (pro-eutectoid), with ferrite and cementite forming at lower temperatures.

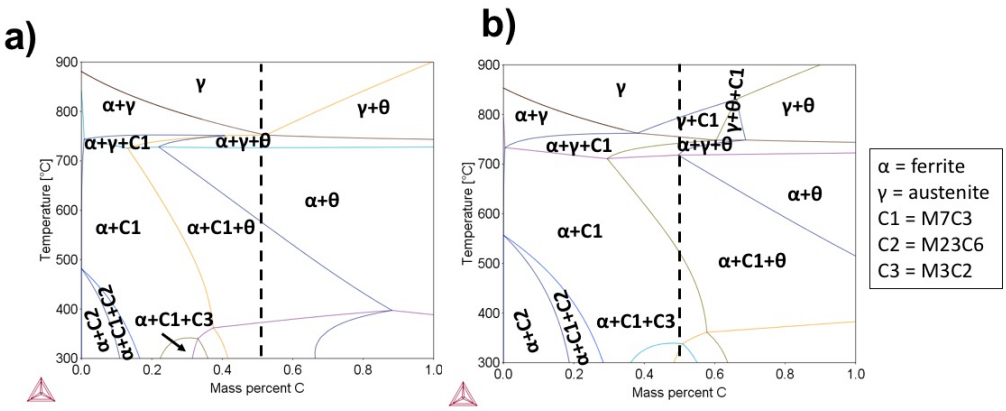

Figure 2.6: Ortho-Equilibrium phase diagram calculations for the chemical compositions of the a) low (1.08 wt.% Mn, 1.08 wt.% Cr) and b) high (1,52 wt.% Mn, 1.68 wt.% Cr) concentration bands as measured by EPMA. Cementite becomes unstable at lower temperatures and Cr-rich carbide precipitation is favoured. Dashed lines indicate the carbon concentration of 51CrV4. Calculations were performed by ThermoCalc software using TCFE5 database.

2.4.3. Effect of carbide precipitation

Generally, carbide precipitation during bainite formation leads to enhancement of the overall kinetics of the transformation. This is especially evident when comparing high Si steels, in which carbide precipitation is inhibited, with lean Si steels, where carbide precipitation takes place. In the present case, 51CrV4 contains a low Si concentration, but it contains Cr and V, both known to be carbide-forming elements. The carbide-forming elements could affect the carbide precipitation process during bainite formation. The behaviour of Cr during carbide precipitation in the bainite transformation constitutes a topic that is still not completely understood [16].

In order to verify if Cr is diffusing during carbide precipitation, chemical composition analysis of the carbides was performed using Scanning Transmission Electron Microscopy - Energy Dispersive Spectroscopy (STEM-EDS). The Mn concentration is very close to the alloy composition of **Table 2.1** in all measurements. In **Table 2.3** the average Mn, Cr concentrations of the carbides measured are shown for the two cases and **Figure 2.7** shows representative spot EDS analysis points, as observed through the STEM. The enrichment of the carbides in Cr is a process that requires long-range diffusion of Cr. This is expected to have a retarding impact on the overall kinetics of the bainite transformation.

The Cr contents of the carbides measured by EDS need to be further interpreted. It is shown in **Figure 2.6** that in the temperature range of bainite formation, alloy carbides should form and especially in the case of high concentrations of Mn and Cr,

Table 2.3: Average chemical composition of carbides, in wt. %, measured with STEM-EDS in bainite.

Temperature (^oC)	Cr (Wt.%)	Mn (Wt.%)
300	2.9 $\pm$ 0.1	1.0 $\pm$ 0.1
420	1.8 $\pm$ 0.1	1.0 $\pm$ 0.1

cementite is not stable at 300 °C. This is only true under the assumption of possible partitioning of substitutional alloying elements during the transformation. In practice, at low temperature, the transformation of austenite to bainitic ferrite and carbides may proceed without partitioning of substitutional elements (para-equilibrium, PE). In this case, it is assumed that Cr does not partition, and that only PE cementite is formed.

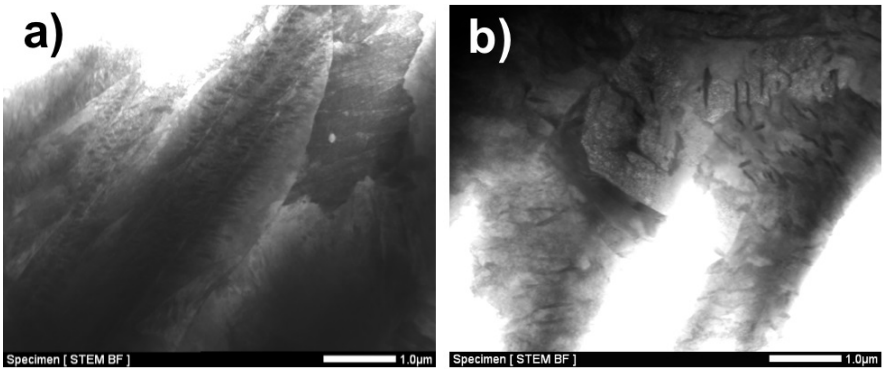

Figure 2.7: STEM Micrographs showing representative spot EDS analysis positions in: (a) lower bainite (300 ^oC) and (b) upper bainite (420 ^oC).

Carbide precipitation is expected to occur in austenite at the interface with bainitic ferrite, where the carbon concentration is high due to the carbon enrichment in austenite. For high carbon concentration (higher than 0.8 wt%), even under full equilibrium, cementite is the only carbide that is stable (**Figure 2.6**). **Figure 2.8** shows the chromium concentration in a nucleus of cementite formed in ortho-equilibrium at 300 °C and 420 °C as a function of carbon concentration in the austenite matrix. The calculations were done using the Thermo-Calc software under the assumption of Cr partitioning between austenite and cementite. It is evident that the chromium concentration in cementite decreases as the carbon concentration in matrix increases, as also reported in the literature [12]. The Cr concentration values measured by EDS for the temperatures 300 °C and 420 °C imply a difference in the maximum C concentration reached during bainite formation at the bainitic ferrite-remaining austenite interface. Further research was performed on the characterisation of the carbides in bainite at different temperatures in the framework of Chapter 3.

Apart from the substitutional elements, during carbide formation diffusion of C is required, which is relatively rapid, as C is an interstitial atom and its diffusivity is several orders of magnitude higher than the one of the substitutionals, like Cr. During bainite formation, when a plate of bainitic ferrite forms, there is driving force for C diffusion into the remaining austenite or into the carbides. An important difference between the two possibilities is that when C diffuses into the remaining austenite, the overall driving force for bainite formation reduces, but when it diffuses into the carbides, the driving force increases. Since in the present case carbide precipitation can be retarded because of the Cr partitioning, C diffuses partly into the austenite and stabilizes it. The carbon enrichment of the austenite can be detected indirectly in the dilatometric signal in the change in length - temperature plot, **Figure 2.1a**. During the final quench, fresh martensite formation starts at different martensite start temperatures. These temperatures decrease as the isothermal holding temperature decreases. Considering that the substitutional alloying elements do not have enough time for long-range diffusion during martensite transformation, carbon is the only element that can affect the martensite start temperature. The enrichment of the untransformed austenite in C and its stabilization provide additional reasons for the local retardation of the bainite transformation.

2.4.4. Inverse bainite

If the local composition is hyper-eutectoid in the quasi-binary Fe-C diagram, cementite can become the leading phase in the bainite formation at high isothermal holding temperatures, close to 500 °C. This results in the formation of the austenite decomposition product that has been reported first by Kinsman and Aaronson [14] and more recently by Kolmskog [10] as inverse bainite, identified in high carbon, Mn, Cr and Mo alloyed steel grades. The dark etching microstructural constituent found in the present study to form at 510 °C after isothermal holding shows similarities with inverse bainite as observed by Kinsman and Aaronson [17], and also recently by Borgenstam et al. [18]. Goldenstein and Cifuentes [15] in their study of austenite decomposition products in a Cr containing steel, mainly above the bay of the TTT diagram, have shown that just below the bay temperatures, the decomposition products have a so-called "arborescent" morphology with needles forming branches, which is also identified in the present case. Additionally, the equivalence of the alloy composition to a hyper-eutectoid steel in the high segregation areas, leads to the suggestion that the microstructure at 510 °C consists of allotriomorphic and Widmanstätten ferrite (formed at early stages) and inverse bainite (formed at later stages) in an austenitic matrix.

2.4.5. Effect of vanadium

The 51CrV4 steel was originally designed to be used in the Quenched and Tempered (Q+T) condition. The intention of the Cr addition is to increase the hardenability, whereas V is added to induce a secondary hardening effect during the tempering step. From the thermodynamic calculations for VC precipitation, it results that VC is stable at temperatures below 910 °C, which is higher than the austenitisation temperature. This means that VC is stable throughout the heat treatment and could play a role in stimulating nucleation of bainitic ferrite at the isothermal stage. Apart from that, since V is not significantly altering thermodynamics of the fcc-bcc interaction, it does not play any other role in the microstructure evolution. By applying an isothermal treatment though, the secondary hardening effect that V induces during tempering is not exploited as it is during Q+T.

2.4.6. The role of chromium - indications for diffusional mechanism

Based on the observations resulting from the experiments performed in this study, it is suggested that the overall bainite formation kinetics is not only influenced by the nucleation, but is also significantly influenced by the growth of the nucleated bainitic ferrite. The influence of growth on the mechanism of bainite formation leads to the suggestion that the transformation can be diffusional in nature. To further support this suggestion, the behaviour of the substitutional elements, and the possible presence of inverse bainite can all be consistently explained by the diffusional theory. Mn and Cr are both well known to retard the bainite formation, especially at isothermal holding temperatures close to the bainite start temperature, by solute drag. They are also responsible for incomplete transformation. These cases are well reported in the literature [19]. Recently, Chen et al. have performed detailed analysis of the solute drag effect caused by the Mn segregation at the α/γ interface in Fe-C-Mn alloys containing low concentrations of C and 3.0 wt% Mn [20]. In their experiments, they have shown that Mn retards the bainite formation significantly. In the present case, the difference in Mn concentration between the high and low segregation regions is not large enough to produce such an effect, and therefore the additional role of Cr is considered critical for producing the observed microstructures. We consider the role of Cr to be particularly important in this case because it is found to affect the resulting microstructure differently at high and low isothermal holding temperatures. At high temperatures, near 500 °C, growth of bainitic ferrite is almost inhibited. It has been suggested that Cr produces a solute drag effect on the moving interface of bainitic ferrite, which dramatically retards the growth of the plates [8]. At

lower temperatures within the bainite formation range, Cr retards the kinetics of the bainite reaction by partitioning into the carbides. In an inhomogeneous material, as the one studied in the present research, the above described phenomenon will result in a banded microstructure in the early stages of the transformation, but if enough time in the isothermal holding step is allowed, the microstructure will eventually become homogeneous. From the experimental observations, this is true for isothermal holding temperatures close and above the martensite start temperature, but when the isothermal holding temperature are higher, still incomplete reaction is evident, which is then attributed to the solute drag effect.

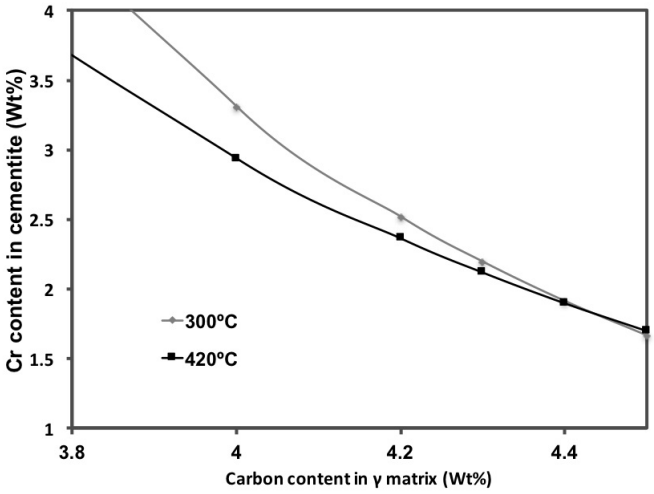

Figure 2.8: Equilibrium concentration of Cr in cementite with respect to the carbon concentration in austenite.

2.5. Conclusions

An isothermal treatment in which bainite is formed was applied to 51CrV4 steel grade as an alternative to quenching and tempering. The bainite formation mechanism was studied and discussed. By performing dilatometer tests and microscopy analysis it was found that:

1. Homogeneous lower bainitic microstructures at holding temperatures close to and above the martensite start temperature can be produced, even though it contains chemical segregation when produced industrially.

2. At higher temperatures, significant retardation or the transformation is observed, leading also to incomplete reaction. Incomplete reaction is observed

mainly at the bands of the material where the concentration of substitutional alloying elements is high due to segregation.

3. It is suggested that Cr retards the bainite formation in two ways, depending on the isothermal holding temperature. At high temperatures, close to the bainite start temperature, Cr retards the growth of the nucleated bainitic ferrite by retarding the interface mobility (solute drag effect). A certain fraction of the rejected C from the newly formed bainitic ferrite can diffuse into the residual austenite, before the rest is consumed in the carbide precipitation. The momentary stabilization of the austenite leads to an overall retardation of the bainitic transformation at isothermal holding temperatures close to and above martensite start temperature.

4. Bainite formation kinetics cannot be solely explained by the bainitic ferrite nucleation kinetics, it is evident that it is closely linked to the bainitic ferrite growth kinetics. Considering also the effect of growth on the kinetics, banded structures appearing at the early stages of the transformation that become homogeneous in the end of the treatment can be consistently explained.

5. Inverse bainite is found to form at 510 °C, attributed to the high local Cr segregation.

6. All the above-described observations lead to the suggestion that the bainite formation could be more accurately described by the diffusional approach in alloys containing significant amounts of Cr.

7. The vanadium addition in this grade does not influence the bainitic transformation. Vanadium carbides form at temperatures within the austenite stability region, and are therefore stable at the temperatures at which upper and lower bainite forms isothermally, and no further precipitation is expected or experimentally verified.

References

1. Yoshiyuki Tomita and Kunio Okabayashi, Metall. Trans. A15 (1984), pp. 2247-2249.

2. Taek-Young Kim and Ho-Kyung Kim, Mater. Sci. Eng: A 58 (2013), pp. 322-329.

3. A. Hultgren, Transanctions of the American Society of Metals 39 (1947), pp. 815.

4. M. Hillert, Royal Institute of Technology, Stockholm, 1960.

5. M. Hillert, Metall. Mater. Trans. A25 (1994), pp. 1957-1966.

6. W. T. Reynolds, S. K. Liu, F. Z. Li, S. Hartfield and H. I. Aaronson, Metallurgical Transactions A21 (1990), pp. 1479-1491.

7. W. T. Reynolds, F. Z. Li, C. K. Shui and H. I. Aaronson, Metall. Trans. A21 (1990), vol. 21, pp. 1433-1463.

8. H. I. Aaronson, W. T. Reynolds, Jr. and G. R. Purdy, Metall. Mater Trans A 35 (2004), pp. 1187-1210.

9. C. Zener, Trans. ASM 167 (1946).

10. T. Ko and S.A. Cottrell, J. Iron Steel Inst. 172 (1952), p. 307.

11. H. K. D. H. Bhadeshia and D. V. Edmonds, Acta Metall. 28 (1980) pp. 1265-1273.

12. H. K. D. H. Bhadeshia, Bainite in Steels, IOM Communications Ltd. London, 2001

13. M.Y. Tu, C.A. Hsu, W.H. Wang and Y.F. Hsu, Mater. Chem. Phys. 107 (2008), pp. 418-425.

14. Peter Kolmskog, PhD Thesis KTH, Stockholm, 2013.

15. H. Goldenstein and J. A. Cifuentes, Metall. Mater. Trans. A37 (2006) pp. 1747-1755.

16. H. K. D. H. Bhadeshia, Materials Science and Engineering: A 1999.

17. K. R. Kinsman and H. I. Aaronson, Metall. and Mater. Trans 1 (1970), pp. 1485-1488.

18. Annika Borgenstam, Peter Hedström, Mats Hillert, Peter Kolmskog, Albin Stormvinter and John Agren, Metall. and Mater. Trans. A42 (2011), pp. 1558-1574

19. H. I. Aaronson, W. T. Reynolds, G. J. Shiflet and G. Spanos, Metall. Trans. A21 (1990), pp. 1343-1380.

20. H. Chen and S. Van Der Zwaag, Act. Mater. 2014, vol. 72, pp. 1-12.

3

Characterisation of isothermally formed bainite microstructures in 51CrV4 spring steel*

In Chapter 2 it was shown that the morphology and the kinetics of the isothermal bainite formation depends strongly on the isothermal holding temperature and the local chemical composition. It was especially shown that there is a very distinct difference in the kinetics of the transformation products between 300 °C, 420 °C and 510 °C. The present chapter aims to provide some smaller-scale information on the transformation products studied in Chapter 2. To achieve this, atomic-scale investigation was performed on 51CrV4 steel, isothermally held at different temperatures within the bainitic temperature range. Transmission electron microscopy (TEM) analysis revealed three different morphologies: upper, lower and inverse bainite. Lower bainite contained elongated cementite precipitates, aligned at an angle towards the length of the bainitic ferrite plate. Atom Probe Tomography (APT) analysis of cementite particles showed no evidence of partitioning of substitutional elements; only

* This chapter is based on the article: C. Goulas, A. Kumar, M.G. Mecozzi, F.M. Castro-Cerda, M. Herbig, D. Raabe, R. Petrov and J. Sietsma, Atomic scale investigation of isothermally formed bainite microstructures in 51CrV4 Spring steel, to be submitted for publication.

carbon partitioned in cementite to the equilibrium value. Carbon in the bainitic ferrite was found to segregate at dislocations and to form Cottrell atmospheres. The concentration of carbon remaining in solution measured by APT was more than expected at the equilibrium. Upper bainite contained cementite as well. Chromium and manganese were found to redistribute at the cementite-austenite interface and the concentration of carbon in the ferritic matrix was found to be lower than the one measured in the case of lower bainite. After isothermal treatments close to the bainite start temperature, another austenite decomposition product was found at locations with high degree segregation, resembling inverse bainite, an acicular cementite plus ferrite phase mixture reported in hypereutectoid steels; this transformation product is always located at the interface of ferrite, which formed around prior austenite grain boundaries. Site-specific APT analysis of the inverse bainite reveals significant partitioning of manganese and chromium at the carbides and at the ferrite/martensite interfaces, unlike what is found at isothermal transformation products at lower temperatures.

3.1. Introduction

The formation of bainite has been attracting scientific interest for almost a century. What makes it attractive is the fact that it combines characteristics of fundamentally different phases, which are martensite and Widmanstätten ferrite; this circumstance is the reason why the mechanism of formation of this phase, a mixture of ferrite and cementite, is still object of controversy. The morphology of ferrite and the carbides distribution depend on the transformation temperature and therefore bainite is usually classified as either upper bainite or lower bainite. When formed at low temperatures, lower bainite shares common characteristics with martensite and it is sometimes even impossible to distinguish them microscopically. This experimental finding suggests that the mechanism of formation of bainite is similar to that of martensite and therefore is diffusionless in nature. On the other hand, an increasing number of experimental and theoretical studies support the similarity between bainitic ferrite and proeutectoid ferrite with Widmanstätten morphology and the idea that bainite growth is determined by carbon diffusion.

Hultgren first proposed in 1947 that upper bainite could form by initial precipitation of ferrite with Widmanstätten morphology followed by cementite precipitation on its sides [1]. The concept was further analysed by Hillert, who has shown that there is no reason to treat Widmanstätten ferrite and bainitic ferrite as different products, as there is no kinetic discontinuity [2]. According to this approach, the bainitic ferrite nucleates at austenite grain boundaries and grows at a rate determined by the

diffusivity of carbon. Aaronson et al., supporting the above-described theory, have considered the effect of alloying elements on the bainitic transformation, and the potential segregation of substitutional elements at the growing phase interface [3].

The diffusionless approach was introduced by Zener in 1946 [4], further developed by Ko and Cottrell [5], and more recently supported by Bhadeshia [6]. According to this approach, a sub-unit of bainitic ferrite, supersaturated in carbon, nucleates on an austenite grain boundary. The growth is instantaneous and displacive and stops because of the plastic deformation of the adjacent austenite. The bainitic ferrite is initially supersaturated with carbon, which needs to be rejected by diffusion into the residual austenite, in which it can form carbides with para-equilibrium composition. Carbon can also directly precipitate in the form of carbides within the bainitic ferrite sub-unit, if insufficient diffusion can take place due to the transformation temperature being low. Once bainitic sub-units have formed, the bainite formation can continue by the autocatalytic nucleation and displacive growth of new sub-units on the tip of previously formed sub-units.

Recent studies have revealed that, although carbon is depleted from bainitic ferrite, bainitic ferrite even after long times retains more carbon than is theoretically predicted by thermodynamic equilibrium. Recent Atom Probe Tomography and Synchrotron X-Ray Diffraction studies observe this phenomenon and some authors claim that the carbon that is trapped in the bainitic ferrite causes tetragonality of its cubic lattice [7-8]. However, the fact that the carbon does not diffuse out of the bainitic ferrite given the time and the driving force still cannot be explained satisfactorily.

The composition appears to be playing a very important role in the morphology of bainite. Especially in high carbon and chromium containing steels, when austenite decomposes at temperatures between 500 and 700 °C, non-classical austenite decomposition products were reported. One of them, formed close to the bainite start temperature (500 °C), is called inverse bainite on the basis of its inverse morphological characteristics with respect to the conventional bainite [9]. Inverse bainite is in fact identified as a phase mixture of carbide plates surrounded by Widmanstätten ferrite. The presence of inverse bainite was used by Borgenstam et al. to support the concept that austenite decomposition occurs by "mirror mechanisms" for compositions lower and higher than the eutectoid composition [10], and thus claim the generality of the diffusional mechanism in bainite formation. By mirror mechanisms it is implied that bainite and inverse bainite are products of austenite decomposition, which are obtained by similar processes, but with their constituents, ferrite and cementite, having opposite roles. In a bainitic microstructure, a leading phase grows from the prior austenite grain boundary with a Widmanstätten morphol-

ogy, followed by the formation of a secondary phase. Following this mechanism, at hypo-eutectoid compositions, the leading phase is ferrite, while at hyper-eutectoid compositions the leading phase is cementite.

Besides carbon, substitutional alloying elements such as Mn, Cr, and Mo are known to affect the formation of bainite in different ways. The presence of these elements in steel retards the growth of bainite by inducing a solute drag effect and can also limit the maximum fraction of bainite that can be obtained from an isothermal treatment at a given temperature (incomplete reaction phenomenon) [11-13].

Cr addition reduces the eutectoid carbon composition of steels, so even alloys with C content as low as 0.4 wt% can produce microstructures similar to the ones found in hypereutectoid Fe-C steels. This is especially applicable to the observation of inverse bainite, which is primarily found in hyper-eutectoid steels. Recent studies reported similar microstructures in Cr containing steels with lower carbon contents [14].

Transmission Electron Microscopy (TEM) studies of inverse bainite microstructures show evidence of a crystallographic orientation relationship between the acicular carbides, the surrounding ferrite and the parent austenite. This was achieved by relating the orientation of retained austenite in partially transformed specimens with the orientation of the carbides and the ferrite sheaves.

Information about the composition of the different constituents of the inverse bainitic microstructure is very limited in literature, most of the studies report the carbides as being of the M_7C_3 type with significant partitioning of Cr from the matrix to the carbide. Detailed study on the composition of the non-classical decomposition products of austenite can help to elucidate the transformation mechanism leading to their formation, as well as the relation between these products and conventional bainite. Due to the fine scale of the microstructure, a high resolution chemical composition analysis technique is required. Atom Probe Tomography (APT) is a very suitable technique for such an analysis, especially if combined with site-specific tip preparation and TEM.

In this chapter, the microstructures obtained by isothermal treatment of 51CrV4 steel within the temperature range of bainite formation are studied by means of transmission electron microscopy and atom probe tomography. TEM provides information about the bainitic microstructure morphology at different temperatures, APT enables a detailed compositional analysis of these microstructures. The compositional information can help elucidate the reasons for the wide morphological variety of bainite in medium carbon low alloy steel grades.

3.2. Experimental procedure

Samples of 51CrV4 steel were received in as rolled condition. The samples were cut out of hot rolled bars with dimensions 95 x 49 x 5500 mm^3. The chemical analysis was performed on 30 x 30 mm2 cross-sections of the bars, perpendicular to the rolling direction, by means of Optical Emission Spectroscopy (OES). The chemical composition of 51CrV4 steel is shown in **Table 3.1**.

Table 3.1: Chemical composition of the 51CrV4 grade as measured by Optical Emission Spectroscopy.

Elements	C	Mn	Si	Cr	V
Wt. %	0.51	1.02	0.33	1.15	0.12
At. %	2.32	1.01	0.64	1.21	0.13

Besides the average chemical composition, local fluctuations in the chemical composition, expected to affect the phase transformations, were measured in the normal direction by Electron Probe Micro Analysis. The details of the measurement, as well as the interpretation of the effect of the segregation on the microstructure formation, was reported in Chapter 2 and previously published by the authors [14]. The concentration profile of Cr and Mn is shown in **Figure 3.1**.

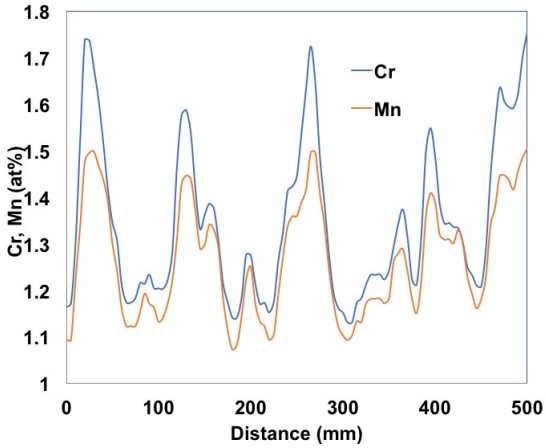

Figure 3.1: Concentration profile of Mn and Cr as measured with EPMA.

The dilatometric specimens with dimensions Φ4 x 10 mm^2 were machined using Wire Electro-Discharge Machining (EDM). The dilatometric tests were performed in a B?hr 805A Quench dilatometer, with the heat treatment schemes shown in **Figure 3.2**. The specimens were placed in the dilatometer with two thermocouples, spot welded, one at the centre and the other 1 mm from the edge in order to control the temperature and observe its gradient during the treatment. All samples were

heated within 60 s to the austenitisation temperature (900 °C) under vacuum and then quenched to an isothermal holding temperature in the range 300-510 °C using helium gas. After the isothermal holding, the samples were quenched to room temperature. The quenching rate was high enough to avoid austenite-to-ferrite transformation according to TTT diagrams for the specific chemical composition. This rate was chosen to be 30 °C/s.

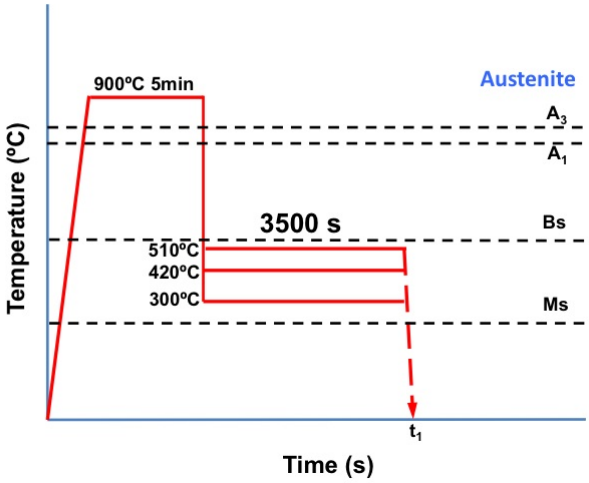

Figure 3.2: Heat treatment schemes used in the dilatometer.

For microstructural characterization, dilatometric samples were mounted on a specially designed sample holder, then ground, polished and etched with Nital 2%. Scanning Electron Microscopy (SEM) analysis was carried out in a Field Emission Gun Scanning Electron Microscope (FEG-SEM) JEOL 6500F operated at 15 kV. For TEM analysis, specimens were prepared from the dilatometry samples corresponding to the full treatments. Although the temperature gradient within the dilatometric specimen during the heat treatment was found to be within 10 °C, in order to ensure that the microstructure observations were consistent with the dilatometry measurements, the sample discs were cut from the central zone of the dilatometric specimen, close to the thermocouple. The TEM discs were manually ground down to 60 μm, and then Ar-ion polished to final electron transparent thickness using a GATAN 691 PIPS system. For the observation, a JEOL JEM-2100 electron microscope operated at 200 kV was used.

APT samples were prepared also from the dilatometry specimens using focused Ion Beam (FIB) milling. Conventional lift-out procedures and Felfer's method were used to produce the atom probe specimens, as described in Ref. [15-16]. Felfer's

method is employed for APT sample preparation to study the acicular cementite in inverse bainite. Its size on the order of tens of nanometres and its non-uniform distribution in the microstructure made it particularly challenging to capture inverse bainite within an APT specimen, if a conventional lift out procedure is employed. Thus, the method applied in the present study incorporated as a first step coarse FIB cutting at 52° and 0° sample tilt. The FIB-cut lamella was then placed at an axial manipulator and rotated 90° manually after opening the FIB chamber as shown in **Figure 3.3**. After rotation, the lamella was lifted out from the axial manipulator and then welded using platinum on electro-polished molybdenum posts [17].

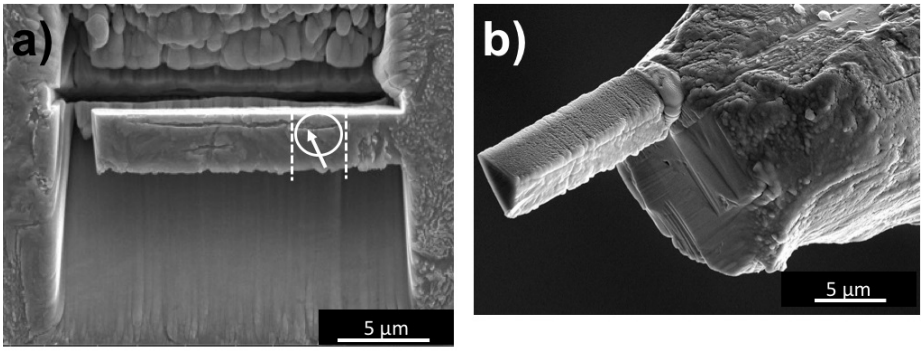

Figure 3.3: Site specific FIB milling of the APT tips. a) SEM micrograph from the location of the site-specific Atom Probe Tomography tip preparation by FIB and b) rotation of the lamella by 90^o with an axial manipulator to have the region of interest close to the atom probe tip (circle with arrow showing the annular milling direction, dashed lines show the cut area of the specific tip).

APT measurements were performed using a local electrode atom probe (LEAP 3000X HR, Cameca Instruments) in voltage mode at a specimen temperature of ~-213^oC (60 K). The pulse fraction and the pulse frequency were 15% and 200 kHz, respectively, for all measurements. APT data analysis was performed using the IVAS software (Cameca Instruments) with proper calibration of the Image Compression Factor (ICF) and K_f constant as per the procedure explained in [18]. A peak decomposition algorithm incorporated in the IVAS software was used to decompose the ($12C_3 13C^{2+}$) peak at a mass-to-charge ratio of 24.5 Da.

3.3. Results

3.3.1. Isothermal treatment at 300 °C

The isothermal treatment at 300 °C, despite the macro-chemical segregation detected by EPMA, produced a homogeneous bainitic microstructure after 1 h of treatment. **Figure 3.4a** shows the bainitic microstructure produced after 1 h holding at

300 °C. Extensive carbide precipitation is evident. The carbides are fine and elongated, aligned at an angle towards the length of the bainitic ferrite plate.

For observation at a larger magnification, TEM was employed. The observation in the TEM confirms the presence of elongated carbides parallel to each other within the ferrite plates; carbides are not found at the plate boundaries, **Figure 3.4b**. Significant presence of dislocations is verified in the specimen and their distribution appears to be homogeneous.

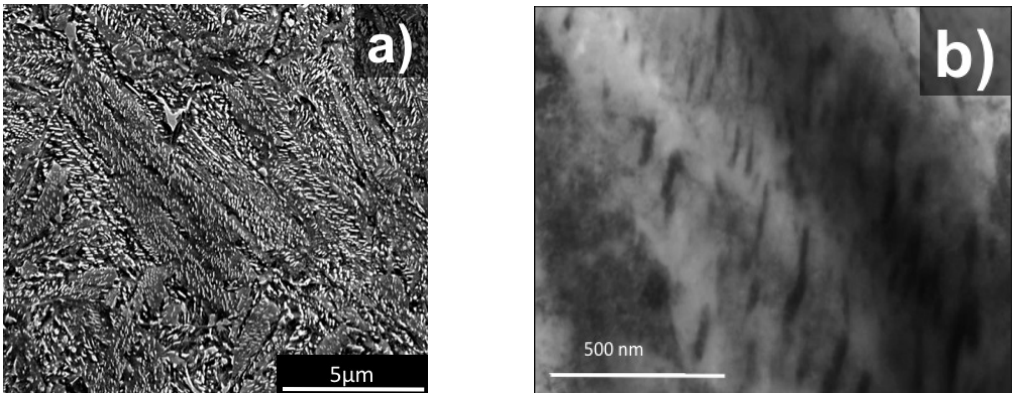

Figure 3.4: a) SEM Micrograph showing bainitic microstructure obtained after isothermal holding at 300 ^{o}C for 1 h. b) Bright Field Transmission Electron microscopy micrograph showing typical morphological characteristics of lower bainite.

In order to obtain compositional information about the carbides and bainitic ferrite, APT tips were obtained from an area containing both bainitic ferrite and carbides by site specific preparation.

In **Figure 3.5**, the reconstructed APT ion maps of C, Cr, Mn and Si are shown. It is evident from the C map that in the analysed volume two large carbon clusters are present. The two large clusters are around 60 nm apart and parallel to each other, resembling the carbides observed in TEM in lower bainite, **Figure 3.4b**. In between those clusters there are numerous smaller C accumulations with not clearly defined shapes. The maps of the substitutional elements in the analysed areas do not show any signs of partitioning between ferrite and cementite, with the exception of Si, **Figure 3.5b**. In fact, Si appears to be the only alloy element that is depleted from the area of the carbides, while slightly accumulating close to the bainitic ferrite/carbide interfaces.

Quantitative chemical information can be obtained by the proximity histograms. **Figure 3.5b** shows the proximity histogram of the lower large C cluster with the zero position at an isosurface of 25 at% C. The proximity histogram shows a car-

bon content of around 25 at.% in the centre of the carbide. Indeed, there is no partitioning of Cr or Mn. The last point of the Cr measurement appears to be high, but the error of this point is high as well, so it can be concluded that there is no significant Cr fluctuation within the carbide. The reduced concentration of Si in the carbides and its increased concentration around the α/θ interface is verified by several measurement points with very limited error margin. The above analysis shows that the carbides formed at 300 °C can be identified as cementite formed under non-partitioning conditions for the substitutional elements (cementite in para-equilibrium conditions), with the Si most probably partitioning during isothermal holding, after carbide formation.

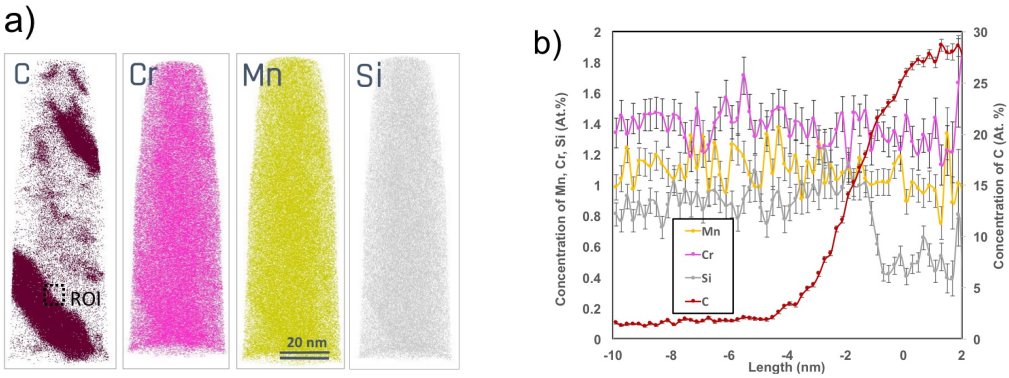

Figure 3.5: a) APT Ion maps of C, Cr and Mn from a sample that was isothermally transformed into bainite at 300 ^{o}C. The C map reveals two cementite particles and C clustering in bainitic ferrite. b) Proximity histogram of the lower carbide, taken in the Region Of Interest (ROI) indicated in the C map of a), showing no partitioning of Cr and Mn. The Si concentration is reduced in the cementite.

In order to analyse the smaller carbon clusters observed in the areas between two adjacent carbides, C isosurface maps were constructed at carbon concentrations between 4 and 11 at.%, **Figure 3.6**. This analysis shows that carbon accumulates in three dimensional features, while the other elements do not redistribute. The carbon concentration at these features reaches 11 at.%. The same analysis was performed for the bulk of the bainitic ferrite, this time excluding areas with a carbon content higher than 1 at.%. In this way, the carbon content in solution in the matrix was estimated. The result shows that the carbon concentration in the matrix is on average 0.65 at.%, higher than the equilibrium value 0.27 at.%, determined from the α/γ line in the phase diagram, calculated with Thermocalc and extrapolated to 300 °C.

3.3.2. Isothermal treatment at 420 °C

In contrast with the isothermal treatment at 300 °C, the treatment at 420 °C does not produce a homogeneous microstructure. The SEM micrographs show that there are areas in the microstructure that transformed into bainite, with distinct features evident after the etching, but other areas remain featureless. The featureless areas can be identified as martensite/austenite islands (M/A) and form during the final quenching from the isothermal treatment temperature to room temperature, Figure 3.7a. The M/A areas contain high concentrations of Cr, Mn and Si. The morphology of bainite after isothermal treatment at 420 °C is different from the one found at 300 °C. The shape of the bainitic ferrite plates is not acicular; the carbides are coarser and are found at the platelet boundaries.

TEM observation provides information at higher magnification, **Figure 3.7b**. The matrix is coarser and shows some granular sub-structure. Dislocations are evident, but there are areas with clearly lower density of dislocations. The carbides are coarser and more elongated than in the case of bainite formed at 300 °C.

Figure 3.8a shows the ion maps for C, Cr, Mn and Si. The C-map reveals two large carbon clusters and a low-carbon matrix, whereas the maps of substitutional elements show a slight enrichment at the interface of the carbides. **Figure 3.8b** shows the proximity histogram plotted from a C isosurface of 25 at%. The proximity histogram shows that the carbon content of the carbide is around 25 at.% in the interior of the particle, but also that there is a slight increase of Cr and Mn content close to the interface. In contrast, the silicon is depleted from the interior of the carbide to the interface, where Si content reaches a maximum of 1.2 at.%, with the composition inside the carbide being around 0.33 at.%. The APT results suggest

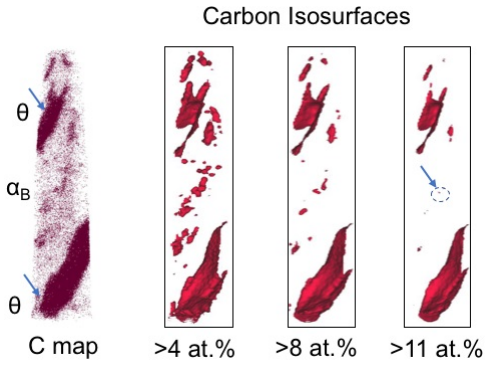

Figure 3.6: APT carbon ion map and carbon isosurfaces of 4 at.%, 8 at.% and 11 at.%. In between the two large carbides, smaller carbon clusters are found in the sample.

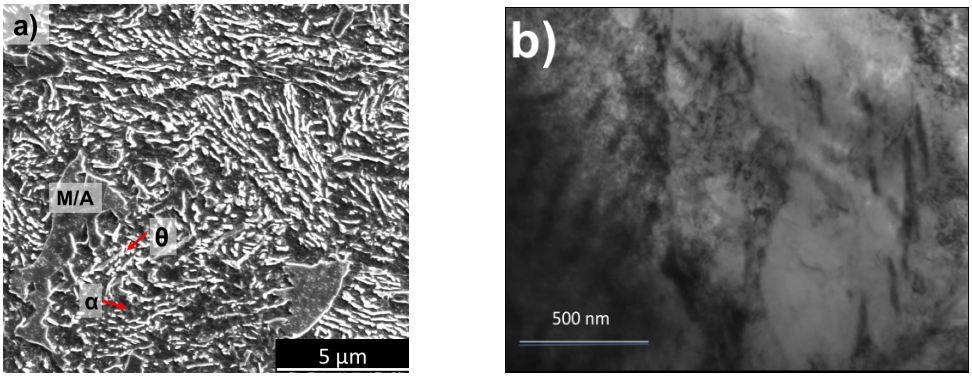

Figure 3.7: a) SEM micrograph showing upper bainitic microstructure obtained after heat treatment at 420 ^{o}C. b) Bright Field TEM micrograph of the same specimen.

that the carbides in this treatment are also cementite, which can be enriched slightly in Cr and Mn and depleted in Si.

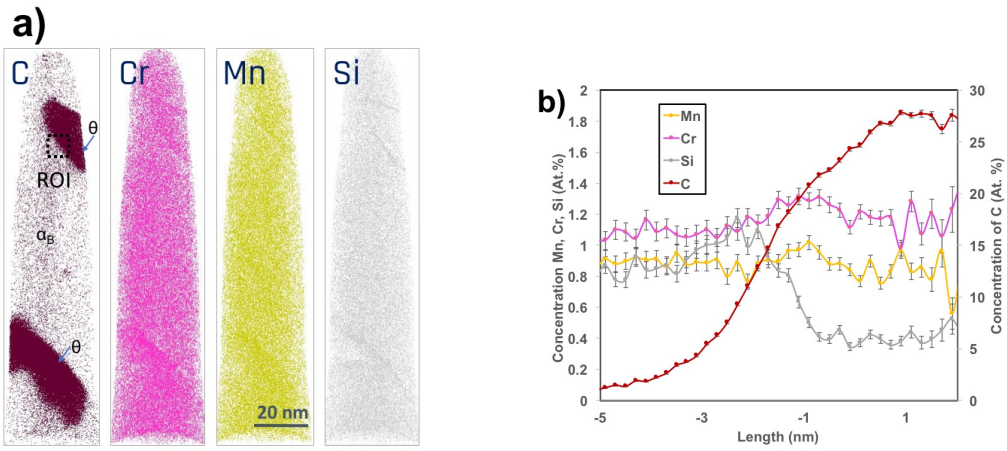

Figure 3.8: a) APT Ion maps of C, Cr and Mn of a specimen isothermally transformed into upper bainite at 420^{o}C. The C maps show two cementite precipitates. There is no C agglomeration at locations apart from the cementite. b) Proxigram of the upper cementite particle shown in a). Cr and Mn exhibit slight partitioning into the cementite, and Si is depleted from the cementite to the surrounding bainitic ferrite. The profile is taken normal to the interface between cementite-ferrite (positive values inside cementite in the ROI indicated in the C map of figure a)).

The carbon content of the bulk was measured in this sample following the same procedure. The results indicate that the carbon content in ferrite of upper bainite is 0.35 at.%, higher than the equilibrium value resulting from the extrapolated α/γ line

in the phase diagram at the selected temperature, calculated by Thermocalc, which is 0.12 at.%.

3.3.3. Isothermal treatment at 510 °C

The specimens that were isothermally treated at 510 °C differed fundamentally from the ones transformed at lower temperatures, **Figure 3.9**. The microstructure characterization reveals multiple microstructural constituents. Allotriomorphic ferrite with Widmanstätten secondary plates are evident at prior austenite grain boundaries. Additionally, an aggregate of acicular carbides surrounded by thin layers of ferrite is found to grow directionally from the α/γ interface, coinciding with the prior austenite grain boundaries, **Figure 3.9a**. In the areas surrounding these aggregates, the microstructure remains unetched, and these areas are identified as M/A resulting from the final quench to room temperature. This is consistent with the observation that the isothermal treatment was interrupted before the transformation was complete.

The TEM analysis of this microstructure focused on the carbide-ferrite aggregates, in order to elucidate the formation mechanism. Bright-Field (BF) TEM micrographs show that the carbides have a needle or fibre morphology. They are generally surrounded by a film of ferrite, but occasionally carbides are found to be directly surrounded by martensite, as indicated by the arrows in **Figure 3.9b**. The martensite is characterised by its different contrast, which indicates higher dislocation density, aided by Selected Area Electron Diffraction (SAED). The carbides are identified to be cementite by means of SAED and Dark Field imaging from $(\bar{3}\bar{1}\bar{1})$ reflection of cementite, **Figure 3.9c-d**. The thickness of the carbides is around 10 nm, while the thickness of the surrounding ferrite is consistently measured to be around 20-30 nm. The aggregates exhibit a certain degree of branching, at an angle of around 60° from the main direction of the aggregate.

The APT elemental maps show multiple areas, in which redistribution of C, Mn, Cr, and is evident, **Figure 3.10a**. There is an area clearly defined by two interfaces enriched in C, Mn and Cr, which outlines the carbide-ferrite aggregate detected in TEM. Within the aggregate, the ferrite film is depleted from C, Cr, Mn and enriched in Si. Approaching the ferrite/carbide interface, the Si concentration reaches a peak and the concentration of C, Cr and Mn gradually increase. Finally, within the cementite, C reaches a peak concentration of around 21 at.%, with the Cr concentration being around 8 at.% and the Mn concentration around 5 at.%, **Figure 3.10b**. The θ/α interfaces are significantly enriched in C, Mn, and Cr and depleted of Si as well, as seen by the proxigram in **Figure 3.10b**.

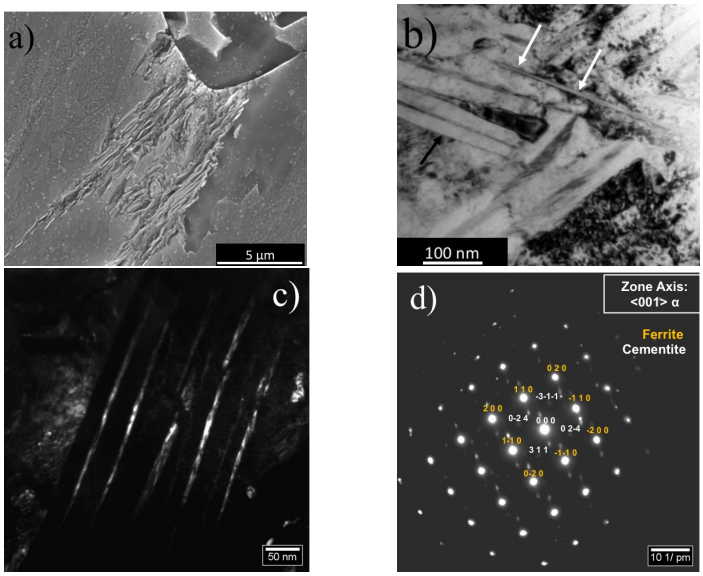

Figure 3.9: a) SEM micrograph showing the microstructure obtained after isothermal holding at 510 ^{o}C for 1 h. b) Corresponding Bright Field TEM micrographs of the same specimen. c) Dark Field image obtained from the $(\bar{3}1\bar{1})$ reflection of cementite d) SAED Pattern of ferrite and cementite, zone axis: <001> ferrite.

3.4. Discussion

3.4.1. Lower bainite (300 °C)

After isothermal transformation at 300 °C, the microstructure is homogeneous at the micro-scale, which means that the sample contains areas that transformed into bainite while containing high Cr, Mn, and Si concentrations. In this particular case, it is interesting to measure the composition of the bainitic ferrite and the carbides in order to examine the possible effect of Cr, Mn and Si on the evolution of the transformation. Therefore, for the sample preparation, the bulk composition of the area was chosen to contain a high concentration of alloying elements, so in case alloying element re-arrangement would occur, it would be evident in the measurement.

APT carbon maps reveal two precipitates with around 25 at.% of carbon, **Figure 3.5**. Cr and Mn maps show no redistribution of these elements between the precipitate and the ferritic matrix. Si on the other hand is found to have a lower concentration inside the precipitate. Since the isothermal treatment is 1 hour long and the exact time of the formation of the specific carbides is not known, we assume that Si, similarly to the other substitutional alloying elements present in the sample, did not partition during the formation stage, as it is also claimed for the

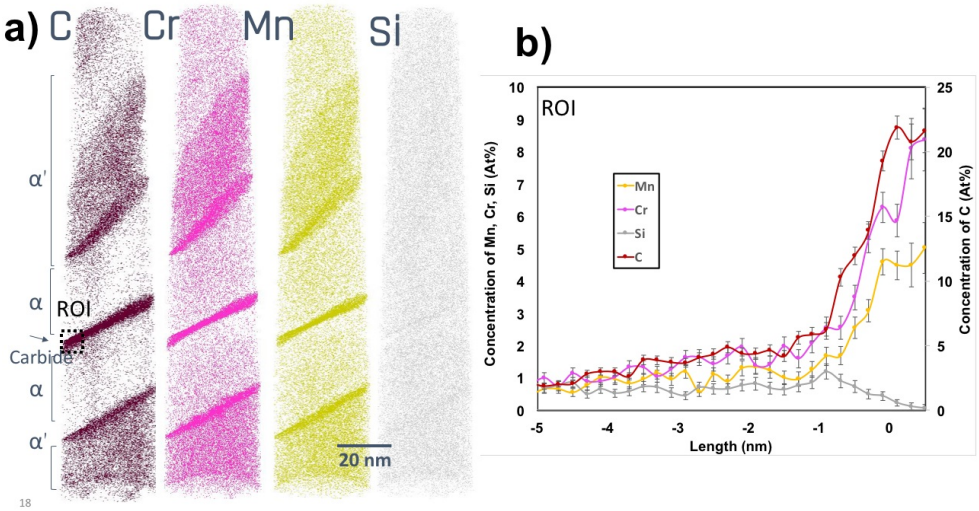

Figure 3.10: APT ion maps of C, Cr, Mn, and Si of a sample isothermally transformed at 510 ^{o}C for 1 h. Significant redistribution of all elements studied is evident. b) Proximity histogram for the Region Of Interest indicated in figure a). The proximity histogram profile showsis taken normal to the concentrationinterface between cementite-ferrite (positive values inside cementite).

case of cementite formation in tempered martensite at similar temperatures [19]. Given the fact that the diffusivity of Si in α iron is higher than the the diffusivities of Cr and Mn at 300 °C, it is suggested that the depletion of Si occurred after the precipitation, during the holding at 300 °C. The depletion of silicon from the precipitates and the accumulation of this element at the precipitate's interface with bainitic ferrite can contribute to the retardation of carbide growth during further isothermal holding. In this framework, the time of the treatment after the precipitation of the carbides has an effect on the microstructure that is similar to tempering. As far as the other substitutional alloying elements are concerned, there is no difference of their concentrations in the carbides and in the bainitic ferrite.

Furthermore, carbon clusters are observed in between the precipitates. Using carbon isosurfaces, Figure 3.6, it is shown that these clusters reach concentrations higher than 11 at.% of carbon. The carbon concentration of these clusters is more than the value of 6-8 at.% reported in literature for Cottrell atmospheres, formed by segregation at the dislocations [16]. However, the concentration is less than expected for transitional carbides or cementite. Given the fact that, according to TEM observations and literature [17], the dislocation density is high for the bainitic ferrite, carbon is expected to segregate at dislocations. Other studies [18] show that close to the precipitates and at the grain boundaries there is an increase in dislocation

density and carbon tends to get trapped at such lattice defects. Carbon clusters were found to be located in between the two precipitates, which could be attributed to an increased dislocation density at these locations. The dislocation density could be high at that location due to high transformation strain accommodation by the bainitic ferrite.

Furthermore, the high carbon concentration observed in the matrix (equal to 0.65 at.%) is consistent with observations of previous studies using APT [19,20] or synchrotron techniques [7,19]. An explanation for the increased carbon solubility in bainitic ferrite has been proposed by Hulme-Smith et al. [21], who support the hypothesis that the higher carbon content observed in ferrite is a consequence of an increased carbon solubility due to the change in symmetry from the conventional cubic unit cell to the tetragonal unit cell. The present observations do however not reveal information on the tetragonality of the bainitic ferrite.

3.4.2. Upper bainite (420 °C)

In upper bainite, the results show that the transformation produces cementite, but in this case some partitioning of Mn and Cr is observed at the cementite-ferrite interface. This trend is consistent with previous observations by APT [22]. In ref. [22] it was suggested that the decomposition of austenite into upper bainite with carbides could occur under NPLE conditions (Negligible Partitioning Local Equilibrium), because of the element profiles measured at the interface of cementite with ferrite. Although the element profiles in the present study have a similar trend, a high concentration of substitutional elements at the interface, supporting the NPLE hypothesis, was not found.

As far as the bainitic ferrite matrix is concerned, there is no carbon segregation inside the ferrite region between the two adjacent cementite particles. This is in agreement with TEM observations showing a lower dislocation density in bainite formed at 420 °C (**Figure 3.6b**). The dislocation density in upper bainite, although it was not directly measured or calculated, it can be expected to reach values of the order of 10^{13} m^{-2}. This assumption is based on the dislocation density value calculated by using tensile test data in tempered martensite sample, as it will be explained in Chapter 5, and on TEM analysis showing that the bainitic ferrite matrix in upper bainite resembles the one of martensite tempered at 480 °C in terms of contrast.

The APT tips from this specimen were prepared using site-specific preparation. In this case, choosing an area of strong segregation for the analysis was not relevant, since these areas do not transform into bainite. Thus, the tips were constructed from a transformed area containing carbides.

3.4.3. Inverse bainite (510 °C)

The SEM micrograph of **Figure 3.9a** shows that the cementite is always found to nucleate at prior austenite grain boundaries. In Chapter 2, it was shown that this cementite is forming in bands where high concentrations of Mn and Cr are found. This segregation implies that the local thermodynamic conditions are different from for the rest of the material, and the austenite decomposition at these locations will follow a different sequence according to the phase diagram isopleths of **Figure 2.6**. The austenite in Cr-rich and Mn-rich regions will decompose following the phase formation sequence of hyper-eutectoid steels. It has been reported in such cases that the so-called inverse bainite can be formed. This type of ferrite and cementite phase mixture is forming with cementite directly precipitating at the austenite grain boundary, initiating the transformation. Ferrite subsequently forms surrounding the cementite. Non-classical austenite decomposition products similar to this have been reported in the past for medium carbon, high chromium steels [23].

In fact, thermodynamic calculations reveal that the addition of substitutional elements in an Fe-C system changes the range of stability of different phases. The phase diagram isopleths of 51CrV4, **Figure 2.6b** for the local composition measured by EPMA at regions with high Mn and Cr segregation with the values reported in Chapter 2, reveals a eutectoid composition of 0.4 wt.% C (1.8 at.%). Therefore, in the high Mn and Cr region the austenite of the investigated steel can decompose by forming pre-eutectoid cementite or M_7C_3 before forming ferrite. Carbides can be found, which are directly surrounded by martensite, without any intermediate ferrite layer, which indicates that the carbides form before the ferrite and thus can act as leading phase for the formation of this microstructure. These facts indicate that the microstructural product formed at temperatures between the temperatures for upper bainite and pearlite formation can be inverse bainite, as was reported for the higher carbon steels in literature [25-28].

Chromium has a special role in the formation of these non-classical structures. It is mainly responsible for the observed shift of the eutectoid composition to lower carbon contents; it significantly retards the bainite formation and it is found to partition in carbides. A solute drag effect can explain the retardation of bainite growth at high temperatures. The requirement for Cr diffusion for the formation of carbides explains the slow reaction kinetics of this transformation.

3.4.4. Thermodynamic considerations - formation mechanism

The morphological and the chemical diversity observed can be further interpreted in terms of thermodynamics. Thermodynamic calculations were performed using

ThermoCalc software with TCFE7 database. The $\alpha/\alpha+\gamma$ and $\gamma/\alpha+\gamma$ boundary lines were calculated in the para-equilibrium condition in the range 600-800 °C and then extrapolated to lower temperatures. In **Figure 3.11** the para-equilibrium $T_{\gamma\to\theta}$ and $T_{\gamma\to\alpha}$ as well as the orthoequilibrium $T_{\gamma\to\theta}$ lines are extrapolated to lower temperatures. Based on our experimental findings, for the temperatures of 300 °C and 420 °C bainite formation can proceed under para-equilibrium conditions. However, at 510 °C, it was experimentally observed that substitutional alloying elements partition to the carbides and at the interfaces. Therefore, in this case local equilibrium conditions can be assumed, which are represented by the ortho-equilibrium $T_{\gamma\to\theta}$ line in **Figure 3.11**.

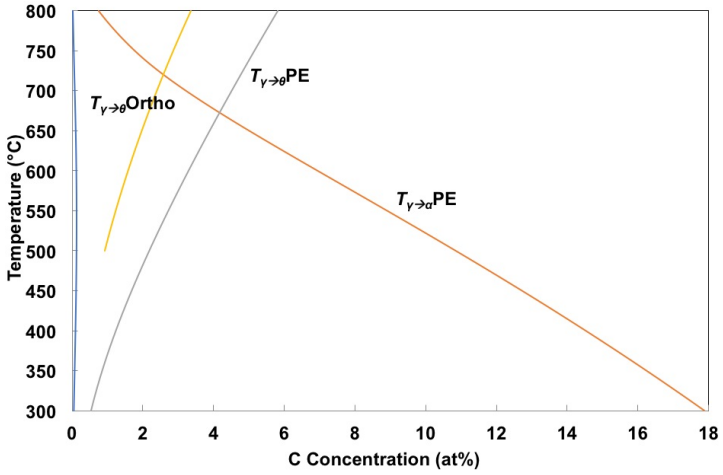

Figure 3.11: $T_{\gamma\to\theta}$ and $T_{\gamma\to\alpha}$ lines under para-equilibrium conditions and $T_{\gamma\to\theta}$ line under ortho equilibrium conditions extrapolated to low temperatures.

For bainite forming at 300 °C, in TEM it was observed that there is an initial, carbide-free spine of ferrite forming without precipitation of carbides. This initial plate grows into the surrounding austenite at a rate governed by the diffusion of C. At some point, the supersaturation of C in austenite is sufficient to allow PE cementite precipitation directly from austenite at the γ/α interface according to **Figure 3.11**. The reaction of cementite precipitation consumes the C from the remaining austenite, thus providing driving force for further grow of the bainitic ferrite without further nucleation being necessary.

For bainite forming at 420 °C, the diffusivity of C is higher, hence the concentration profile at the interface is broader. The undercooling is still high enough for the transformation to occur by a shear mechanism. The higher diffusivity can explain the coarser ferrite plates and the high undercooling its morphology. The cementite

in this case is also coarser, but it has another different feature: it is not aligned at a specific orientation, but it follows the γ/α plate boundaries. This happens because cementite forms at the carbon rich areas in the remaining austenite, surrounding the newly formed bainitic ferrite plates.

In the sample, isothermally treated at 510 °C, ferrite was found at the prior austenite grain boundaries, hence called allotriomorphic. However, it presented facets and sometimes acicular morphology or even degenerate Widmanstätten features. This can be attributed to the low driving force for Widmanstätten ferrite formation.

Inverse bainite formation initiates with precipitation of carbides of Widmanstätten morphology at the prior austenite grain boundaries. Ferrite will form surrounding these carbides because carbon will be consumed for the carbide formation, triggering the formation of ferrite. The ferrite grows to a specific width and then, according to apt analysis, significant segregation of Cr and Mn is found at the α/α' (previously γ) boundary. It is therefore suggested that the coarsening of the ferrite ceases because of solute drag.

3.5. Conclusions

In the present study, bainite microstructures, which were produced by an isothermal treatment of 51CrV4 medium carbon, low alloy spring steel have been characterized by SEM TEM and APT. It was found that:

1. Bainitic ferrite contains more carbon in solution than is predicted from the thermodynamic equilibrium. The carbon content of the bainitic ferrite becomes higher as the transformation temperature decreases. This could be attributed to the possible tetragonality of bainitic ferrite, allowing higher solubility of C in α-Fe.

2. The substitutional alloying elements (Mn, Cr) did not partition to the carbides during lower bainite formation. Silicon was depleted from the carbides. This is a process occuring after the precipitation (tempering).

3. During upper bainite formation, segregation of Cr and Mn occurred at the cementite-bainitic ferrite interface.

4. A peculiar microstructure consisting of acicular carbides and ferrite formed at temperatures close to the bainite start temperature. It can be suggested based on the calculated thermodynamics that this microstructure is inverse bainite.

5. During inverse bainite formation, alloying elements can diffuse within the time frame of the transformation. APT measurements show that Mn and Cr partition to the boundaries of bainitic ferrite and into the carbides.

6. The difference in the chemical composition of the carbides in inverse bainite and the formation temperature can explain their presence and their morphology.

References

1. A. Hultgren: Trans. ASM 39, 1947, pp. 815.

2. M. Hillert, Royal Institute of Technology, Stockholm, 1960.

3. M. Hillert, Metall. Mater. Trans 25A, 1994, pp. 1957-66.

4. C. Zener, Trans. ASM, 1946, vol. 167, pp. 550-95.

5. T. Ko and S.A. Cottrell: J. Iron Steel Inst., 172 (1952), p. 307.

6. H.K.D.H. Bhadeshia and D.V. Edmonds, Acta Metall. 28 (1980), pp. 1265-73.

7. R.K. Dutta, R.M. Huizenga, H. Gao, M. Amirthalingam, A. King, M.J.M. Hermans and I.M. Richardson, Metall. Mater. Trans. 45A, (2014) 12 pp 5281-5285.

8. C.N. Hulme-Smith, M.J. Peet, I. Lonardelli, A.C. Dippel and H.K.D.H Bhadeshia, Mater. Sci. Technol. 31 (2015) 2 pp. 254-256.

9. H. Goldenstein and J.A. Cifuentes, Metall. Mater. Trans. 37A (2006) pp. 1747-1755.

10. A. Borgenstam, P. Hedstr?m, M. Hillert, P. Kolmskog, A. Stormvinter, J. Agren (2011) Metall. Mater. Trans. 42A (6), pp. 1558-1574.

11. W. T. Reynolds, S. K. Liu, F. Z. Li, S. Hartfield and H. I. Aaronson, Metallurgical Transactions A21 (1990), pp. 1479-1491.

12. W. T. Reynolds, F. Z. Li, C. K. Shui and H. I. Aaronson, Metall. Trans. A21 (1990), vol. 21, pp. 1433-1463.

13. H. I. Aaronson, W. T. Reynolds, Jr. and G. R. Purdy, Metall. Mater Trans A 35 (2004), pp. 1187-1210.

14. C. Goulas, M.G. Mecozzi and J. Sietsma Metall. Mater. Trans. 47A (2016) 6 pp 3077-3087.

15. K. Thompson, J. Sebastian, S. Gerstl, Ultramicroscopy, 107 (2007), p. 124.

16. Felfer, P.J., Microsc. Res. Tech. 75 (2012) 4 pp. 484-491.

17. Herbig, M., P. Choi, and D. Raabe, Ultramicroscopy 153, (2015) pp. 32-39.

18. Gault, B., et al. J. Appl. Phys. 105, (2009) 3 pp. 34.

19. A.J. Clarke, M.K. Miller, R.D. Field, D.R. Coughlin, P.J. Gibbs, K.D. Clarke, D.J. Alexander, K.A. Powers, P.A. Papin, G. Krauss, Acta Mater. 77 (2014) pp 17-27.

20. Timokhina, I.B., Liss, K.D., Raabe, D., Rakha, K., Beladi, H., Xiong, X.Y., Hodgson, P.D., J Appl. Crystall., 49, (2016) pp. 399-414.

21. J. Cornide, G. Miyamoto, F. G. Caballero, T. Furuhara, M. K. Miller, C. García-Mateo, , Solid State Phenom. 172-174, (2011), pp. 117-122.

22. E.V. Pereloma, Mater. Sci. Technol. 32 (2016) 2, pp. 99-103.

23. C. Garcia-Mateo, J.A. Jimenez, H.W. Yen, M.K. Miller, L. Morales-Rivas, M. Kuntz, S.P. Ringer, J.R. Yang and F.G. Caballero, Acta Mater. 91, (2015) pp 162-173.

24. C.N. Hulme-Smith, I. Lonardelli, A.C Dippel and H.K.D.H. Bhadeshia, Scr. Mater., 69 (2013) 5, pp. 409-412.

25. Kaya, A.A., Edmonds, D.V. (1988) Metall Trans 29A, pp. 2913-2924.

26. K.R. Kinsman and H.I. Aaronson: Metall. Trans., 1970, vol. 1, pp. 1485-88.

27. H.J. Lee, G. Spanos, G.J. Shiflet, and H.I. Aaronson: Acta Metall. 36 (1988), pp. 1129-40.

28. G. Spanos, H.S. Fang, D.S. Sarma, and H.I. Aaronson: Metall. Trans. 21A (1990), pp. 1391-1411.

4

The effect of shot peening on 51CrV4 spring steel with bainitic and tempered martensitic microstructure*

In the two previous chapters, we focused on the microstructure, the mechanism of its formation and its specific features. As the motivation of this work is linked to spring production, we confirmed that the performance of a spring is closely linked to its fatigue properties. Springs obtain their fatigue properties from their microstructure, but also to a great extent from surface treatments. Shot peening is a widely-used and low-cost method for improving the fatigue properties of engineering components. In the present chapter, using high-resolution electron microscopy and Finite Element Modeling, we compare bainitic and tempered martensitic microstructures produced by the same steel grade and with the same hardness, asking how each microstructure accommodates the strain caused by the shot peening treatment. This difference in strain accommodation can influence the peening parameters, the desired residual stress distribution, and full surface coverage, which are important

* The effect of shot peening on 51CrV4 with bainitic and tempered martensitic microstructure, by C. Goulas, C. Jiménez-Peña, F. Castro-Cerda, M.G. Mecozzi, D. Debruyne, R. Petrov, J. Sietsma, submitted for publication to J Mater. Proc. Technol.

prerequisites for improving the fatigue life of components.

4.1. Introduction

Shot peening (SP) is one of the most important and widely used surface treatments used as a post manufacturing process in order to increase fatigue life and fatigue limit of engineering components. During shot peening, projectiles (usually spherical steel shots, short steel wire pieces, glass or ceramic beads) are accelerated to the surface of a target component. A layer at the surface of the component deforms because of the shot impact and compressive stresses (parallel to the surface) are generated in the deformed layer, while also the roughness is increased. The improvement of fatigue performance in SP components that is often observed is mostly related to these compressive residual stresses [1]. SP is also used as a forming process to shape large, relatively thin parts, for fine local forming, for correcting dimensional inaccuracies and to improve tolerances [2].

The SP process can be controlled by the parameters of shot size and type, shot velocity, peening angle and time [3], peening coverage, Almen peening intensity and resulting residual stress. The coverage is important to be at least 100% to ensure the beneficial effect of the SP on the fatigue life of the component. It is evaluated by optical investigation using a x10 magnifying glass. Under this magnification, it is accepted that when in the 98% of the area examined no prior machining marks are evident, then the coverage is assumed to be 100%. Multiples of 100% of coverage are then calculated based on time, so a 200% coverage means that the SP was performed for the double time necessary to reach 100%. Intensity is the second controlling parameter. For measuring SP intensity, a standard method is used developed by J.O. Almen in the 1940's [4]. For this method, using the conditions applied for shot peening, a component, a standard cold rolled steel strip specimen, is peened. Afterwards, due to the stresses induced, the strip becomes curved. The height of curvature arc is called Almen Intensity. Based on the thickness of the Almen strip used, there are three different Almen scales, A, N, and C. "A scale" strips are used for shot peening with cast and cut-wire shots, C scale strips are thicker than A scale and appropriate for high intensity shot peening, and N scale strips are thinner than A scale strips and are used for low intensity shot peening with glass or ceramic beads.

It is well established that SP produces a nano-crystalline layer at the surface of the component because of the severe plastic deformation induced by the shot impacts [5]. The nano-crystallisation of the surface provides additional reasons for the fatigue life enhancement besides the compressive residual stresses [6]. This

nanocrystalline layer is most frequently reported in cases in which coverage exceeds 100%, often called severe shot peening or ultrasonic shot peening (USSP). However, nano-crystalline layers have been also reported after normal SP processes [7].

The EBSD technique has been used in the past to investigate the microstructurally affected layer by SP due to the plastic deformation. The strain caused by the SP creates local changes in the orientation of the crystal lattice, which can be effectively illustrated by local misorientation maps. Messe et al. [8] used kernel average misorientation maps in combination with the intergranular misorientation maps to measure the depth of the SP layer in Ni-based superalloy. Using these maps, they were able to reveal the non-uniform effect of the shot peening depending on their shape and orientation [8]. D.J. Child et al. have shown, using EBSD measurements, that the microstructurally affected layer by shot peening does not coincide with the depth that residual stresses can be detected by XRD [9]. The result of the SP is difficult to be predicted, as it is a function of various parameters that are mutually dependent. Finite Element Modelling (FEM) has been used in several studies as a tool to predict the effect of the SP treatment [10]. Hassani-Gangaraj et al. included in their simulation a dislocation model to obtain more refined results [11].

Currently, heat treatment routes alternative to the typical Quenching and Tempering (Q+T) are being investigated to produce components with equivalent properties while reducing energy consumption [12]. One of the main alternatives is austempering instead of quenching, which can lead to a bainitic instead of a martensitic microstructure. Bainite and martensite are known to have very similar hardness and microstructural features, but little is known if these microstructures will produce a different result after SP. As SP is a very common surface treatment process in the automotive industry, changes of the target's response to the SP treatment because of microstructural changes need to be further investigated. Ling-Wen et al. briefly reported a correlation of microstructure and shot peening result related to the roughness in Ti alloys. They show that the target's ductility can influence the roughness [13].

In the present work, we introduce a comparative study of shot peening of components made of the same spring steel grade, 51CrV4, with the same hardness, but with different initial microstructures: lower bainite, produced by austempering, and tempered martensite, produced by quenching and tempering. The intrinsic properties of each microstructure are found to play an important role in the end result of the SP.

4.2. Experimental procedure

4.2.1. Heat treatment of the specimens

Rectangular specimens (20x50x10 mm^3) were machined from a 51CrV4 hot rolled bar (49 x 95 x 985 mm^3), and were subsequently heat-treated. After complete austenitisation, one set of components was austempered to produce lower bainite and the second set was first quenched in water to room temperature and then tempered to match the hardness of the austempered components. Detailed description of the heat treatment cycles is found in **Figure 4.1**.

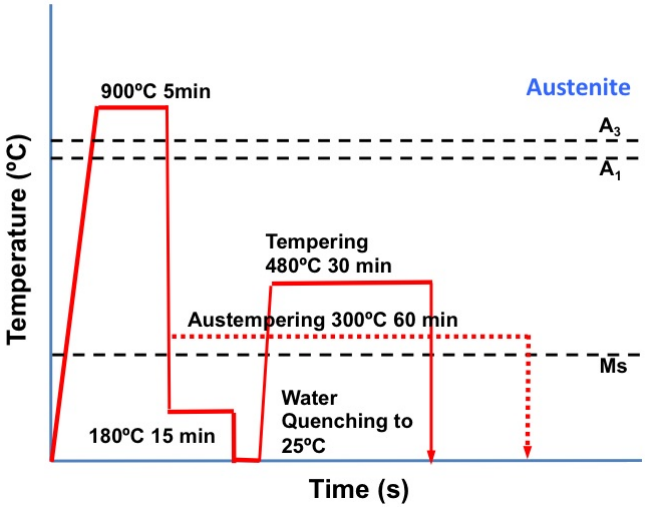

Figure 4.1: Heat treatment schedules used to produce bainite (dotted line) and tempered martensite (solid line) with the same hardness in 51CrV4.

Bainite: The heat treatment consisted of an austenitization step of 5 min at 900 ^oC in a salt bath followed by an isothermal holding stage of 1 h at 300 ^oC in a second salt bath. The treatment ended with water quenching to room temperature. The influence of the final cooling step (water quenching or air cooling) was found to be negligible, because the hardness of the water quenched samples after bainitic transformation was the same as the hardness of samples, which were air cooled. This is because the full bainite transformation is obtained within 1 h in 51CrV4 at this temperature, as confirmed by previous dilatometry experiments [12].

Tempered Martensite: The specimens were heated up to 900 ^oC and soaked for 5 min in a furnace with protective Ar atmosphere. Next, they were quenched in salt bath at 180 ^oC and held for 15 min. After that, the samples were water quenched to room temperature and finally tempered in salt bath at 480 ^oC for 30 min. The

intermediate quenching was used to prevent quench cracking and to minimize the sample distortion. Surface machining to remove decarburized layer was applied after the heat treatment.

4.2.2. Shot peening experiments

Final machining of the surface of the specimens was performed before the SP to obtain roughness *R*a = 0.8 μm $\pm$ 0.1 μm. A wheel blasting machine of hanger type was used for the study. The shot type chosen for this treatment was conditioned cut steel wire 1.0 mm $\pm$ 0.1 mm controlled by the use of a series of screens. The flow rate of the shots was in all cases 90 kg min-1. The speed of the shots was measured by a high-speed camera for different rotational speeds of the accelerating turbine. The shot speed varied between 36 m s^{-1} and 72 m s^{-1}. The speed of 60 m s^{-1}, as a result of a wheel rotational speed 2500 rpm, was found to produce a good combination of coverage and roughness at the exposure time permitted by the machine limitations (automated exposure time 20 s). Almen tests were performed before each trial to measure the peening intensity and to assess qualitatively the coverage. For the treatments investigated, Almen A scale tests were considered appropriate. Coverage was considered complete when no prior machining marks were evident on the Almen strips under examination with x10 magnification stereoscope. Before each measurement, three tests were performed. For the specific test conditions, the Almen intensity measured was 0.60 mm (A scale).

4.2.3. Analysis by stereo-microscopy, light optical microscopy and EBSD

The peened samples as well as the Almen strips were evaluated by means of stereo microscopy (surface evaluation) and optical microscopy (evaluation of the cross section). The cross sections treated with the conditions fulfilling the criteria of full coverage and acceptable roughness were chosen based on the evaluation and were prepared for EBSD analysis. Bainitic and tempered martensitic specimen were carefully sectioned with a precision cutting machine. In order to protect the sub-surface and near-surface features, the specimens were clamped between two metal steel plates, ground and polished by standard metallographic procedures up to a surface finish of 0.25 μm, using OP-S colloidal silica solution as a final step for 30 min. Electron backscatter diffraction (EBSD) analyses were performed on a FEI Quanta^{TM} 450-FEG-SEM operated at 20 kV, beam current corresponding to FEI spot size 5 for aperture 30 μm and working distance of 16 mm. The sample was tilted 70^{o} towards the EBSD detector and the EBSD patterns were acquired

with a Hikari detector operated with EDAX-TSL-OIM Data Collection version 6 software in hexagonal scan grid. The step size was 50 nm. The orientation data was post-processed after excluding points with Confidence Index lower than 0.1 and the grains were defined as a group of points containing at least 5 neighbouring points found at least in two rows and exhibiting misorientation higher than 5^o with their other neighbours.

4.2.4. Roughness measurements

Surface roughness measurements were also performed on each of the surfaces. Measurements were performed using a Bruker Contour white-light interferometer. S_a parameter was used to characterize the roughness. The parameter S_a describes the surface area roughness taking into account multiple profiles, as opposed to the conventionally used parameter for roughness characterisation, R_a, which measures only one particular profile. S_a is calculated by:

$$S_a = \frac{1}{A} \iint_A \left| Z(x,y) \right| dxdy \tag{4.1}$$

where the integration is performed over the surface area of the specimen A, and Z(x,y) is the function representing the height of the surface relative to the average plane defined by the least squares method.

4.2.5. Tensile tests of the heat-treated microstructures

Standard tensile specimens were machined out of 51CrV4 bars and subsequently heat treated in salt baths according to the heat treatment schemes of **Figure 4.1**. The specimens were prepared in sets of 5 per condition. The tensile tests were performed with a cross-head velocity of 3 mm min^{-1} on an INSTRON 5501 tensile machine. As bainitic specimens do not show a clear yield point, the extended Kocks Mecking plot was used to accurately determine the yield strengths of the bainitic and the quenched and tempered specimens, as shown in [14].

4.2.6. Finite Element Modeling

In order to analyse the development of residual stresses and plastic strain caused by the shot peening process, a finite element simulation of shot peening was developed. A 3D model was constructed using the commercial finite element code Abaqus 6.13-1 to simulate single shot impacts. From these simulations information on the strain accommodation and the residual stress distribution is obtained. Then, multiple shot impacts were simulated to evaluate the interaction of the strain fields

produced by the individual impacts. The analysis was divided into two parts: the shot, modelled using Abaqus Explicit, and the elastic recovery modelled in Abaqus Standard. The mesh of the target part was formed by 8-node linear brick elements. The optimal mesh size was found with a mesh convergence study and it was 15 μm in the impact area, where higher stress gradients are expected. Only one quarter of the target was modelled in order to reduce computational time. Symmetric boundary conditions were applied in the two planes of symmetry and the target's bottom was restrained. The spherical shot was modelled as an analytical rigid sphere with diameter of 1 mm. Initial velocity of 60 m/s was applied in the reference point of the ball (centre). The 3D model is illustrated in **Figure 4.2**, together with a schematic view of the specimen shape. For the sake of clarity, the full target geometry is represented instead of the quarter used in the model.

Two sets of mechanical properties were considered in the analysis, the one of the bainitic microstructure and the one of the tempered martensitic microstructure. The elastic material parameters were set to Young's Modulus E = 210 GPa and Poisson's ratio v = 0.3 for both materials. The material plastic behavior of the target was modelled using the von Mises yield surface with the data extracted from tensile tests that were performed with cylindrical dog-bone specimens following the exact same heat treatment as the rectangular specimens.

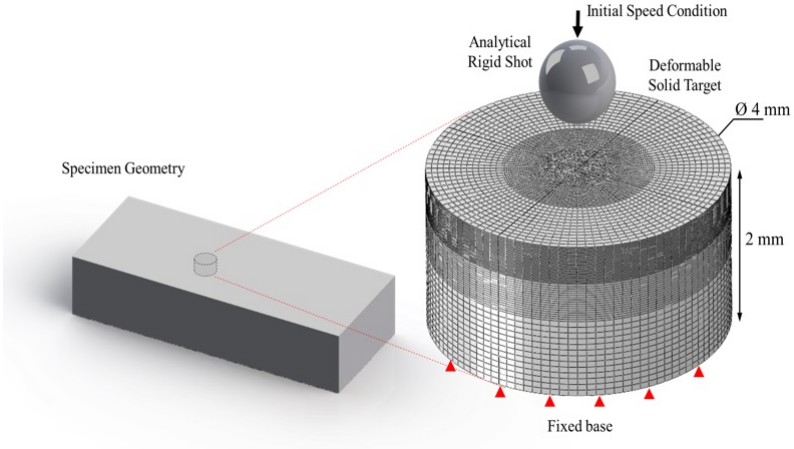

Figure 4.2: Finite Element Model of a single shot impact.

4.3. Results and Discussion

4.3.1. Microstructure characterization

The cross sections of shot peened specimens were used for microstructure characterisation. As the microstructures in both cases are very fine, Scanning Electron Microscopy was used to resolve the morphologies of the two microstructures. In **Figure 4.3**, lower bainite microstructure is shown. It consists of bainitic ferrite plates with length varying between 3 and 8 μm, and a width of 0.8 to 1.5 μm and fine cementite particles precipitated mainly within ferrite plates, aligned and at an angle towards the growth direction of the plate. As almost no martensite/retained austenite (MA) islands are seen (apart from a small one in **Figure 4.3b**), bainite formation is considered to be complete during the isothermal treatment, verifying previous dilatometry findings [12].

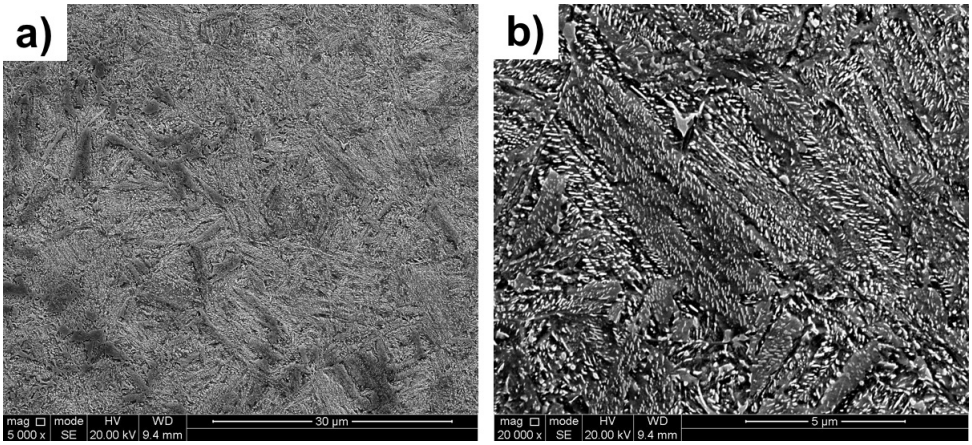

Figure 4.3: Scanning Electron Microscopy micrographs of lower bainitic microstructure.

In **Figure 4.4**, the tempered martensitic structure is shown. The microstructure consists of tempered martensite laths that are 2-5 μm long and 0.35-0.8 μm wide, with cementite carbides precipitated both within laths and following the lath boundaries, at multiple orientations.

There are specific morphological characteristics of the two structures that originate from the different formation mechanisms of the microstructural constituents. In the case of bainite, the plates of the bainitic ferrite are coarser than the laths of tempered martensite. On the other hand, the size of the carbides in the case of tempered martensite is larger than the ones found in bainite, for this particular treatment. This can be explained as the carbides in bainite form during the transformation and they do not coarsen significantly afterwards until the end of the treatment. On the

other hand, the carbides in martensite form during tempering at a temperature that is higher than the temperature chosen for the bainitic treatment and they coarsen during the tempering treatment. The martensitic matrix is supersaturated in carbon, so the carbon and other carbide forming elements (if the temperature allows) diffuse to the carbides and lead to their coarsening during tempering. Another reason for the size difference between the carbides found in lower bainite and the ones found in tempered martensite is the diffusivity of carbon in the phase in which the carbides form. In the case of tempered martensite, the carbides form in a martensitic matrix, which is essentially bcc. In bainite on the other hand, carbides are forming in the remaining austenite while bainitic ferrite is still growing.

The size of the bainitic ferrite plates and the martensite laths as well as the distribution of carbides are microstructural parameters that can affect the mechanical properties and, consequently, the effect of shot peening on it.

After the microstructure is shot peened, observation by means of SEM does not reveal the effects of the treatment on the microstructure. For this purpose, Electron Back Scatter Diffraction was employed. The EBSD maps are very helpful in analysing the deformed layer in the microstructure caused by the shot peening process, by providing visual and quantitative data. For the current analysis we used the Image Quality (IQ) map with superimposed grain boundaries and the Kernel Average Misorientation (KAM) map.

In the IQ maps, grain boundary networks are superimposed, **Figure 4.5** and **Figure 4.6**. The grain boundaries were defined as low angle for misorientation angles between 5^o-15^o, and high angle, in case of misorientation higher than 15^o.

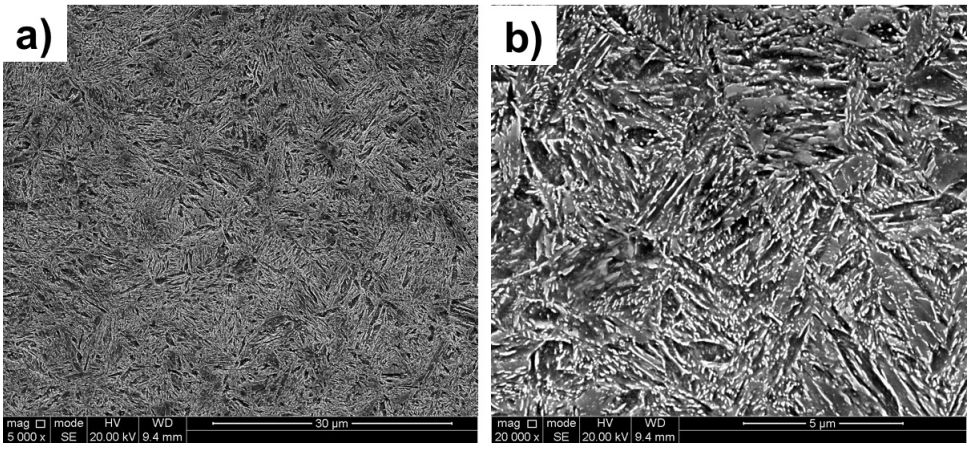

Figure 4.4: Scanning Electron Microscopy micrographs of tempered martensitic microstructure.

Grain substructures are also evident in the case of the surface specimens, on the IQ plot of which the boundaries 2^o-5^o are additionally plotted. Calculations using the grain definition criteria described in section 4.3.3. (Experimental Procedure) show that the bainitic microstructure is coarser than the martensitic, **Figure 4.7**. In the case of the bainitic specimen, the coarser grains develop sub-structure with the trend of forming low angle grain boundaries. From the top 5 microns from the surface, the deformation is very severe, so no microstructural information can be obtained due to the unsuccessful indexing.

The KAM maps of **Figure 4.8** and **Figure 4.9** show that the strain induced by the shot peening causes increased misorientation values close to the surface for both bainite and tempered martensite microstructures. However, the microstructurally affected layer of the martensitic structure is thinner than the one observed in the bainitic specimens. Additionally, KAM charts for bainite and martensite show that the martensite exhibits higher misorientation values close to the surface than the bainite, with a high number of points exhibiting misorientation higher than 2^o.

For the bainitic specimens, coarser bainite plates closer to the surface tend to form sub-grains because of the plastic deformation. On the other hand, the martensitic microstructure is much more refined, so the points exhibiting the highest misorientation values are located at the grain boundaries. In both cases, it can be seen that at the surface KAM maps there is an increased number of points, which remain unindexed. These points have CI less than 0.1, so they were excluded from the post processing. It is significant to mention that directly at the surface, indexing is impossible, even with the finest step size possible for the technique, 50 nm. Analysis of the surface layer is possible only with very high resolution techniques, like Transmission Electron Microscopy.

4.3.2. Mechanical properties

The mechanical behaviour of the two microstructures is expected to influence the effect of the shot peening treatment. Mechanical testing of the heat-treated materials is necessary to gain insight into the mechanical properties of the two microstructures. The results show that although the hardness is similar in the two kinds of samples (46 HRC $\pm$ 1.5), there are important differences in the mechanical behaviour of the microstructures. The shot peening treatment induces plastic deformation at the surface of the components. Using information derived from the standard engineering stress-strain curves, the consequences of the shot peening treatment on the two microstructures, such as the final roughness and the residual stresses, will be compared and discussed.

In **Figure 4.10a** full tensile curves are shown. Both structures yield at similar

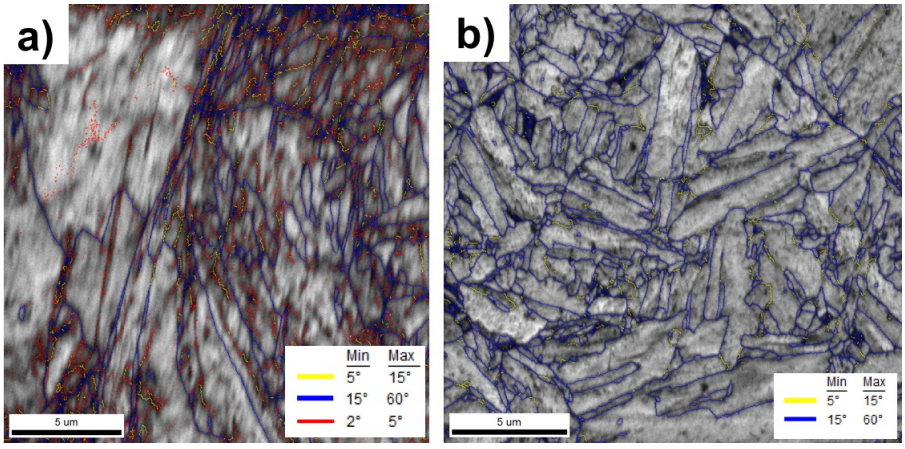

Figure 4.5: Image Quality EBSD maps of the bainitic specimen. a) Surface. b) Bulk.

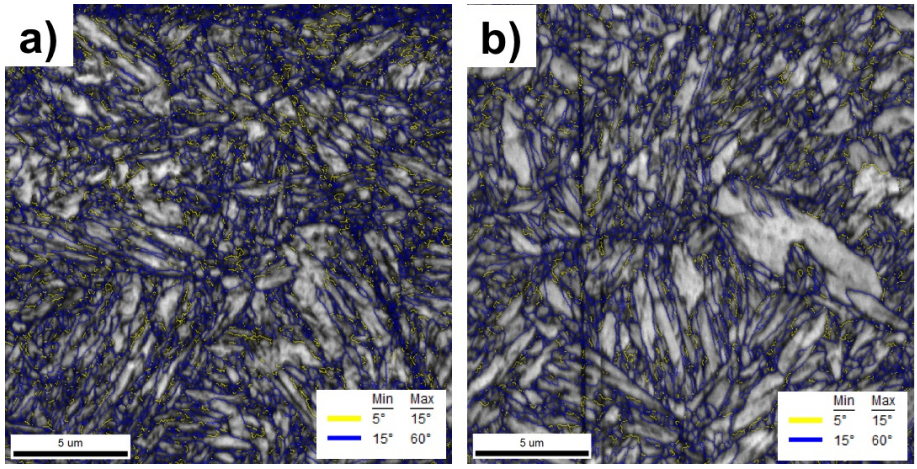

Figure 4.6: Image Quality EBSD maps of the tempered martensitic specimen. a) Surface. b) Bulk.

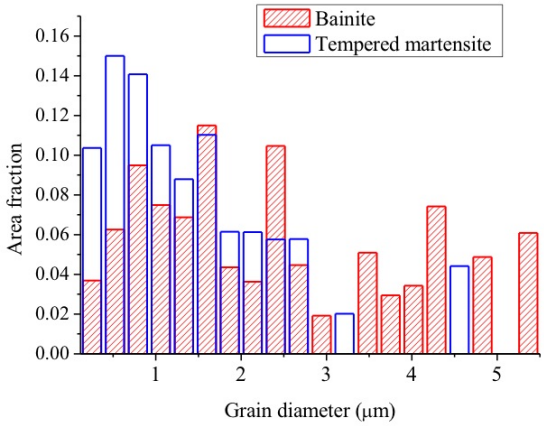

Figure 4.7: Grain size comparison between bainite and tempered martensite.

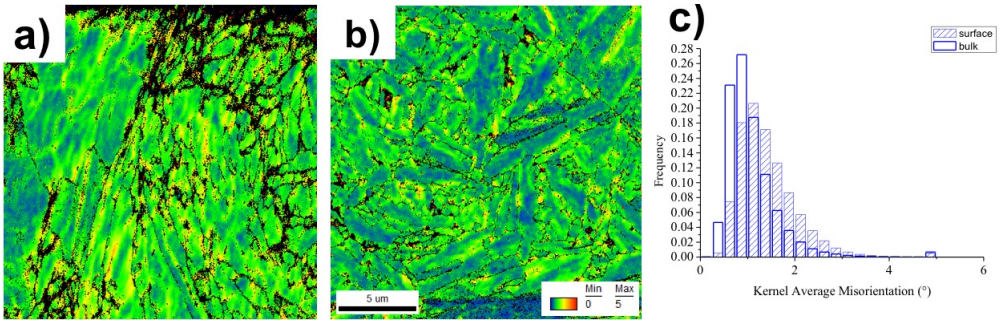

Figure 4.8: EBSD Kernel Average Misorientation Maps for a) the surface, b) the bulk of the bainitic specimens after SP. The scale is the same for a) and b).

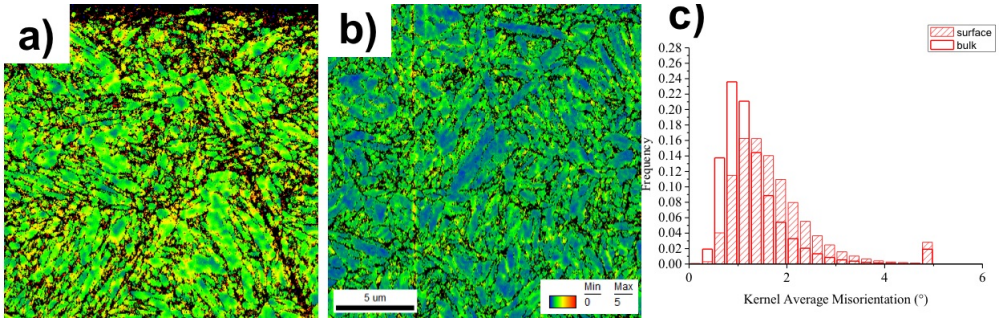

Figure 4.9: EBSD Kernel Average Misorientation Maps for a) the surface, b) the bulk of the tempered martensitic specimens after SP.

under similar stress levels. Tempered martensite shows a sharp yield point in contrast with the bainite, which exhibits continuous yielding behaviour. **Figure 4.10b** shows the extended Kocks-Mecking analysis as suggested in [14] for the curves of **Figure 4.10a**, which allows the precise determination of the yield stress by the distinct change in slope. This is particularly useful in the case of bainite, in which the yield strength determination is challenging due to the absence of a clear yield point in the tensile curve.

Using the above analysis, it is found that the bainitic microstructure shows yield strength (R_p) 1405 MPa $\pm$ 10 MPa. After reaching the yield strength, further loading leads to extensive work hardening, leading to an ultimate tensile stress of 1780 MPa $\pm$ 20 MPa. The total elongation measured was 8 % $\pm$ 0.5 %. On the other hand, the martensitic microstructure was different. Although the yield stress is similar to the bainitic specimens (1379 MPa $\pm$ 10 MPa), the post-yield behaviour shows very limited work hardening, leading to R_m of 1425 $\pm$ 10 MPa. The total elongation in this case is very similar to the bainitic specimens (8.5% $\pm$ 0.65%).

4.3.3. Surface roughness measurements

Surface roughness of the peened specimens was evaluated by means of white light interferometry. In **Figure 4.11**, the image obtained from the interferometer for the two specimens is shown. There are no prior machining marks evident, thus the coverage is considered to be 100% for both cases. In **Figure 4.11c** the average roughness values are shown for a range of shot speeds. It is observed that that the roughness of the tempered martensitic specimens is consistently lower than the one observed in the bainitic specimens.

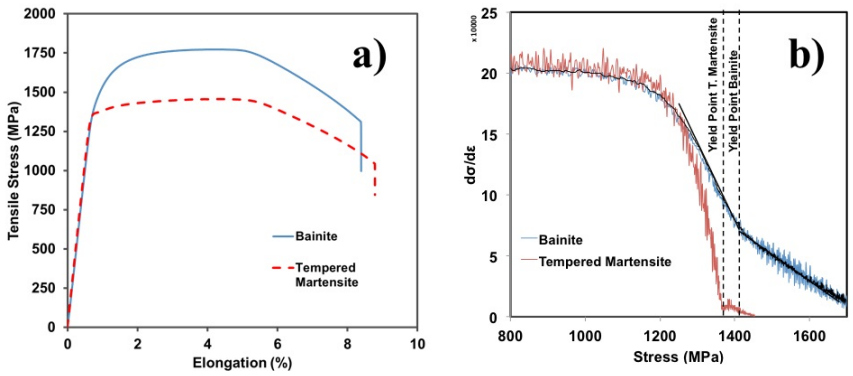

Figure 4.10: a) Tensile curves of standard specimens heat treated according to the schemes of Figure 1. b) Extended Kocks-Mecking Plot for the two types of specimens, showing the yield stress (R_p).

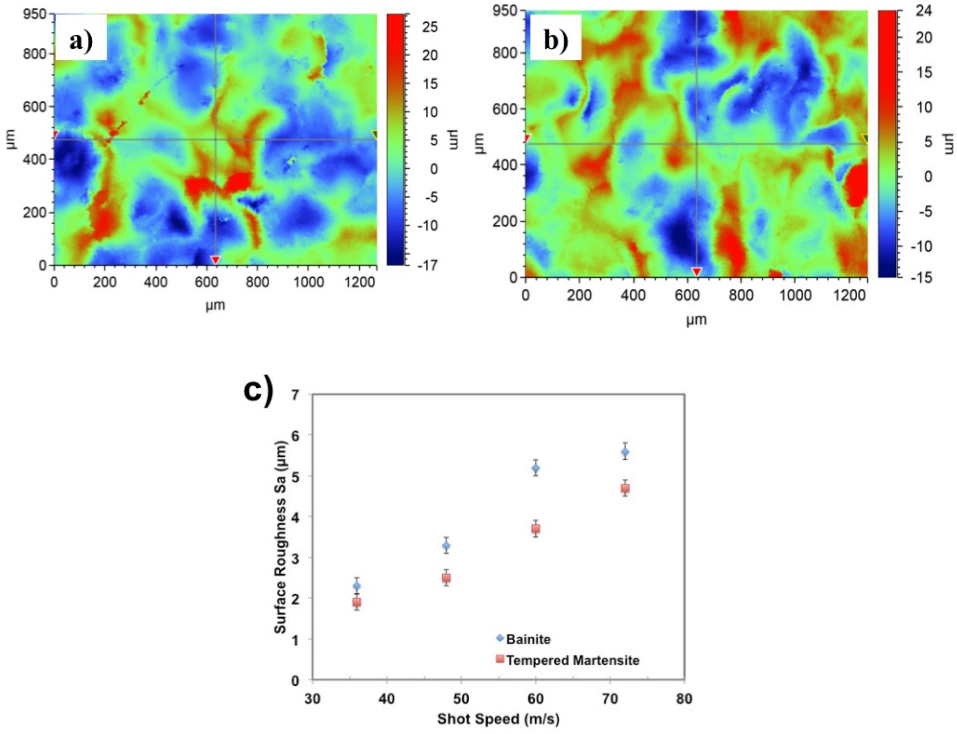

Figure 4.11: Maps of the surface roughness of the two microstructures. a) bainite, b) tempered martensite. c) Comparison of roughness values, average of 5 measurements, error bar represents the standard deviation.

The difference in the work hardening behaviour of the two microstructures, as found in the tensile test, can provide an explanation for the difference in the roughness and in the strain accommodation between the two studied microstructures. As far as the roughness is concerned, the bainitic specimen exhibits higher roughness because the initial impacts deform the surface plastically and produce dimples. As the bainite gets deformed, it work hardens, so the subsequent impact can only produce a smaller dimple. Thus, with the progress of the peening process, it becomes increasingly difficult for the new dimples to eliminate the increased roughness induced during the first impacts. This is not the case for martensite. Since the martensitic specimens have shown a relatively little work hardening in the plastic deformation zone, the shot impacts are more likely to create dimples of approximately the same size throughout the process, as the ridges around the dimples and the valleys are expected to show similar mechanical properties due to the limited extent of work hardening. For this reason, a tempered martensitic microstructure as initial microstructure is more likely to produce a shot peened component with lower roughness, if compared to a component with a bainitic microstructure.

4.3.4. Finite Element Modeling

The effectiveness of the shot peening treatment depends on a variety of parameters and optimization of their combination in an industrial environment is usually performed by trial and error. In order to provide a deeper understanding of the peening process, the described experiments were simulated using Finite Element Modeling (FEM). The FEM provides a visual and quantitative result of the shot indent, and can contribute to the understanding of the differences in the performance of the two microstructures (bainite and tempered martensite).

In **Figure 4.12**, the residual stresses after the impact of a single shot of 1 mm of diameter are displayed. It is shown that the residual stress field consists of a core of compressive stresses which is surrounded by regions in which tensile stresses appear. The map on the left corresponds to the impact of the shot on a bainitic target, while in the map on the right the target is tempered martensite. It is evident that the residual stress fields, although they have morphological similarities, they exhibit interesting differences.

The response of the two microstructures to the impact of a single shot can be compared analysing the distribution of the tensile and compressive stresses developed along a line parallel to the surface in correspondence of the maximum compressive stress as showed in **Figure 4.13**. It can be observed that the bainitic microstructure results in higher compressive residual stresses and slightly lower tensile stresses. The results shown in **Figure 4.14** indicate that for the material with

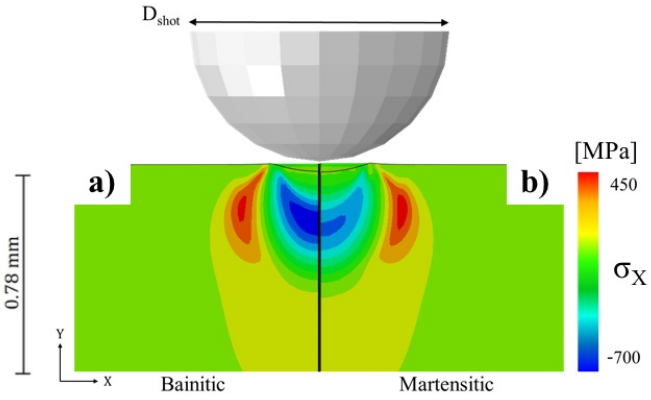

Figure 4.12: In-plane component of residual stresses resulting from the shot impact in: a) bainitic, b) martensitic target.

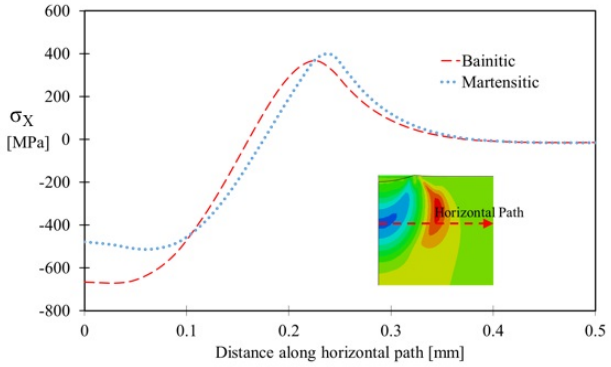

Figure 4.13: Residual stress distribution at the depth with the maximum residual stresses.

martensitic microstructure the residual compressive stresses as a function of the distance to the surface are lower and the plastic deformation is higher than for the material with bainitic structure.

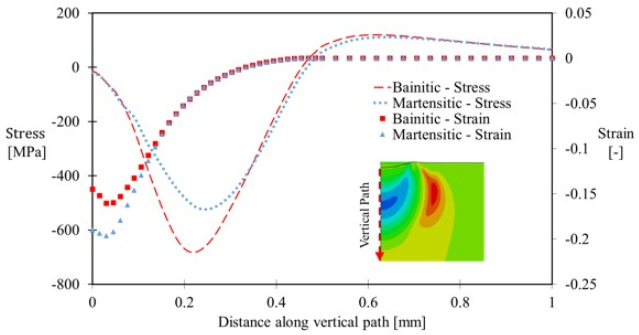

Figure 4.14: Residual stresses and plastic deformation along the vertical path. In both cases, bainite is compared with tempered martensite.

Complete surface coverage is critical for a successful SP treatment. Occasionally, geometrical aspects of the peened component or insufficient peening time may result in incomplete coverage. The FEM single impact simulations show that the beneficial compressive stresses are surrounded by a ring of potentially harmful tensile stresses. To eliminate the tensile stresses, the impacts need to occur close enough for the compressive stress fields to interact with each other. If this is not the case, the tensile stress fields add up to each other and create potential favourable fatigue failure initiation sites. To elaborate more on the important of coverage, the simulation of **Figure 4.2** was repeated for two sequential impacts after the initial one. In this way, is was possible to examine the effect of the pre-existing first impact on the impacts occurring afterwards on a pre-deformed and work-hardened material. In **Figure 4.15**, the residual stress field after the successive impacts at the cross section of the sample at the centre of the first impact is illustrated for two microstructures and shots of 1 mm diameter.

In **Figure 4.15a** the second impact occurs further away from the first one, so that the two dimples are created at areas, which are previously non-deformed. In **Figure 4.15b** the consecutive impacts occur at the ridge of the previously created dimple, 200 μm away from the centre of the first impact. The case of **Figure 4.15a** would be typical of coverage less than 100%, while **Figure 4.15b** illustrates a case of coverage starting to be complete. Apart from the beneficial compressive stress regions, tensile stress regions surrounding the ones of compressive stresses also exist, as a result of the shot impacts. In order for the effect of SP treatment to be-

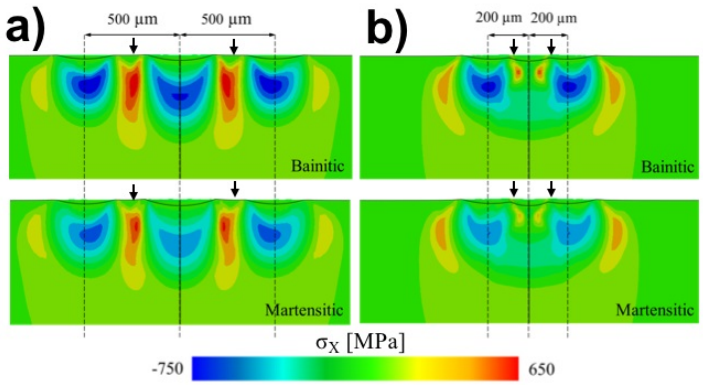

Figure 4.15: Sequential shot impacts on martensitic and bainitic targets a) Distance between impact points 500 μm, arrows indicate non-deformed surface. b) 200 μm, all surface is deformed as seen from the deflected black line. Top row: Bainitic target. Bottom: Tempered martensitic target.

come beneficial for fatigue life enhancement the layer of compressive stress needs to be continuous. Thus, the tensile stresses need to be annihilated by sequential impacts, at distances that cause the compressive stress fields to overlap. The contour plot shows that for the case with closer successive impacts, the residual stresses compressive and tensile, annihilate each other. In the case of bainitic specimens with residual stress fields created by impacts at the same distance from each other as in the case of tempered martensitic targets, there is still tensile residual stress remaining when the impacts occur at 200 μm distance. This means that, although in the case of bainitic microstructure higher beneficial compressive residual stress can be obtained, higher coverage would be required to create a continuous compressive stress field. Otherwise, in case of incomplete or insufficient coverage, the tensile stresses at the surface between shot impacts can act as potential crack nucleation sites during service. Higher coverage in terms of process control, would mean longer shot peening time.

4.4. Conclusions

Isothermal bainitic treatment is being investigated as an alternative, energy efficient heat treatment route for spring production. The heat-treated components are typically shot peened for fatigue life enhancement. In the present study, we show that:

1. The EBSD KAM maps show that the microstructurally affected layer is larger in bainitic targets than in the tempered martensitic ones. This is related to the difference in grain size between the two structures. The tempered martensitic

microstructure is much finer than the bainitic microstructure, the grain boundary density influences the strain accommodation.

2. The tensile tests analysed using the Kocks-Mecking plot show that bainite exhibit slightly higher yield strength than the tempered martensite, while the ultimate tensile stress of bainite is significantly higher and total elongation values are comparable.

3. Although the bainitic and tempered martensitic microstructures exhibit similar yield strength, the different work hardening behaviour affects the strain accommodation and the residual stress distribution. Shot peening on bainitic targets produces higher compressive stresses than the ones observed in tempered martensitic targets.

4. The fact that the microstructural differences lead to different residual stress distribution according to FEM, means that the two microstructures would require different peening parameters to obtain the optimum fatigue life enhancement.

5. The tensile residual stresses in the bainitic specimens, surrounding the compressive stresses, according to FEM simulations, are higher in magnitude. This fact could make the bainitic microstructure less tolerant in shot peening process flaws, as incomplete coverage.

6. White light interferometry measurements show that bainitic specimens exhibit higher roughness values compared with the tempered martensitic. This can be explained by the fact that bainite work hardens after primary impacts, making it less probable to deform by a subsequent impact. Tempered martensite shows limited work hardening, and thus is more probable to produce a smoother surface after peening.

References

1. S.Wang, Y. Li, M. Yao, R. Wang, J Mater. Proc. Technol. 73 (1998) 64-73.

2. A. Gariépy, H. Miao, M. Lévesque, Comprehensive Materials Processing Peen Forming (book chapter) 3 (2014) 295-329.

3. S. Kyriakou, Proceedings of 6th international conference on Shot Peening San Francisco, 1996, 183-190.

4. J.O. Almen, P.H. Black, Residual Stresses and Fatigue in Metals, McGraw Hill 1963.

5. S.M Hassani-Gangaraj, K.S. Cho, H.-J.L. Voigt, M. Guagliano, C.A. Schuh, Acta Mater. 97(2015) 105-115.

6. S.Bagheri and M. Guagliano, Surface Eng. 25 (2009) No1 3-14.

7. B. Okolo, F.Perez-Willard, J. Hawecker, D. Gerthsen, A. Wanner, J Mater. Process. Technol., 183 (2007) 160-164.

8. O.M.D.M. Messe, S. Stekovic, M.C. Hardy, and C.M.F. Rae, JOM 66 (2014) 12 2502-2515.

9. D.J.Child, G.D. West, R.C. Thomson, Acta Mater. 59 (2011) 4825-4834.

10. M. Guagliano, J. Mater Process. Technol 110 (2001) 277-286.

11. S.M. Hassani-Gangaraj, A. Mordi, M. Guagliano, IOP Conf. Series, Mater. Sci. Eng. 63 (2014) 012038.

12. C.Goulas, M.G. Mecozzi, J. Sietsma, Metall. Mater. Trans. A (2016).

13. A.LingWen, S.W.Wang, R.M. Ren, X.X.Yan, Applied Mech. And Mater. 55-57 (2011) 1138-1141.

14. P.van Liempt, J. Sietsma, Mater. Sci. Eng. A 62 (2016) 80-87.

5

Fatigue Properties of 51CrV4 with Bainitic and Tempered Martensitic Microstructure*

Chapter 5 focuses on the influence of heat treatment on the fatigue properties of 51CrV4 spring steel with fully bainitic and tempered martensitic microstructure. This study examines the influence of two different microstructures, one fully bainitic and the other tempered martensitic, on the fatigue performance of 51CrV4 spring steels. Microstructure characterization, which was performed by means of Scanning Electron (SEM) and Transmission Electron Microscopy (TEM), shows that lower bainite and tempered martensite exhibit different microstructural features, which are the martensite lath/bainite plate size, dislocation structure, and the size and distribution of carbide precipitates. Static mechanical properties were investigated by standard tensile tests. The results show a higher ultimate tensile strength for bainite than for tempered martensite. Kocks-Mecking analysis was employed to determine the yield stresses of the two microstructures precisely. The yield strengths were found to be similar. A physically-based model that was used to characterize the dislocation structure provided a valuable insight into the mechanical response of the two microstructures. Rotating-bending fatigue tests were carried out to evaluate the fa-

* Fatigue Properties of 51CrV4 with Bainitic and Tempered Martensitic Microstructure, by C. Goulas, K.O. Findley, F.M. Castro Cerda, M.G. Mecozzi, R.H. Petrov and J. Sietsma, to be submitted for publication to Mater. Sci. Eng: A.

tigue performance of the two microstructures. The fatigue performance of bainite was found to be superior to that of the tempered martensite. Fracture analysis of the fatigue specimens by stereo-microscopy and SEM reveals different morphology of the fracture surfaces for bainite and tempered martensite. On the fracture surfaces of tempered martensite, multiple initiation sites and ratchet marks are evident, while the fracture of bainite initiates mostly at a single point at surface inclusions. Final fracture zones of tempered martensite are dominated by micro-void coalescence. In contrast, the same zone in bainite mainly consists of quasi cleavage features, indicating lower fracture toughness for bainite.

5.1. Introduction

During the last years, the strict efficiency and CO_2 emission regulations steered the automotive industry to research and focus on reducing the overall weight of vehicles. This is achieved by optimising the function and reducing the weight of each individual component. Although much has been achieved for the Body-In-White with the successful development of the different generations of advanced high strength steels, other mechanical components, not constructed by thin sheet steel, are still produced by using conventional steels and heat treatments. One of these components are the flat springs, a type of spring often used in the suspension system of trucks. Flat springs are heavy components manufactured from conventional hot rolled bar of medium or high carbon low alloy steel. They typically gain the required strength level after a quenching and tempering (Q&T) heat treatment.

Quenched and tempered components have a tempered martensitic microstructure, that provides a good combination of strength, ductility, and fatigue resistance and meets the performance requirements for even the most demanding automotive applications [1]. Although the performance of Q&T components is considered sufficient, Q&T often results in quench cracking, distortion or undesired residual stresses [2]. Recently, research on spring steels focuses on springs with bainitic microstructures, instead of the typically used tempered martensitic microstructures. Bainite combines high strength with good ductility, while production of components with bainitic microstructures by heat treatment can be more cost and energy efficient in comparison to Q&T treatments. In a bainitic treatment, there is no need for a tempering step, so the heat treatment can be completed in one reheating cycle directly after hot forming. Without tempering, an indispensable, energy-intensive and costly step of the heat treatment can be omitted, and at the same time, quench cracking and distortion are minimized and even completely avoided.

The comparison of the mechanical properties and performance of components

with bainitic and tempered martensitic microstructure has been investigated in the past for various steel grades. Several studies have shown that components with a bainitic microstructure obtained by austempering (isothermal transformation in lower bainitic range) can exceed the mechanical performance of the same component if heat treated by quenching and tempering. Hehemann et al. found that austempered steels with lower bainitic microstructure have higher impact toughness than their equivalent treated by Q&T [3]. Tartaglia et al. showed that austempering results in slightly higher hardness, higher yield strength, ultimate tensile strength, and fatigue properties than Q&T treatment in a medium carbon, low alloy steel [4,5]. Similar findings were confirmed by other studies in high strength steels [6]. However, other studies have shown that Q&T steels perform better in fatigue than austempered steels, under the same monotonic properties [7]. Therefore, there is no definite answer for which heat treatment and microstructure results in better fatigue properties. Understanding the underlying microstructural reasons that lead to a certain fatigue behaviour becomes a necessity [8].

The purpose of this study is to investigate the microstructure and the fatigue properties of one medium carbon spring steel grade, 51CrV4, heat treated in two different ways. One heat treatment is isothermal bainitic (austempering) and another is quenching followed by high temperature tempering. The microstructural features playing the most important role in fatigue performance are identified via in-depth characterization. Stress (S) vs Number of loading cycles (N) curves are constructed through standard rotating bending fatigue tests. Tensile tests, fracture analyses and estimation of dislocation density using a recently developed model [9,10] help to elucidate the fatigue behaviour of 51CrV4 with tempered martensitic and bainitic microstructure.

5.2. Experimental procedure and sample preparation

5.2.1. Material

Hot rolled bars of 6 m long and 16 mm diameter were used in the study. The detailed composition as measured by Optical Emission Spectroscopy (OES) is shown in **Table 1**.

Table 5.1: Chemical composition of the 51CrV4 grade as measured by Optical Emission Spectroscopy.

Elements	C	Mn	Si	Cr	V
Wt.%	0.51	1.02	0.33	1.15	0.12

5.2.2. Fatigue and tensile specimen design and preparation

Hourglass-shaped fatigue specimens, as shown in **Figure 5.1**, were utilized for rotating bending fatigue (RBF) testing. Standard dog-bone tensile specimens were designed according to the standard ASTM E8M [11]. The samples, machined out of the 51CrV4 hot-rolled bars, were heat treated in salt baths according to the schemes of **Figure 5.2** to produce two different microstructures, isothermal bainite and tempered martensite with the same hardness. Final mirror finish was achieved by manual grinding using SiC papers and then polishing using diamond paste. Grinding and polishing were both performed along the specimen axis. The final roughness of the specimens (R_a) was less than 0.2 μm.

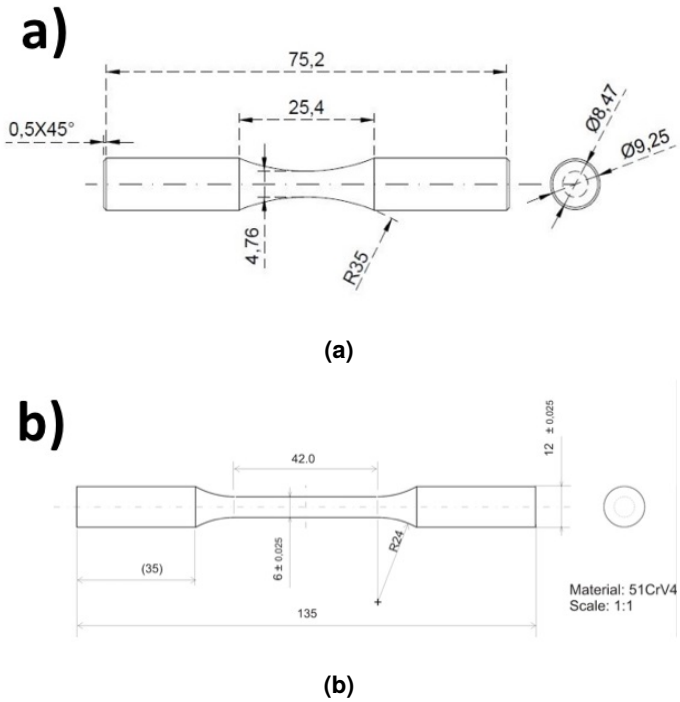

Figure 5.1: TSchematics of the specimens used for the mechanical tests: a) Rotating bending fatigue specimens. b) Tensile specimens. All dimensions in millimetres.

5.2.3. Heat treatment

After complete austenitisation for 5 min at 900 ^oC, one set of specimens was austempered at 300 ^oC for 1 h to produce lower bainite (dotted line in **Figure 5.2**) and the second set was initially quenched in salt at 180 ^oC, then quenched in water un-

til room temperature and finally tempered in a different salt at 480 ^{o}C for 30 min (solid line in **Figure 5.2**). The resulting hardness after both heat treatments was 46 HRC $\pm$ 1 HRC. The tempering time of the second treatment was adjusted for the hardness of both treatments is the same.

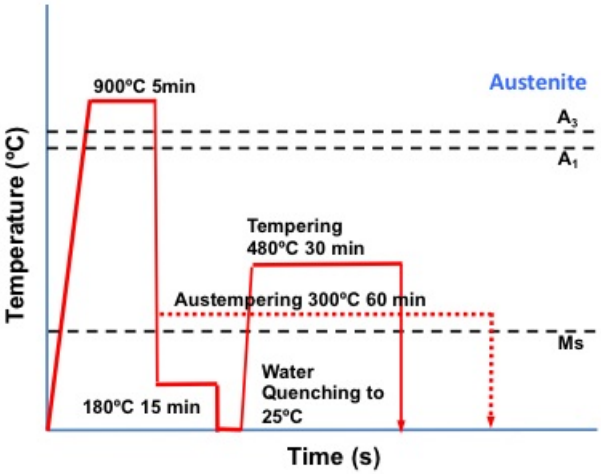

Figure 5.2: Heat treatment schedules used to produce bainite (dotted line) and tempered martensite (solid line) with the same hardness in 51CrV4.

5.2.4. Mechanical properties tests

The tensile tests were performed on an INSTRON 5500 tensile test machine at a strain rate of 10^{-3} s^{-1} with an extensometer of 25 mm attached to the centre of the gauge length. The Rotating Bending Fatigue tests were performed on 4 General Motors cantilever RBF200 machines at a frequency of 60 Hz. The frequency was chosen to avoid sample resonance, which was observed to reduce the fatigue life. No heat increase was observed during the tests. The four machines were calibrated to each other by using a calibration specimen with the same geometry as the actual specimens, on which a strain gauge was attached. The applied momentum in these experiments is adjusted by moving a weight over a calibrated beam. The strain resulting from each weight increment on the calibrated beam was recorded in order to ensure that the outcome of each machine is the same.

5.2.5. Stereo-microscopy, optical microscopy and SEM

The fractured specimens from the mechanical tests were preserved in a desiccator to prevent oxidation of the fracture surfaces until the analysis. The fracture surfaces

were observed by stereomicroscopy, and images were taken using a digital camera equipped with a macro-focusing bellows system. Higher magnification analysis was carried out in a FEI Quanta 450 FEG SEM operated at 20 kV. For the microstructural characterization, the specimens were cut out of the grip location of tensile specimens that were not used for the test. The samples were prepared following standard metallographic techniques. For etching, 2% Nital (ethanol 98% with 2% HNO3) was used.

5.2.6. Specimens for TEM analysis

For the preparation of TEM specimens, the heat treatments were repeated in a dilatometer on cylindrical specimens 10 mm long and 4 mm diameter, which were machined out of the same hot rolled bar. The results of the dilatometry for the bainite treatment are described in detail in Chapter 2 and [12]. After the treatment, the dilatometry specimens were then sliced to produce 0.7 mm discs, which were manually grinded to 80 μm thickness. Final thinning of the specimens was carried out on a Struers TenuPol-5 twin-jet electropolisher with an electrolyte consisting of 82 % vol. ethanol, 13 % vol. perchloric acid, and 5 % vol. glycerol at 20 ^{o}C and polishing voltage of 18.0 V. Electropolishing continued until perforation of the discs was achieved.

5.3. Results

5.3.1. Microstructure characterization

For the microstructure analysis by Scanning Electron Microscopy, the specimens treated in the salt bath and analysed in the framework of the study of Chapter 4 were used, since the heat treatments used in this study are the same. In **Figure 5.3a**, lower bainite microstructure is observed. It consists of bainitic ferrite plates with length varying between 3 and 8 μm, width of 0.8 to 1.5 μm, and fine cementite particles precipitated mainly within them, aligned and at an angle with respect to the growth direction of the plate. A minor fraction of martensite/austenite micro-constituents can be identified, as indicated by the arrow in **Figure 5.3a**.

In **Figure 5.3b**, tempered martensitic structure is shown. The microstructure consists of tempered martensite blocks 2-5 μm long and 0.35-0.8 μm wide as measured by linear intercept method, with cementite carbides precipitated both within and at the lath boundaries at seemingly random orientations.

There are specific morphological characteristics of the two structures that originate from the different transformation mechanisms. For the sake of consistency, in the present study the authors will accept the morphological definition of martensite

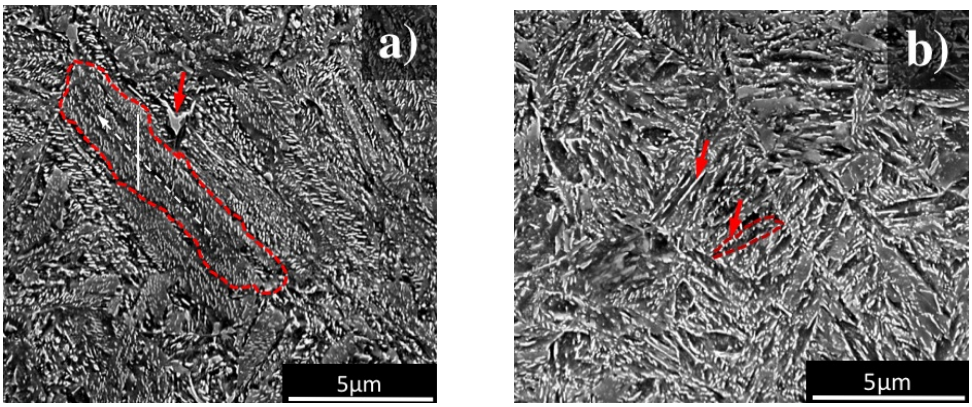

Figure 5.3: Scanning electron microscopy micrographs of the specimens with: a) bainitic microstructure, b) tempered martensitic microstructure.

sub-structure proposed in [13]. The plates of the bainitic ferrite are coarser than martensitic blocks of tempered martensite, and the size of the carbides in the case of tempered martensite are coarser than those found in bainite, for this particular treatment. This is consistent considering the temperature of each isothermal heat treatment. It is also important to mention the location of carbide precipitation. In bainitic structure, the carbides precipitate during the advancing of the α/γ interface [14], while the carbides in martensite are precipitating during tempering and are coarsening according to the tempering conditions [15]. To characterize the differences in both microstructures in more detail, high resolution microstructural analysis was also carried out by means of transmission electron microscopy.

The observation of the sample heat-treated isothermally at 300 ^{o}C for 1 h by Transmission Electron Microscopy revealed a bainitic ferrite plate matrix and aligned carbide precipitates, see. **Figure 5.4**. The precipitates are aligned at an angle with respect to the growth direction of the plate, which is a characteristic feature of the lower bainite microstructure. In both bright field images of **Figure 5.4**, there is a bright region in the middle of the bainitic ferrite plate, parallel to the growth direction of the plate. The strain contrast indicates homogeneous distribution of dislocations. In **Figure 5.4a** there is a prior austenite grain boundary crossing the micrograph from the top left to the bottom right. The difference in orientation between the two prior austenite grains is illustrated by the different diffraction contrast of bainite plates.

After quenching and tempering, the microstructure consists of lath martensite with carbide precipitates located both at the block boundaries and inside the blocks,

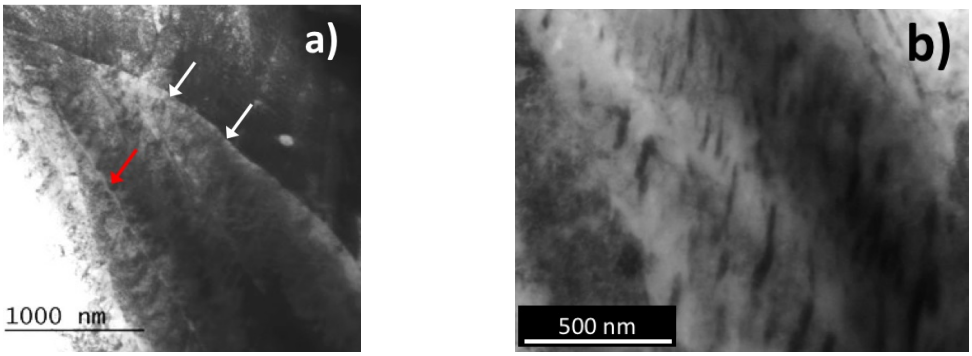

Figure 5.4: Bright Field TEM micrographs showing typical lower bainite microstructure of bainitic ferrite and aligned cementite precipitates. a) a prior austenite grain boundary is evident, marked with white dashed line. A carbide-free midrib is evident, a feature often found in bainite formed in medium carbon steels, marked with the red arrow. b) Higher magnification of a) showing the aligned carbides.

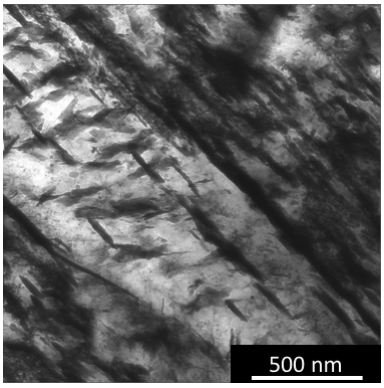

Figure 5.5: Bright Field TEM micrograph of tempered martensitic microstructure.

as shown by the bright field TEM image in **Figure 5.5**. The carbides are coarser than those observed for bainite and they appear in multiple orientations. The average size of martensite blocks was $3 \pm 0.5\ \mu$m, the average width of plates was $0.2 \pm 0.1\ \mu$m, measured by linear intercept method from the SEM micrographs. The dislocation substructure is different from the one observed in the case of lower bainite. As indicated by contrast in the micrographs, dislocations seem to be concentrated around the carbides and at the lath boundaries, while at the interior of the lath the dislocation density appears to be lower, because of the recovery taking place during high temperature tempering.

5.3.2. Mechanical Properties

The tensile results show that there are important differences in the mechanical behaviour of bainite and tempered martensite.

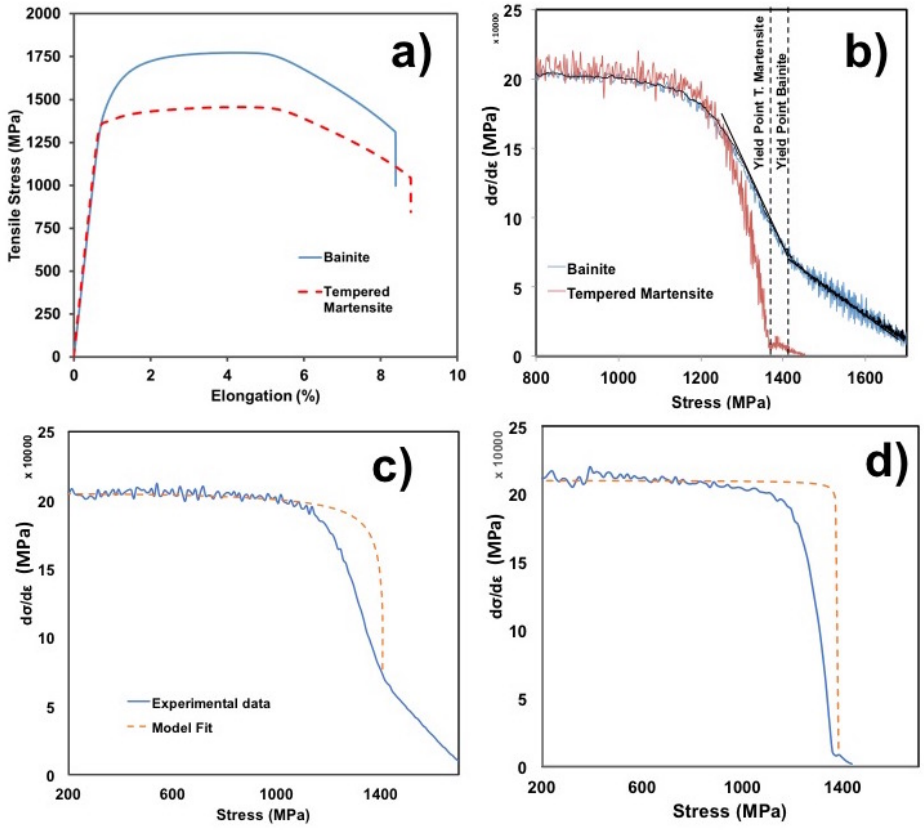

Figure 5.6: a) Tensile curves of standard specimens heat treated according to the schemes of Figure 1. b) Extended Kocks-Mecking plot of the two types of specimens, showing the yield stress (R_p). To determine the yield strength of bainite, two lines are fitted, one at the pre-yield region and one at the post yield region. c) Extended Kocks-Mecking plot fitted with the model described in [6-7] for quantifying the dislocation structure of bainite. d) The same plot applied for tempered martensite.

In **Figure 5.6a** full tensile curves are shown. Both structures yield under similar stress levels. Tempered martensite shows a sharp yield point in contrast with the bainite, which exhibits continuous yielding behaviour. **Figure 5.6b** shows the extended Kocks-Mecking analysis for the curves of **Figure 5.6a**; this analysis allows an accurate determination of the yield stress especially in the case of bainite, in

which the yield strength determination is challenging due to the absence of a clear yield point.

Using the above analysis, it was shown that the bainitic specimens have a yield strength of 1405 MPa $\pm$ 10 MPa. After reaching the yield strength, further loading leads to extensive work hardening and an ultimate tensile stress of 1780 MPa $\pm$ 20 MPa. The total elongation measured was 8 % $\pm$ 0.5 %. On the other hand, the martensitic specimens were different. Although the yield strength is similar to the bainitic specimens (1379 MPa $\pm$ 10 MPa), the post yield behaviour shows very limited work hardening leading to ultimate tensile strength around 1425 $\pm$ 10 MPa. The total elongation in this case is very similar to the bainitic specimens (8.5 % $\pm$ 0.65 %). In both cases, the reduction of area due to necking was measured to be 45 % $\pm$ 5 %.

Figure 5.7 shows the S-N curves from the RBF tests. It is evident that bainite exhibits superior fatigue behavior, having a fatigue endurance limit around 800 MPa compared to 600 MPa for tempered martensitic specimens. A fatigue life of 10^7 cycles (open marks in the plot) was considered runout. Three consequtive specimens that reached 10^7 cycles without failure, was considered as runout. The data points were fitted with the Basquin equation in the finite life region (10^4-10^6 load reversals) and with a horizontal line up to the endurance limit (2 x 10^7 load load reversals).

There is a change in the slope of both S-N curves at fatigue lives around 10^6 cycles, after which a small decrease in loading results in orders of magnitude of increase in fatigue life. The results for bainite were more scattered than those for tempered martensite. It is interesting to report that it was not possible to obtain points for the curve of tempered martensite in the 10^6 cycle region, since with a small reduction of stress amplitude the specimens reached the run-out threshold.

5.3.3. Fracture analysis

Representative specimens with bainitic or tempered martensitic microstructures that have failed after a comparable number of loading cycles were selected for fractographic analysis.

Stereo-microscopy was used for an evaluation of the fracture surfaces of the fatigue specimens. Significant differences were observed in the fracture behavior between bainite and Q+T, **Figure 5.8** and **Figure 5.9**.

Analysis of the fracture surface of bainitic specimens showed that under high stresses the initiation points were very few, or even one, **Figure 5.8a**, **Figure 5.8b**. The fracture surface was flat and rough, oriented perpendicular to the loading direction with a clear distinction of the stages of the fatigue failure. While the appearance of the fracture surface did not change for the specimens failed under low stresses,

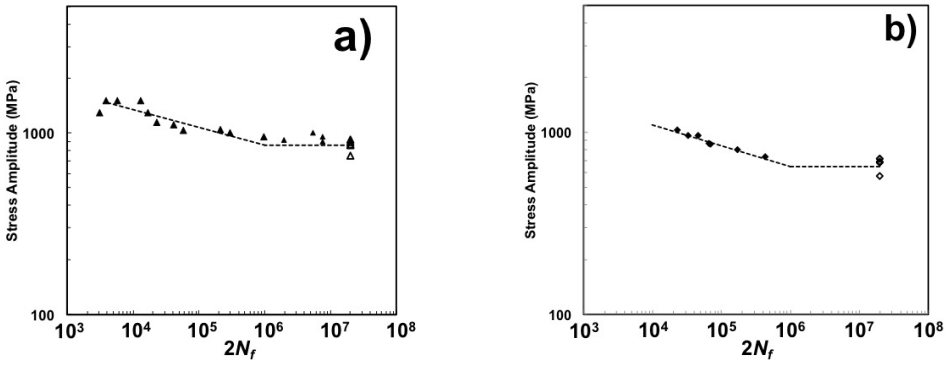

Figure 5.7: RBF results for polished specimens. a) Bainitic microstructure b) Tempered martensitic microstructure. Specimens with bainitic microstructure exhibit higher fatigue limit than quenched and tempered specimens.

Figure 5.8c, **Figure 5.8d**, subsurface initiation was identified after 7.5 x 10^6 cycles, **Figure 5.8d**.

The analysis of the fracture surface of specimens subjected to high stresses (around 1050 MPa for quenched and tempered and around 1300 MPa for bainitic), see **Figure 5.8a, Figure 5.8b, Figure 5.9a, Figure 5.9b**, reveal that both bainitic and tempered martensitic specimens have cracks initiated at the surface. The tempered martensitic specimens had multiple simultaneous initiation points at high stresses. The coalescence of the cracks during propagation leads to the formation of ratchet marks and quite irregular fracture surfaces. The glossy appearance of the fracture surfaces seen in **Figure 5.9a** can be attributed to the smearing of the two sides of the cracked specimen before failure. Under lower stresses (650-750 MPa) a single crack initiation point is present and ratchet marks are not evident in the tempered martensitic specimens of **Figure 5.9c, Figure 5.9d**.

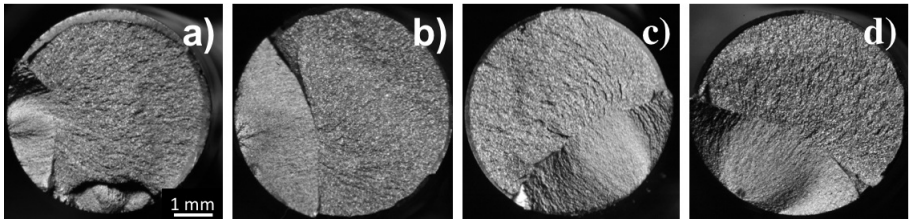

Figure 5.8: Fracture surfaces of bainitic specimens: a) 1514 MPa 5.700 Cycles b) 1303 MPa 13.400 Cycles c) 1041 MPa 58.600 Cycles d) 955 MPa 7.470.000 cycles.

Scanning electron microscopy was employed to analyze the crack initiation re-

gions and the fracture surfaces at different stages of the fatigue failure, **Figure 5.10a-f**. Fatigue striations were found in the Stage II crack growth regions of the fracture specimens in both cases, with their size being similar, **Figure 5.10b** and **Figure 5.10e**. Stage II crack growth stage refers to the stage at which a well defined crack grows normal to the direction of maximum tensile stress. The images were taken at approximately equal distances from the crack origin. The final failure fractographs were very different. The martensitic specimen showed a final failure governed by microvoid coalescence, while in the bainitic specimen the final failure zone is dominated by quasi-cleavage features.

5.4. Discussion

5.4.1. Relation of microstructure to tensile properties

The present study shows that a change in the heat treatment scheme in spring steels can have an important impact on the fatigue performance. The reason stems in the morphology of each developed microstructure, particularly in platelet and block sizes, carbide precipitate size, distance between carbides, and dislocation structure. In treatments with the same austenitisation temperature, which leads to a same prior austenite grain size, bainitic ferrite is coarser than tempered martensite. This is expected to influence the fatigue performance [16]. The precipitates in bainite are finer than the ones found in martensite, although the austempering treatment is longer in time. This is attributed to the fact that the carbides in bainite form during bainitic ferrite formation, in contrast with the tempered martensite, in which the carbides form exclusively during tempering.

Martensite is a phase forming with high dislocation density during quenching, due to the character of the martensitic transformation. In addition, it accommodates in its lattice the carbon that was present in the austenite. During tempering, two phenomena occur affecting the microstructure and the mechanical behaviour of martensite: carbon is depleted from the bcc lattice forming carbides and recovery

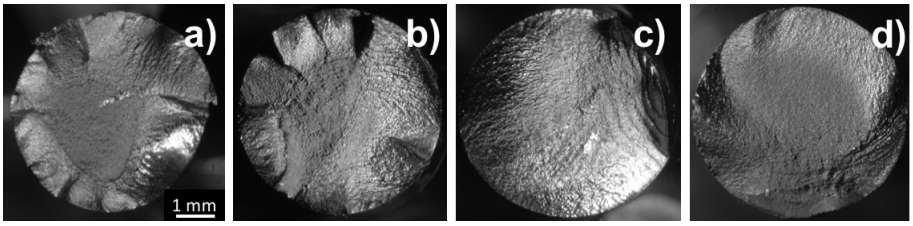

Figure 5.9: Fracture surfaces of tempered martensitic specimens: a) 1026 MPa 11.300 Cycles b) 960 MPa 16.300 Cycles c) 865 MPa 33.100 Cycles d) 645 MPa 167.800 cycles.

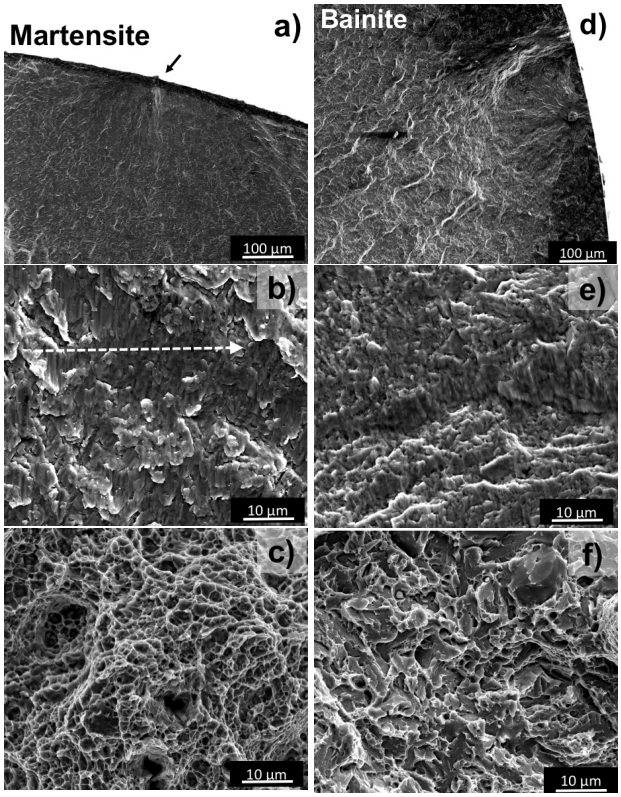

Figure 5.10: Scanning electron microscopy fractographs of fatigue samples with tempered martensitic and bainitic microstructure, both failed after 104 cycles. a-c: tempered martensite. d-f: bainite. a) initiation site at the surface. b) fractograph, showing striations, from a location belonging to Stage II crack growth. c) final failure by microvoid coalescence. d) initiation at inclusion. e) stage II fractograph showing striations and similar features as b). f) fractograph from final failure area, showing quasi-cleavage features.

of dislocations takes place. Thus, high temperature tempering leads to a structure with the dislocations mostly present close to the lath boundaries and around the precipitates. Bainite on the other hand, can be expected to contain a lower dislocation density [17]. Lower bainite forms in 51CrV4 steel at lower temperatures than those used for high temperature tempering, at which dislocation recovery does not occur. To gain further insight into the reasons explaining the different behaviour of the two types of specimens, we use a recently proposed dislocation model to characterise the dislocation structure of the two microstructures [9, 10].

The dislocation structure determines the anelastic contribution to the pre-yield deformation behaviour. Under a given stress below the yield stress, dislocation

segments bow out in a reversible manner, causing the so-called anelastic strain. This strain leads to the instantaneous Young's modulus that is given by

$$\Theta_{pre} = \frac{\bar{M}^2 E s^3 \sqrt{1-s^2}}{\bar{M}^2 E s^3 \sqrt{1-s^2} + \rho L^2 (1+\nu)(s - \sqrt{1-s^2} arcsin(s))} \tag{5.1}$$

where Θ_{pre} is the slope of the stress-strain curve, $(\frac{d\sigma}{d\varepsilon})$ for stresses lower than the yield stress, $\bar{M}$=3.06 is the Taylor factor for steels, E = 210 GPa is the theoretical elastic modulus of the crystal lattice, s is the stress normalized by the critical stress (average stress under which the dislocations become Frank-Read sources), ρ is the dislocation density, L is the average dislocation segment length and ν = 0.30 is the Poisson's ratio.

Applying **Equation 5.1** to the data of the extended Kocks-Mecking plots in **Figure 5.6** enables an approximation of the dislocation density and the average dislocation segment length for bainite and tempered martensite, for which the data are given in **Table 5.2**. The ranges of the reported ρ and L values represent the results obtained by using maximum and the minimum values for the pre-yield slope and the yield stress respectively. The dislocation segment length defines the applied stress, under which the dislocations will become Frank-Read sources [9]. Longer dislocation segments will become Frank-Read sources under lower stress than short segments.

Table 5.2: Dislocation structure characteristics for lower bainite and tempered martensite.

Microstructure	ρ(m^{-2})	L(nm)
Bainite	1.74 x 10^{14} - 2.67 x 10^{14}	43 $\pm$ 1
Tempered Martensite	2.55 x 10^{13} - 6.65 x 10^{13}	45 $\pm$ 1

Based on the dislocation density estimation carried out using **Equation 5.1** and data from **Figure 5.6**, it was found that the decrease of dislocation density of the martensite after tempering is significant, leading to a value almost an order of magnitude less than the one for bainite. Although the calculated average dislocation segment lengths are similar for the two microstructures, the difference in work hardening rate curves (cf. Figure 5.6b) suggests that, in the distribution of dislocation segment lengths, the range of lengths is wider for bainite than it is for tempered martensite.

The wide range of dislocation segment lengths in bainite could justify the gradual change of slope of the work hardening rate curve in **Figure 5.6c**.

5.4.2. Fatigue and fractography

In the finite-life region of the S-N curves, the Basquin equation describes the relation between the stress amplitude,σ_α, and the number of cycles to failure N_f, as

$$\sigma_\alpha = \sigma'_f(2N_f)^b \tag{5.2}$$

where σ'_f represents the fatigue strength coefficient, and b is the fatigue strength exponent.

The Basquin equation parameters for the finite life region were determined from a logarithmic plot of the stress amplitude vs number of load reversals (twice the number of loading cycles). The Basquin parameters are shown in **Table 5.3** and are similar to the values reported in literature for other heat treated, medium carbon low alloy steels [18]:

Table 5.3: Basquin Equation Parameters for Isothermal Lower Bainitic and Tempered Martensitic 51CrV4 specimens.

Microstructure	σ'_f(MPa)	b
Bainite	3359	-0.099
Tempered Martensite	3182	-0.115

Based on the tensile properties of bainite and tempered martensite, it was interesting to observe differences in the fatigue properties as well. The bainitic specimens with a higher Ultimate Tensile Strength showed higher fatigue limit than the tempered martensitic specimens [19].

The fractographic analysis revealed that multiple crack initiation occurs in tempered martensite, while this is uncommon for bainitic specimens. Considering that the surface was mirror polished in both types of specimens, it can be argued that crack initiation is connected to microstructural features. In high cycle fatigue, most of the fatigue life is consumed for crack nucleation to occur. In this case, the fatigue limit can be related to the resistance of the microstructure to crack nucleation. In high strength quenched and tempered and bainitic steels, crack nucleation usually occurs at non-metallic inclusions and not at microstructural features [20]. In order for cracks to nucleate at microstructural features, plastic damage and slip band formation needs to occur under fatigue loading, which has less probability to occur in high strength materials.

In the present study, multiple initiation sites are identified in tempered martensitic specimens, while usually single-point initiation occurs in bainite. Given the fact that both types of specimens were produced by the same bar of 51CrV4 steel, the inclusion distribution and size can be considered to be equal in both cases. This means

that two competing crack nucleation mechanisms are active - the one which is related to inclusions and the other which is related to local plasticity. The difference in strength between bainite and tempered martensite can make one mechanism dominant or the other. In the lower strength tempered martensite, cracking due to plasticity-related fatigue damage in the microstructure is more likely to occur than in higher strength lower bainite. The extensive precipitation is evident in martensite, as seen in **Figure 5.5**, could facilitate the plasticity induced failure. Cementite precipitates, not only weaken the block boundaries, but also soften the martensitic matrix, especially the near-boundary area, promoting inhomogeneous slip and slip localization [8]. In contrast, in bainite the microstructure is stronger and the precipitates are finer, making the inclusions the most probable sites for fatigue crack initiation. This difference in the crack initiation mechanisms can explain the larger scatter of points on the S-N curve of bainite. Since the crack nucleation is controlled by inclusions, the probability of having an inclusion at the surface or close to it defines the fatigue life. On the other hand, if the crack initiation is connected to the microstructural features, localised slip can occur anywhere at the surface.

In the propagation zone, the fractographs of the two microstructures exhibit striations which could be helpful in quantifying the crack propagation distance per loading cycle. The analysis of **Figure 5.10b** and **Figure 5.10e** reveals that the distance between the striations is very similar for bainite and tempered martensite for similar fatigue lives and at equal length from the crack origin.

As far as the final failure zone is concerned, the bainitic specimens showed in all cases quasi-cleavage features, **Figure 5.10c**, while the tempered martensitic specimens failed in most specimens studied by a mechanism dominated by microvoid coalescence, **Fig 5.10f**. The smearing of the two sides of the tempered martensitic specimens indicates that the final failure did not occur in a single loading cycle, but the specimen resisted the total fracture for a few cycles, leading to a fracture surface with shiny propagation zones and ductile final failure. In contrast, the quasi-cleavage features of bainite and the absence of smearing indicate that final fracture occurred suddenly after reaching a certain critical stress. This difference could be explained by the difference in dislocation structure between bainite and high temperature tempered martensite. The tensile behavior of bainite indicates that the dislocations are mobile, so they can contribute to work hardening. On the other hand, in high temperature tempered martensite the dislocations are partially recovered and most of the remaining dislocations are sessile, either because of the segregation of carbon and formation of Cottrell atmospheres or because they are pinned by precipitates. The quasi-cleavage final failure of bainite could be an indication of low toughness of this microstructure [21].

5.5. Conclusions

In the present paper, we present a comparative study on the fatigue properties of the widely used 51CrV4 spring steel, in isothermal bainitic and tempered martensitic condition. Through detailed microstructure characterization, mechanical properties tests and fracture analysis, it is concluded that:

1. The bainitic microstructure, under tension, undergoes significant work hardening before reaching the ultimate tensile strength.

2. A physically based model was successfully applied to characterize the dislocation structure of bainite and tempered martensite. It was found that the dislocation density of bainite is higher than the one of tempered martensite, while the average dislocation segment length is similar for both microstructures.

3. 51CrV4 exhibits improved fatigue behaviour in the bainitic condition in comparison to the quenched and tempered condition.

4. The fatigue properties in the present case seem to be linked to the post-yield behaviour of the material and not by the yield strength.

5. Fatigue failure in bainite was not found to initiate on microstructure-related defects in the case of bainite. It was located either at the surface or at subsurface (Al, Ca) spherical inclusions. On the other hand, the multiple initiation points found in high temperature tempered martensite can be associated with plasticity-related fatigue damage. This difference shows that different crack initiation mechanisms are triggered depending on the strength of the material.

References

1. G. Krauss, Quench and Tempered Martensitic Steels: Microstructures and Performance. ASM international, Materials Park, Ohio, USA, 2015.

2. K. Brandenberg, K. Hayrynen, and J.R. Keough, Austempered Gears and Shafts: Tough Solutions, Gear Technol., 18 (2001) 2 pp. 42-50.

3. R.F. Hehemann, V.J. Luhan, and A.R. Troiano, Trans ASM, 49 (1957) pp. 409-426.

4. J.M. Tartaglia, K.A. Lazzari, G.P. Hui, and K.L. Hayrynen, Metall. Mater. Trans A 39 (2008) 3 pp. 559-576.

5. J.M Tartaglia. & K.L. Hayrynen, J. of Materi Eng and Perform 21 (2012) pp. 1008-1024.

6. H. Hengerer, Sulzer Tech. Rev., 51 (1969) 2 pp. 72-79.

7. P. Raviazz and C. Giometto, Rev. Met., 67 (1970) 6 pp. 531-538.

8. C.S. Lee, K.A. Lee, D.M. Li, S.J. Yoo, W.J. Nam, Mater. Sci. Eng. A: 241 (1998) 30-37.

9. P. van Liempt and J. Sietsma, Mater Sci. Eng. A 662 (2016) pp. 80-87.

10. Z. Arechabaleta, P. van Liempt and J. Sietsma, Acta Mater. 115 (2016) pp. 314-323

11. ASTM E8/E8M - 15a "Standard Test Methods for?Tension Testing of Metallic Materials", ASTM international, 2015.

12. C. Goulas, M.G Mecozzi, J Sietsma, Metall. Mater. Trans. 47A (2016) 3077-3087.

13. Phase transformations in Steel vol. 2, Chapter 2: Morphology and substructure of martensite in steels, T. Maki, 2012, Elsevier.

14. A. Borgenstam, M. Hillert, J. ?gren, Acta Mater. 57 (2009) 11 pp. 3242-3252.

15. G. R. Speich and W. C. Leslie, tempering of steel, Metall. Trans. 3A, 1972, 1043-1054.

16. Tomita, Y. & Okabayashi, K. Metall. Trans. 17A (1986) pp. 1203-1209.

17. G.Spanos, H.S.Fang and H.I. Aaronson, Metall. Mater. Trans. 21A (1990) pp. 1381-1390.

18. M.L. Hayne, P.I. Anderson, K.O Findley, C.J. Van Tyne, Metall. Mater. Trans. 44A (2013) pp 3428-3433.

19. P.G. Forrest, Fatigue of Metals, Pergamon Press, London, 1962.

20. K.O. Findley, R.L. Cryderman, A.B. Nissan, D.K. Matlock, Iron and Steel Technol, 10 (2013) pp. 234-243.

21. D.R. Johnson and W.T Becker, J. Mater. Eng. and Perform. 2 (1993) pp. 255-263.

6

Microstructure evolution of medium carbon low alloy steel under rapid thermal cycles*

Abstract

This chapter contains an alternative approach to heat treating spring steels by using ultrafast induction heating. Rapid thermal cycles may lead to chemical heterogeneity on a microscopic scale, which can be used to create multiphase microstructures in a single process step. For this reason, a comparative study on the microstructural changes after conventional (20 $^oC/s$) and ultrafast (300 $^oC/s$) heating is performed on a soft annealed, medium-carbon low-alloy steel with an initial microstructure consisting of ferrite and spheroidised cementite. The heating is followed by very short soaking at high temperature (austenitic range) followed quenching to room temperature. The ultrafast heating leads to the formation of compositional gradients within austenite as confirmed by transmission electron microscopy (TEM) and diffusion simulations performed with the software Dictra. A thorough investigation of the microstructures by TEM shows that the initial chromium-rich carbides dissolve only

* The effect of heating rate on the microstructure of a soft annealed medium carbon steel, by S. Papaefthymiou, C. Goulas, F.M. Castro Cerda, N. Geerlofs and R. Petrov, Steel Res. Int. 87 (2017)

partially during the rapid heat treatment. The product microstructure after an Ultra-Fast Heat Treatment (UFHT) is thus a mixture of undissolved carbides embedded in a very fine combination of martensite and bainite. It is shown that the phase distribution after the UFHT is directly related to carbon gradients in the microstructure.

6.1. Introduction

Advanced high strength steels (AHSS), applied in automotive body-in-white, led to reduced weight, emissions and increased passenger safety, meeting political and environmental dictates. Steel is able to successfully compete with light alloys due to strengthening effects of the microstructures (ultimate tensile strength (UTS): higher than 1.5 GPa; total elongation: 12-20%). Strengthening mechanisms, i.e. solid solution and carbide strengthening, are well known and fully exploited. Additionally, Transformation Induced Plasticity (TRIP) and Twinning Induced Plasticity (TWIP) effects are nowadays exploited based on the continuous annealing furnace technologies that were designed for the development of these steel families [1-5]. Current approaches to develop steel concepts focus on incorporating ultra-fine grained nano-precipitate hardening phases, mainly of ferrite and bainite. Novel processing routes are required [6-9], which are not only based on ferrite (α) grain refinement. The volume fraction, morphology and distribution of retained austenite (γR) and/or martensite (α') strongly affect the mechanical properties of advanced high strength steels [4, 6-8]. Mechanical behaviour of steels can benefit from multiphase microstructures consisting of hard and soft phases because the stress and strain partitioning can be optimised to enhance tensile strength and ductility [4, 6-8]. Ultra-Fast Heat Treatment (UFHT) of low and medium carbon steel has been proposed as a realistic approach [9, 10] to produce third generation AHSS, given the wide range of final microstructures and hence of mechanical properties that can potentially be reached.

Rapid thermal cycles may lead to chemical heterogeneity on a microscopic or even nano-scale in steel and a set of multiphase microstructures in a single process step can be achieved. This concept is in fact well known [11-14] from welding metallurgy and induction hardening of medium carbon steels. Rapid heating has been widely studied from the microstructural point of view in laboratory scale set-up [15] and recently at industrial scale by G. Cola in the form of "flash bainite", a microstructure product of a very short heat treatment process, which involves flame heating and water quenching [16]. This heat treatment produces a very fine, multiphase microstructure with properties equivalent to the ones obtained by other well established Advanced High Strength Steel (AHSS) heat treatments, using commercially

available medium carbon steel grades without high Silicon (Si) and high Manganese (Mn) contents.

The formation of austenite from spheroidised microstructures has been broadly studied under isothermal and anisothermal conditions [13, 17-24]. It has been early established that the nucleation of austenite in such initial microstructures takes place at cementite-ferrite and ferrite-ferrite interfaces and the growth stage is controlled by carbon diffusion. Similar features hold when anisothermal formation of austenite takes place in the ferrite and austenite intercritical region. When high heating rates are applied, it has been found that the austenite formation can be accomplished by a massive mechanism in either a ferrite and spheroidised cementite [15] or ferrite and pearlite [18, 25, 26] initial microstructure. Schmidt et al. used the temperature T0 to define the thermodynamic threshold at which the transition from diffusion controlled to interface controlled transformation during heating can take place [25], in spite of Hillert [27] already having shown that the actual limit for massive product formation does not fall within the two phase region and can therefore not be defined by T0. Carbon gradients have been widely reported [15, 17, 28] to be present in the microstructure after fast heating experiments. Mixtures of martensite (α') and bainite (αB) have been reported as the main transformation products of rapid heating cycles.

For accurate control of the microstructure after an ultrafast cycle, the transformation behaviour needs to be understood and exploited. This can lead to altogether fundamentally new alloy design paths. The goal of this study is to characterise and understand the microstructure formation during conventional (20 $^{o}C/s$) and ultrafast (300 $^{o}C/s$) heating cycles. The approach has been to examine the potential application of UFHT to create multiphase microstructures in one step, without the necessity of complicated, continuous annealing lines.

6.2. Experimental procedure

6.2.1. Dilatometry

Dilatometry experiments form a reliable method to perform precision heat treatments for the present study. Samples of a Cr-Mn-steel were received in a shape of hot rolled bars with dimensions 95 mm width x 49 mm thickness x 5500 mm length in soft-annealed condition with a microstructure of spheroidised cementite and ferrite. Chemical composition analysis was performed on 30x30 mm2 cross sections of the bars, transverse to the rolling direction, by means of Optical Emission Spectroscopy (OES) and the results are shown in Table 6.1. Dilatometric plate shaped samples (10 mm length x 4 mm width x 2 mm thickness) and cylindrical samples (10 mm

length and 3 mm diameter) were prepared using Wire Electro-Discharge Machining (EDM) from cross sections cut out of hot rolled bars. The dilatometry tests were performed in a Bähr 805A Quench dilatometer. Experiments were performed with two thermocouples: one at the edge and the second, the control thermocouple, at the centre of the sample in order to check the temperature gradient and, thus, to make sure that the transformations take place throughout the sample. It was found that for the plate shaped specimens, even in the cases in which the sample cross section was not cylindrical, the temperature variation was within 10^oC. All samples were heated in vacuum at either $20^oC/s$ or $300^oC/s$ to peak temperatures (TP) of 900^oC and 950^oC respectively for a maximum holding time at the peak temperature of 0.3 s. Subsequently, the samples were quenched with helium at -300oC/s to room temperature. The dilatometric data were post-processed by the lever rule method and the austenite fractions formed during heating were quantified.

Table 6.1: Chemical composition of the medium carbon low alloy steel used in the study (Element (wt.%)).

C	Mn	Si	P	S	Cr
0.42	1.43	0.40	0.009	0.010	1.23

6.2.2. Microstructure characterisation

For the Optical Microscopy (OM) observations, samples obtained from the dilatometer were sectioned at the position of the control thermocouple and then mounted on a sample holder with the plane of the cut being the observation plane for the microstructure characterisation. This ensured that the thermal cycle at the observation plane was the one measured by the thermocouple. Sample preparation included grinding with silicon carbide (SiC) abrasive papers up to 2400 grit, polishing with 3 μm and 1μm diamond paste and a final step of colloidal silica solution. Chemical etching for revealing in a first step the microstructure was performed with Nital 2%. Afterwards, the same sample preparation was repeated and the etching was performed this time with 10% aqueous sodium metabisulphite tint etching solution. The aim of this second etching was to reveal the multiphase microstructure and to distinguish the areas of interest (e.g. carbides, retained austenite, bainitic ferrite) for subsequent study with higher magnification techniques. The etching was performed three times in each sample to ensure that colour effects are reproducible. Disk specimens for TEM were cut from the dilatometry samples, manually ground to a thickness of 80 μm and then the final thinning was carried out with precision ion polishing system (PIPS). Scanning Electron Microscopy (SEM) analysis was carried out in a Field Emission Gun SEM (FEG-SEM) operated at 10 kV equipped with

a Back-Scatter Electron (BSE) detector and an Energy Dispersive Spectroscopy (EDS) detector.

Transmission electron microscopy (TEM) measurements were conducted with a high resolution JEOL JEM-2100, operating at 200 kV, equipped with an Oxford energy-dispersive X-ray spectroscopy (EDS) microanalysis system.

Electron Back-Scatter Diffraction (EBSD) analyses were performed using FEI Quanta^{TM} 450-FEG-SEM operated at 20 kV, with a beam current corresponding to FEI spot size 5 for an aperture of 30 μm and a working distance of 16 mm. The sample was 70^{o} tilted towards the EBSD detector and the EBSD patterns were acquired with a Hikari detector operated with EDAX-TSL-OIM-Data Collection version 7 software in hexagonal scan grid. Step size was 50 nm. The orientation data were analyzed using the following grain definition: misorientation higher than 5and a minimum of 5 points per grain. Points with a confidence index (CI) lower than 0.1 (usually less than 0.5% of all raw data) were excluded from the measurement.

6.2.3. Hardness measurements

Using optical microscopy observations at 1000x magnification, selected Vickers micro-hardness measurements $HV_{0.5}$ were performed to identify the hardness in several points within the microstructure. Based on the colour etching we aimed to identify the low and high segregation regions and to monitor the hardness in such areas.

6.2.4. Dictra Simulations

Simulations of the distribution of alloying elements during the different thermal cycles were carried out in order to study the kinetics of austenite formation and the compositional gradients in both parent and new formed phases. The simulations were performed using the Dictra software, which allows the computation of diffusion-controlled transformations in multicomponent metallic systems. The general description of the software and the models can be found elsewhere [29-31]. The microstructure was simulated assuming an initial spherical representative volume and phase distribution as indicated in **Figure 6.1**. The dimension of the fine and coarse particles, r_θ, were set based on the size of cementite particles measured in the experimental microstructure; the domain dimensions r_T were adjusted to get in both simulations the same cementite volume fraction, f_θ, equal to the experimental value. The simulation input parameters are reported in **Table 6.2**. Heating cycles consisting of three thermal stages (heating, holding and quenching) were simulated. The heating rates in one case were 20 $^{o}C/s$ (conventional) and in the other 300 $^{o}C/s$

(ultrafast), whereas the holding time and quenching rate were kept constant for both cases equal to 0.3 s and -300 $^oC/s$, respectively. In order to reproduce the experiments, the actual onset of austenite formation was considered ($A_1^{20^oC/s}$ and $A_1^{300^oC/s}$), instead of the equilibrium transition temperature. The peak temperature T_P was considered as the temperature of formation of 100% austenite. It was assumed that the temperature remains constant during the short stay of 0.3 s at the peak temperature. In the case of cooling, the process was stopped at the thermodynamic A_1 temperature, calculated with ThermoCalc software. The $A_1^{20^oC/s}$, $A_1^{300^oC/s}$ and T_P temperatures were obtained from dilatometric experiments.

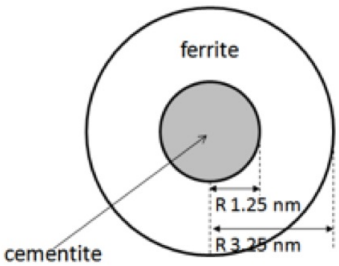

Figure 6.1: Model of the ferrite and cementite initial microstructure used to simulate the thermal cycle.

Table 6.2: Parameters introduced in the Dictra calculations. $f\theta$ is the volume fraction of cementite, values are in μm.

	r_θ	r_T	f_θ
Fine	12.53 x 10^{-3}	32.2 x 10^{-3}	0.06
Coarse	0.25	0.64	0.06

Diffusion calculations were performed using DICTRA version 2015b, MOBFE3. Carbon diffusion in austenite is an active process during ultrafast heating. Additionally, the local conditions at the γ/α interface affects the progress of the transformation. For this reason, simulations of the microstructure during heating at different heating rates were carried out. The simulations were performed using the Dictra software, which allows computing the diffusion-controlled transformation kinetics in multicomponent metallic systems. A ferrite and cementite aggregate was simulated assuming an initial spherical representative volume and phase distribution as indicated in **Figure 6.1**. Two heating rates were simulated: 20 $^oC/s$ and 300 $^oC/s$. It was assumed that instantaneous formation of austenite occurs, when the system reached the $\alpha \rightarrow \gamma$ equilibrium range. The specific initial chemical composition of each phase was estimated with ThermoCalc at a temperature in the range of fer-

rite and cementite equilibrium (677 ^oC). Calculated volumetric phase fractions were estimated neglecting the effect of carbon on the phase density.

6.3. Results

6.3.1. Dilatometry

Application of the UFHT via dilatometry ensures the monitoring of phase transformations. The dilatometric curves in **Figure 6.2** show that the formation of austenite during heating is complete at each heating rate before reaching the peak temperature, since there is an evident change of slope after reaching A_{c3}. The change in length versus temperature (**Figure 6.2a**) curves of the two treatments reveal a significant shift of the A_{c1} and A_{c3} temperatures, as well as an increase of the martensite start temperature (M_s) on cooling, as the heating rate is increased. **Figure 6.2b** shows that the overall austenite formation is displaced to higher temperatures when the heating rate is increased from 20 $^oC/s$ to 300 $^oC/s$.

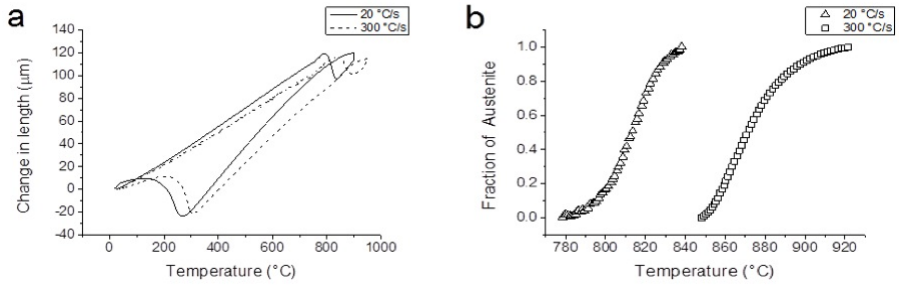

Figure 6.2: Dilatometric curves of a) change in length and b) austenite phase fraction versus temperature, for conventional and high heating rate.

6.3.2. Microstructure characterisation

The initial microstructure was a typical soft annealed microstructure with a very fine ferrite plus spheroidised cementite with a hardness of 220 $HV_{0.5}$ ($\pm$15 $HV_{0.5}$). The ferrite grain size of the initial microstructure ranges within 2-6 μm. **Figure 6.3a** shows a representative Optical Microscopy photo of the as-received fine spheroidised microstructure. **Figure 6.4a** shows a detailed TEM micrograph of the as-received fine spheroidised cementite as well as chromium carbide. The carbides are evenly and homogeneously distributed within the ferrite matrix, as it is evident from Figure 6.3a; their size, estimated by TEM analysis, varies between 10 nm and 250 nm. The chemical composition of the carbides was analysed using spot EDS analyses in the

TEM. **Figure 6.4a** illustrates some large carbides present within the microstructure. According to Selected Area Diffraction (SAED), observed carbides are of two types: (i) chromium enriched cementite which was found next to (ii) chromium carbides. **Figure 6.4b** shows small carbides embedded in a sub-grain structure of ferrite, from where representative EDS microspot chemical analysis were carried out. **Table 6.3** summarizes the chemical analysis of the spots in **Figure 6.4b**, which refer to both the ferrite matrix and the carbides in as-received material; the chemical analysis of carbides in the material after ultrafast heat treatment is reported as well in the table. It is evident that there is Cr enrichment in the carbides. Since the EDS measurements were performed on thin foils and not on carbon replicas, it is very likely that the interaction volume of the foil also includes the ferrite matrix, and that can affect the accuracy of the measurement. Selected Area Diffraction (as shown in Figure 6.4a) gives more robust conclusions on the type of carbides present and Atom Probe Tomography should be employed for accurate quantification of the chemical composition.

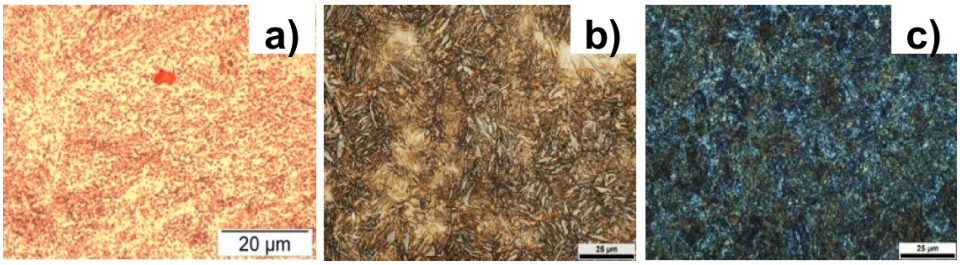

Figure 6.3: Optical microscopy of (a) initial material in the soft annealed condition, (b) sample after conventional heating rate (20 $^{o}C/s$) and quenching, and (c) sample after UFHT (300 $^{o}C/s$) and quenching. Etched with sodium metabisulphite.

Table 6.3: TEM - EDS microspot chemical analysis of different locations of the as received (Figure 6.4b) and UFHT material (wt. %).

Cr	Mn	Location
9.5	7.0	Carbide
12.4	6.0	Carbide
0.9	1.0	Matrix
0.9	0.1	Matrix
3.3	2.8	Carbide after UFHT

The microstructure observations in OM of the UFHT samples reveal a very fine microstructure, by which it was almost impossible to distinguish the phases present with general purpose etching (Nital 2%). The tint etching, though, coloured the phases of interest (e.g. martensite and bainitic ferrite) differently. According to De

et al. [32], martensite is expected to be etched in brown, while ferrite phases are coloured blue, retained austenite as well as carbides white. Thus, it was possible to establish that the sample heated and quenched conventionally (20 $^{o}C/s$) produced a fully martensitic microstructure coloured brown by the tint etchant, as shown in **Figure 6.3b**. On the other hand, the UFHT samples were tinted with multiple colours, indicating the presence of multiple phases, although dilatometry does not show indications of other phases than martensite forming. **Figure 6.3c** shows that the phase morphology could not be resolved by Optical Microscopy; thus, higher magnification techniques were employed. Hardness measurements ($HV_{0.5}$) were performed, with results shown in **Table 6.4** in addition to the OM observations. These have shown that the UFHT samples exhibit lower hardness than the conventional martensitic samples in concordance with the multiple phases and micro-constituents indicated by selective etching. The presence of bainite would explain the lower hardness values found in UFHT (300 $^{o}C/s$), compared to conventional treated sample (20 $^{o}C/s$).

Table 6.4: The Vickers micro-hardness ($HV_{0.5}$) for the three microstructures considered in this study.

Microstructure	$HV_{0.5}$
Initial microstructure	220 ± 15
Microstructure after conventional heat treatment	780 ± 15
Microstructure after UFHT	549 ± 15

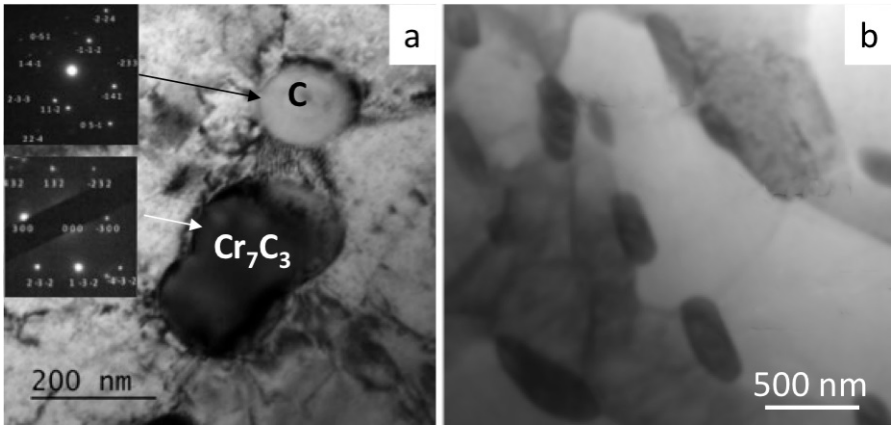

Figure 6.4: (a) Transmission Electron Microscopy (TEM) image (bright field) depicting detailed the spheroidised cementite and chromium carbide in the as-received Cr-steel microstructure. Black arrow points to a cementite (C) spheroid whereas white arrow indicates a Cr_7C_3 type carbide. Diffraction patterns indicate two types of carbides, Cr_7C_3 and cementite. Zone axis <02$\bar{3}$>. (b) Scanning TEM micrograph of carbides in the as received spheroidised microstructure showing the spots of the EDS analysis.

TEM analysis showed that the microstructure of the UFHT sample consists of a mixture of bainite and martensite. The average packet size of these mixed martensitic/bainitic areas is 5-6 μm. The microstructure is homogeneously dispersed with clearly visible carbides with sizes smaller than 1 μm. Thus, the phases identified as white by the tint etchant in the OM, in the SEM using spot EDS analysis were shown to be rich in chromium, which is a strong indication the presence of Cr carbides and/or Cr enriched cementite.

Further microstructural investigation was performed by TEM. Both martensite and bainite were present in the UFHT microstructure with martensite being the dominant phase, **Figure 6.5**.

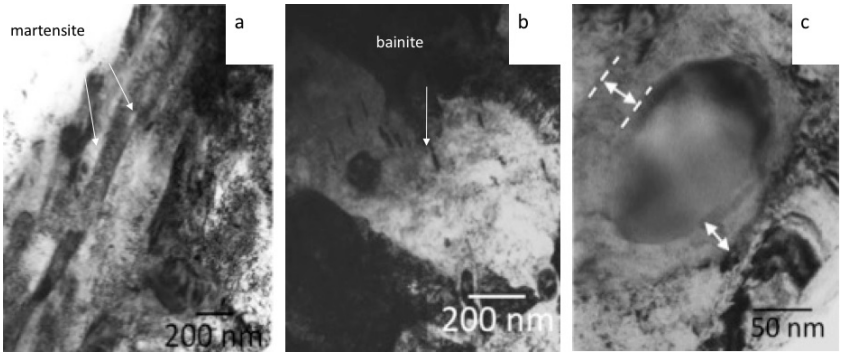

Figure 6.5: Transmission Electron Microscopy (TEM) micrographs of the UFHT specimen (reheated to 900oC at 300oC/s, held for 3s, then quenched) showing: (a) Martensite, (b) Bainite, (c) Partially dissolved carbide [33]. White arrows indicate the region of partial dissolution of the carbide.

Figure 6.5 illustrates the microstructure after UFHT (300 $^oC/s$) and quenching. The microstructure consists of martensite (α') laths (20-50 nm width and 500-1000 nm length), coexisting with fine lower bainite and small spherical carbides, many of which were partially dissolved. Significant differences in the local dislocation density between martensite (**Figure 6.5a**) and bainite (**Figure 6.5b**) were observed by TEM. The contrast and the specific patterns in the bright field TEM images show indications for lower dislocation density in bainitic ferrite and low carbon martensite. The arrangement of the carbides in the microstructure is employed as a criterion to distinguish different phases (or phase mixtures) in the microstructure. There are areas, in which aligned, elongated carbides are evident within ferrite with lower dislocation density, as evaluated based on contrast: these areas could be considered to resemble the bainite phase mixture. Secondly, other areas do not show any aligned carbides while ferrite is more acicular, similar to lower bainite or auto-tempered low carbon lath martensite. In the areas with the higher dislocation densities (based on contrast), limited presence of carbides was verified. This structure is most likely

higher carbon martensite.

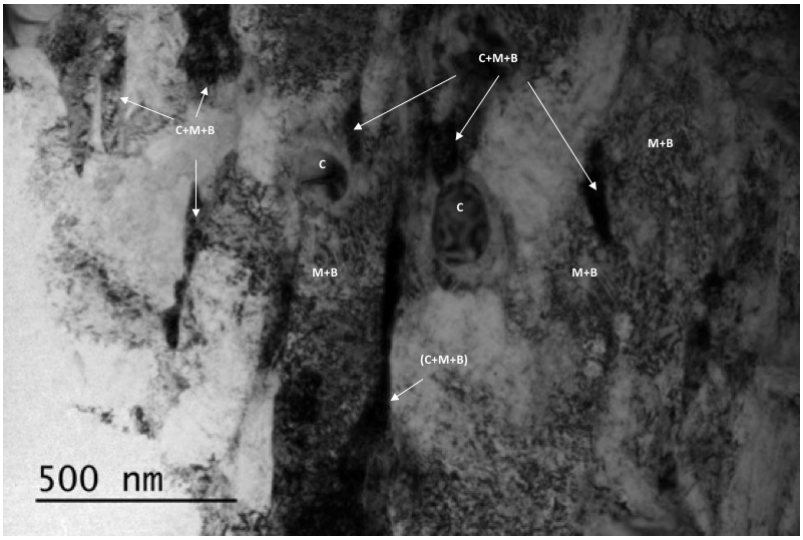

Figure 6.6: TEM micrograph (bright field) of microstructure after UFHT. In the image, the C, M and B stand for cementite, martensite and bainite, respectively.

A very important feature of the microstructure is the presence of partially decomposed carbides, e.g. in **Figure 6.6**, in which several partially dissolved cementite particles are shown. The areas labelled as (C+M+B) are mixtures of small undissolved carbides (as shown in **Figure 6.5c**), martensite and bainite. The surrounding microstructure consists mainly of martensite. **Figure 6.6** also illustrates large, partially dissolved chromium carbides (which is of the same type, size and morphology as the original chromium carbides in the as-received spheroidised microstructure as shown in **Figure 6.4a**). Around large carbides, a shaded ring with a variable width is evident. The presence of similar shaded rings is observed in **Figure 6.5c**, with a width of 40 nm. The observation of a ring around the carbides is possible by mass contrast effect, which can be a consequence of the diffusion of substitutional alloying elements during the carbide dissolution.

6.3.3. Dictra simulations

Figure 6.7a shows the alloy element profile in ferrite, cementite and austenite in a region close to the initial position of the ferrite/cementite interface (dotted line) after ultrafast and conventional heat treatment; it is evident that austenite, nucleated at the ferrite/cementite interface grows in both phases. Notice that the compositional gradients in UFHT (300 $^{o}C/s$, solid lines in **Figure 6.7a**) in austenite are broader

than after the simulation at 20 $^{o}C/s$ (dashed line in **Figure 6.7a**). This occurs in combination with a larger degree of dissolution of cementite achieved during UFHT, as evinced by the austenite-cementite interface position versus time, shown in **Figure 6.7b**. From this figure is also evident that the dissolution of cementite is much faster during UFHT than during the conventional heating. This is closely related to the much larger increase in temperature during the time range shown. Qualitative information about cementite dissolution can be obtained from dilatometry curves, **Figure 6.2a**, which show that while the ferrite to austenite transformation has been completed for both heating rates, the cementite dissolution seems to be incomplete in the UFHT sample. In addition, it is important to mention that the width of the compositional gradient around the carbide for UFHT, as derived by Dictra calculation, is of the same order of magnitude (20 nm) as the contrast rim which surrounds carbides, as shown by TEM images (Figure 6.5c).

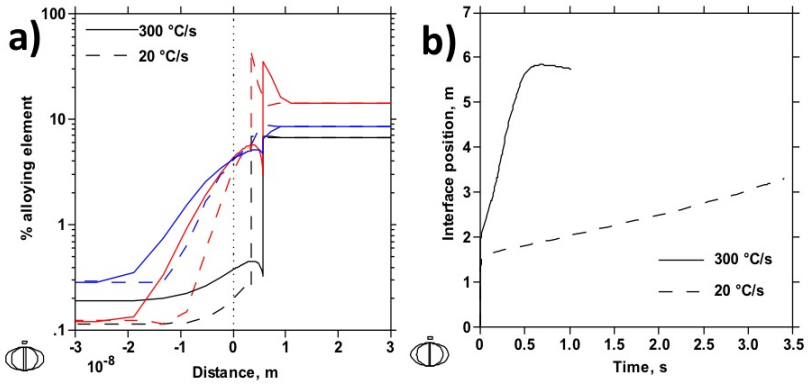

Figure 6.7: Plots of (a) composition versus distance from the interface and (b) position of the austenite-cementite interface versus time at the end of the heat treatment. The interface position is defined as zero at t = 0. Solid lines show the simulations for UFHT (300 $^{o}C/s$), whilst dashed lines show the results for conventional (20 $^{o}C/s$) heating rate, respectively. Colours in figure (a) are black for C, blue for Mn and red for Cr. The vertical lines in figure (a) indicate the final positions of the interface, with austenite on the left and cementite on the right.

6.3.4. Discussion

In general, the carbides can be classified as those found in the initial microstructure (**Figure 6.4**) and the ones formed during the heat treatments (**Figure 6.5, Figure 6.6**). In the first category, two carbide size ranges were found: small carbides, ranging from 10 nm to 50 nm, and the large ones ranging from 150 nm to 250 nm. The aligned carbides present within bainite after UFHT (**Figure 6.5b**) and those in the vicinity of martensite (Figure 6.6) belong to the second category and their size is

one order of magnitude smaller than that of non-aligned partially decomposed carbides, i.e. the chromium carbides. The formation of the smaller aligned carbides is expected to have occurred during quenching, whereas the bigger chromium carbides are those remained partially undissolved after the rapid thermal cycle.

6.3.5. Microstructure evolution

The ultrafast cycle can be analysed in three distinct segments, heating, soaking and quenching, as shown in **Figure 6.8**, which need to be considered both as a whole and separately.

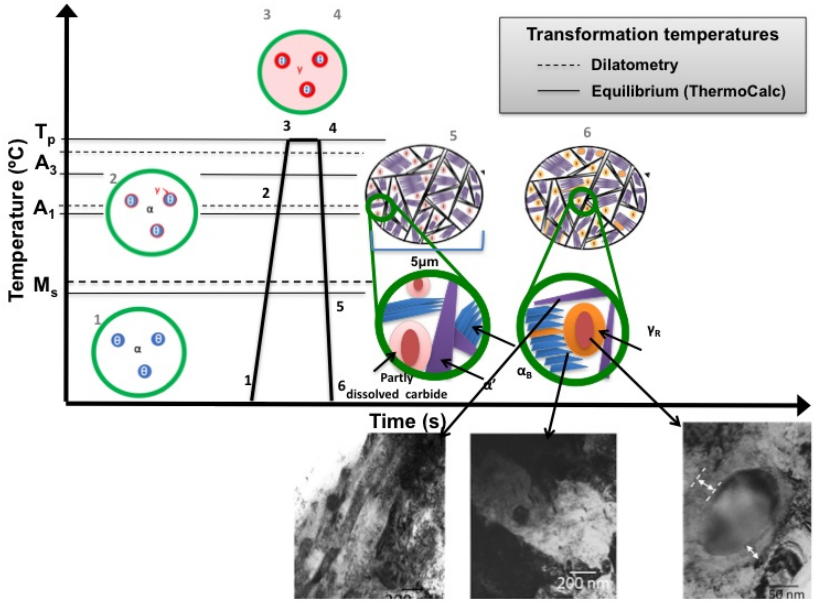

Figure 6.8: Schematic representation of the microstructure evolution during UFHT. Stage 1: Microstructure consists of ferrite plus spheroidised cementite. Stage 2: At the A_c1 temperature, austenite starts nucleating at the cementite/ferrite interface (red). Stage 3: austenite grains grow and more start to appear at triple junctions and ferrite grain boundaries. Stage 4: Above A_c3 temperature, the microstructure is austenitic, but with inhomogeneous chemical composition. Stages 3-4: Austenite transformation is complete, carbides are dissolving, there is compositional gradient in the microstructure. Areas at the viscinity of carbides are richer in carbon than areas that originate from ferrite. Stage 5: during quenching, martensite (purple) and bainite (blue) can form. At stages 5 and 6, the carbide rings (pink) are meta-stable austenite grains enriched in carbon and alloying elements. A_c1 and A_c3 at equilibrium were calculated with ThermoCalc and Ms empirically.

The three segments can be analysed as follows:

Heating from room temperature into the austenite (γ) phase field (see points $1 \rightarrow 3$ in Figure 6.8). At temperature just above A_1, (see point 2 in **Figure 6.8**) the

ferrite-to-austenite ($\alpha \rightarrow \gamma$) transformation features vary when occurring at either low or high heating rates as documented in the previous sections. The austenite formation begins with the nucleation process followed by growth. Studies of austenite formation from similar initial microstructure [17, 21, 22] have pointed out that the nucleation takes place at the intersections of ferrite-ferrite grain boundaries with cementite, indicated here as F-F-C boundaries. In the case of the present experiments, the asymmetrical shape of the ring found around carbides (e.g. **Figure 6.5c**) might be explained by the nucleation of austenite at one of such F-F-C boundaries and subsequently spreading sidewise along the ferrite-cementite interface, producing a more pronounced gradient of alloying elements at the nucleation point at F-F-C boundary thus creating the somewhat asymmetric contrast layer detected by TEM images. At a different scale, metallography of irregular austenite rings around cementite in a very early stage of transformation have been published elsewhere, for example, in **Figure 7** and **Figure 8** of ref. [19]. The preferential F-F-C nucleation sites described above might explain the distinct thickness of the austenite layers surrounding cementite, which was not acknowledged in ref. [19].

Dilatometry curves reveal a shift of the A_{c1} and A_{c3} temperatures as a function of the heating rate in experiments for the same steel grades [32, 33] (see **Figure 6.2**). This phenomenon has been reported before (e.g. in [32]). When increasing the heating rate from 20 $^{o}C/s$ to 300 $^{o}C/s$, A_{c3} increases by more than 100 ^{o}C, while the increase for Ac1 is smaller (up to 50 ^{o}C). The increase of ferrite to austenite transformation temperatures as the heating rate is increased can be explained in terms of a delay of austenite nucleation. Nucleation is a process that requires time to be accomplished, and when the heating rate is accelerated, the onset of austenite formation will take place at higher temperatures [32, 33]. The delayed nucleation of austenite is expected to affect largely A_{c1} temperature.

The local chemical composition of the matrix has an additional effect on the shift of the transformation temperatures during rapid heating. Since the carbides of the original microstructure remain partially undissolved, the carbon content of the matrix that transforms into austenite under rapid heating is poorer in carbon than the one transforming to austenite after slower heating. The chemical composition of the matrix affects mostly the finishing temperature of the austenite transformation (A_{c3}).

From the dilatometric experiments it is difficult to establish whether the mechanism of growth of austenite is diffusion controlled or interface-controlled, possibly varying in certain temperature ranges. The metallography shown in **Figure 6.3b** and **Figure 6.3c** can be interpreted as indirect consequence of diffusion-controlled and mixed-mode austenite formation mechanisms. The fully martensitic microstruc-

ture displayed by the material heated at 20 $^oC/s$ and quenched can be explained by the homogeneous carbon distribution in austenite, whereas the mixture of phases found in material subjected to UFHT (300 $^oC/s$) and quenched could be a consequence of the gradient of hardenability, product of the gradients in carbon and substitutional alloying element composition. It needs to be noted that substitutional alloying element gradients could be observed also at the material heated at 20 $^oC/s$ even though the time above A_3 temperature would allow complete carbide dissolution and the carbon composition to be homogeneous. This could potentially trigger different transformations locally upon cooling in a conventionally heated specimen as well, but experimentally it was found that in such specimens only martensite formed.

Ultra-short stay (0.3 seconds) at the peak temperature (T_p) (see points 3-4 in Figure 6.8) is very important due to the restriction of both austenite grain size and carbon homogenization. Petrov et al. [34, 35] have shown that short holding times (around 0.3 s) at T_p can cause considerable austenitic grain growth in low carbon steel [36].

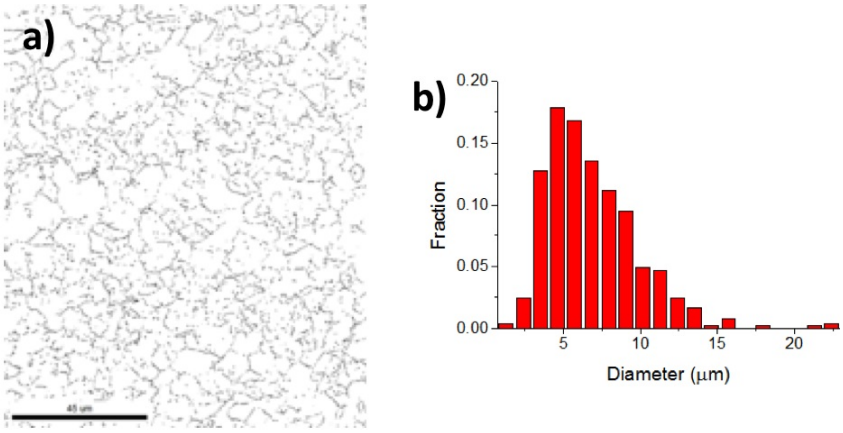

Figure 6.9: a) PAG boundary map for the UFHT sample as obtained by EBSD, b) PAG size distribution corresponding to a).

Figure 6.9 shows the prior austenite grain (PAG) boundary map obtained by EBSD as determined elsewhere for the UFHT sample [37]. PAG boundaries are reconstructed by plotting neighbouring points exhibiting a crystallographic misorientation between 20^o and 45^o. By further post-processing this data using the software ImageJ, the average PAG size is 5.9 μm and the distribution has a standard deviation of 3.5 μm. It is evident that the PAG are significantly smaller than the prior austenite grains for the as received microstructure, reported by the supplier to be

20 $\pm$ 3 μm. Such a small PAG size is expected to affect the austenite to bainite or austenite to martensite transformation kinetics.

As shown by the Dictra simulations, the time interval is not sufficient for existing carbides to completely dissolve. Estimating the distance for carbon diffusion as $x = \sqrt{D_C t}$, where D_C is the diffusivity of carbon in austenite (calculated from [38] and data for carbon content in austenite obtained from Dictra) and t is the holding time, the distances for T_p = 830^oC and Tp = 930^oC are 0.9 μm and 1.8 μm, respectively (calculated for the time at T_p). Neglecting the influence of overlapping carbon gradients, it can be expected that the austenite between small carbides (**Figure 6.5b**) does not contain carbon gradients and within the austenite between large carbides (**Figure 6.5c**), where the distances are of the order of 2 μm, carbon gradients might be present. This fact stresses that local chemical composition can trigger different transformations during subsequent quenching. It needs to be noted that carbon diffusion occurs also during heating.

Quenching: after a full quench (see points 4 $\rightarrow$ 7 in **Figure 6.8**) from austenite with a homogenized carbon distribution, the expected microstructural product is martensite (α'). It is observed by Lolla et al. [16] and by our research that in the case of ultrafast cycles, a mixed bainitic-martensitic α_B - α') microstructure is obtained, **Figure 6.5**. A noticeable shift in the starting of transformation during cooling has been measured in dilatometric experiments (**Figure 6.2a**). In the case of the conventional thermal cycle (20 $^oC/s$) the change in length during cooling of dilatometric specimens indicates the formation of martensite, as shown in **Figure 6.3b**. For UFHT the change in length can represent two possibilities, (i) the formation of bainite or (ii) the formation of martensite. It is reasonable to expect that bainite was the first product formed during continuous cooling. Under this assumption, it can be expected that there are zones in the microstructure with local hardenability variations, due to the fact that the same cooling rate results in a fully martensitic microstructure after heating at 20 $^oC/s$. Assuming martensite formation, condition (ii), the presence of carbon gradients can explain this shifting in the onset of martensite formation, since a low carbon content in austenite implies a high M_S. According to Dictra calculations, the carbon content of austenite formed under UFHT (300 $^oC/s$) is lower than the carbon content of austenite formed during the conventional (20 $^oC/s$) heat treatment. One should, therefore, conclude that both bainite and martensite formation can have taken place, since carbon is not homogeneously distributed after UFHT. The exact parameters that control the transformation products and kinetics during quenching, after rapid reheating, are not well documented, although evidence of simultaneous formation of bainite and martensite has been presented for isothermal transformations [39]. In the present work, some experi-

mental indications have been provided that bainite and martensite can form during the last stage of UFHT. The definition of the exact mechanism, whether martensite and bainite can obtained simultaneously during quenching after rapid heating would require further investigation.

6.3.6. Conclusions

- Ultrafast heat treatments with a heating rate of 300 $^{o}C/s$ produce a mixed microstructure consisting of undissolved carbides, bainite and martensite, whereas heat treatments at heating rates of 20 $^{o}C/s$ produce the conventional mixture of undissolved carbides in a fully martensitic microstructure.

- The mixed microstructure product of ultrafast heat treatment (300 $^{o}C/s$) is indirect evidence of the presence of carbon gradients in austenite.

- Ultrafast heat treatments produce a contrast rim observed by TEM, which is attributed to the heterogeneous distribution of alloying elements in austenite during cementite dissolution. Such compositional gradients have been calculated with Dictra software, showing a width of the same order of magnitude as observed by TEM.

References

1. V.F. Zackay, E.R. Parker, D. Fahr, R. Bush. The enhancement of ductility in high strength steels, Trans. ASM 60 (1967).

2. G. Frommeyer, O. Grässel. High-strenght and ultra-ductile FeMn (Al,Si) TRIP/TWIP light-weigth steels for structural components in automotive engineering, Stahl und Eisen 122 (2002) 65-69.

3. H.K.D.H. Bhadeshia. Bainite in Steels, IOM Communications Ltd, UK, 2001.

4. D. De Knijf, A. Puype, C. Fojer, R. Petrov. The influence of ultra-fast annealing prior to quenching and partitioning on the microstructure and mechanical properties, Materials Sci. Eng. 627A (2015) 182-190.

5. D.P. Koistinen, R.E. Marburger. Acta Metall. 7 59-60.

6. H. Zhang, D. Ponge, D. Raabe. Designing quadplex (four-phase) microstructures in an ultrahigh carbon steel, Mater. Sci. Eng. 612A (2014) 46-53.

7. W. Bleck, S. Papaefthymiou, A. Frehn., Steel Res. Int. 75 (2004) 704-711.

8. C. García-Mateo, F.G. Caballero, H.K.D.H. Bhadeshia. Development of Hard Bainite, ISIJ International 43 (2003) 1238-1243.

9. E. De Moor, P.J. Gibbs, J.G. Speer, D.K. Matlock. A.S. Processing, Strategies for Third-Generation Advanced High-Strength Steel Development, AIST Trans. 7 (2015).

10. F. Castro Cerda, C. Goulas, I. Sabirov, S. Papaefthymiou, A. Monsalve, R. Petrov, Mater. Sci. Eng. 672A (2016) 108-120.

11. V.N. Gridnev, V.I. Trefilov, Dokl. Akad. Nauk SSS. 95 (1954) 741-743.

12. N.N. Lipchin, T.G. Kryukova, N.L. Oslon, Metalloved. I Termicheskaya Obrab. Met. 8 (1964) 5-8.

13. K.J. Albutt, S. Garber. J. Iron Steel Inst. 204 (1966) 1217-1222.

14. G.E. Abrosimova, G.I. Kohanchik, A.M. Markov, A.V. Serebryakov. On the $\gamma \rightarrow \alpha$ transformation in plain carbon steel by rapid thermal treatment, Scr. Metall. 13 (1979) 531-534.

15. Y.Y. Meshkov, E.V. Pereloma. Phase Transformations in Steels, Elsevier (2012).

16. T. Lolla, G. Cola, B. Narayanan, B. Alexandrov, S.S. Babu., Mater. Sci. Technol. 27 (2011) 863-875.

17. R.T. W.J. Kaluba, J. Foct. The bainitic mechanism of austenite formation during rapid heating, Acta Mater. 46 (1998) 5917-5927.

18. E. Schmidt, Y. Wang, S. Sridhar, Metall. Mater. Trans. 37A (2006) 1799-1810.

19. G. Molinder, Acta Metall. 4 (1956) 565-571.

20. G.R. Speich, A. Szirmae, Trans. AIME. 245 (1969) 1063-1073.

21. R.R. Judd, H.W. Paxton, Trans. AIME. 242 (1968) 206-215.

22. E.S. Davenport, E.C. Bain. Trans. AIME. 90 (1930) 117-154.

23. E.C. Bain, ASM Int. (1939).

24. M. Hillert, K. Nilsson, L.E. Torndahl.,J. Iron Steel Inst. (1971) 49-66.

25. E.D. Schmidt, E.B. Damm, S. Sridhar., Metall. Mater. Trans. 38A (2007) 698-715.

26. V.I. Savran, S.E. Offerman, J. Sietsma, Metall. Mater. Trans. 41A (2010) 583-591.

27. M. Hillert. Thermodynamics of the Massive Transformation, Metall. Mater. Trans. 15A (1984) 411-419.

28. T. Lolla, G. Cola, B. Narayanan, B. Alexandrov, S.S. Babu, Mater. Sci. Technol. 27 (2011) 863-875.

29. J.O. Andersson, T. Helander, L. Höglund, P. Shi, B. Sundman, Calphad. 26 (2002) 273-312.

30. A. Borgenstam, L. Höglund, J. Agren, J. Phase Equilibria. 21 (2000) 269-280.

31. J.O. Andersson, L. Höglund, B. Jönsson, J. gren. Fundamentals and Applications of Ternary Diffusion, Elsevier (1990).

32. A.K. De, Speer, J. G., Matlock, D. K., Advanced Mater Proc 161 (2003) 27-30.

33. S. Papaefthymiou, C. Goulas, F. Castro Cerda, J. Sietsma, R. Petrov, Microstructural evolution during ultrafast heat treatment of medium carbon steels. International Conference on Solid-Solid Phase Transformations in Inorganic Materials (PTM). Whistler, Canada 2015.

34. R.H. Petrov, A. Puype, D. De Knijf, L. Kestens. Ultrafast heating of advanced high strength steels. International Conference on Solid-Solid Phase Transformations in Inorganic Materials, 2015.

35. R.H. Petrov, F. Hajy Akbary, J. Sidor, M.J. Santofimia, J. Sietsma, L. Kestens. International Virtual Journal of Machines, Technologies, Materials VI (2012) 68-71.

36. S. Papaefthymiou. Annals of Materials Research (2016).

37. N. Bernier, L. Bracke, L. Malet, S. Godet, Mater. Charact. 89 (2014) 23-32.

38. J. Agren. Scripta. Metall. 13 20 (1986) 1507-1510.

39. P. Kolmskog, A. Borgenstam, M. Hillert, P. Hedstrom, S.S. Babu, H. Terasaki, Y.I. Komizo, Metall. Mater. Trans. 43A (2012) 4984-4988.

7

General discussion, industrial implementation and suggestions for future work

The final chapter of the thesis aims to summarize the findings on the potential utilization of isothermal bainitic heat treatments for automotive spring production. For this purpose, we compare the results obtained in laboratory experiments to results obtained by full-scale industrial trials. It has been shown that the lab scale results are very promising, as the fatigue and tensile performance of the bainitic microstructure has been found to be superior to that of microstructures resulting from the standard quenching and tempering treatment. The results of the industrial trials have shown the same trend, but the performance improvement observed is insignificant, because of the presence of surface decarburization, geometrical effects (stress concentrations on the spring due to design) and heat treatment inaccuracies. However, cost reduction has been achieved by reducing the energy consumption during the production of trailing arms with bainitic microstructure. The challenges of upscaling the process as well as suggestions for future research and improvements are discussed in this last chapter.

Nowadays, springs for automotive applications are made of medium carbon high

strength steels, in quenched and tempered (Q&T) condition. This thesis investigated the possibility of heat treating these conventional high strength steel grades by austempering as an alternative to Q&T. The results at lab scale have shown that 51CrV4 can be effectively used in an isothermal bainitic treatment to produce a homogeneous lower-bainitic microstructure with improved tensile and fatigue performance.

It has been shown that the effect of chemical inhomogeneity in the industrially produced 51CrV4 resulting from casting has an impact on the isothermal bainite formation. This is investigated in medium carbon low silicon spring steel. The analysis by means of dilatometry and microscopy of the microstructure at different times during transformation has shown that chemical segregation of substitutional alloying elements strongly retards the transformation kinetics and limits the maximum achievable bainite fraction. During holding at temperatures close to and above the martensite start temperature, a homogeneous lower-bainitic microstructure can be eventually obtained, whereas at higher temperatures, incomplete bainitic reaction is evident, making these temperatures unsuitable for industrial application. It has also been found that at the early stages of the transformation, differences in the bainite formation kinetics, due to local inhomogeneities in Cr and Mn concentration, result in retardation of the growth of bainite in the high Mn- and Cr- concentration regions. The calculated difference in nucleation rates between the enriched and the depleted areas is not by itself sufficient to explain the microstructures obtained and thus significant influence of growth on bainite formation is concluded.

Nanoscale characterization work by Transmission Electron Microscopy (TEM) revealed three different morphologies: upper, lower and inverse bainite, depending on the austempering temperature. Lower bainite has been found to contain elongated cementite precipitates, aligned at an angle towards the length of the bainitic ferrite plate. Atom Probe Tomography (APT) analysis of cementite particles has shown no evidence of partitioning of substitutional elements; only carbon partitioned into cementite, reaching the equilibrium value. Carbon in the bainitic ferrite has been found to segregate at dislocations and to form Cottrell atmospheres. The concentration of carbon remaining in solution measured by APT has been more than expected for equilibrium. Upper bainite has been found to contain cementite as well. Chromium and manganese have been found to redistribute at the interface and the concentration of carbon in the matrix was measured to be lower. After isothermal treatments close the bainite start temperature, another austenite decomposition product has been found at locations with strong segregation, resembling inverse bainite, an acicular carbide plus ferrite phase mixture reported in hypereutectoid steels. Site-specific APT analysis of the inverse bainite has revealed significant partitioning

of manganese and chromium at the carbides and at the ferrite/martensite interfaces, unlike what is conventionally found in isothermal transformation products at lower temperatures.

Since the heat treatment is intended for spring production, fatigue performance is of central interest. Shot peening is a widely used and low-cost method to improve fatigue properties of steel engineering components. By changing the heat treatment from quenching and tempering to austempering, it is likely that the optimum shot peening parameters would not be the same for the newly designed treatment. Therefore, we have examined the results of the shot peening treatment, when it is applied to components of the same steel grade and similar yield strength (R_p), with either bainitic or tempered martensitic microstructure. It was observed that the resulting surface roughness for the tempered martensitic specimens is consistently lower than for the bainitic specimens, which can be explained by the limited work hardening of the tempered martensite compared to the bainite. Using Electron Back Scatter Diffraction (EBSD) and Finite Element Modelling (FEM), we explore in detail the deformation behaviour of the two microstructures. Modelling results show that the two microstructures accommodate strain differently, due to their different microstructural features such as platelet size and carbide distribution. FEM simulations have shown that shot peening of a bainitic microstructure, in comparison with a tempered martensitic microstructure, results in higher compressive stresses below the dimple of the shot and limited surrounding tensile stresses. This difference in strain accommodation can influence the shot peening parameters to obtain full coverage of the shot peened surface, which is an important prerequisite for improving the fatigue life of components.

Furthermore, the fatigue properties of 51CrV4, after quenching and tempering and after austempering have been compared. Rotating bending fatigue tests have been carried out to evaluate the fatigue performance of the two microstructures. The fatigue performance of bainite has been found to be superior to that of the tempered martensite. Fracture analysis of the fatigue specimens by stereo-microscopy and SEM reveals different fracture morphologies for bainite and tempered martensite. On the fracture surfaces of tempered martensite, multiple initiation sites and ratchet marks are evident, while fracture of bainite has initiated mostly at a single point at surface inclusions. Final fracture zones of tempered martensite have been dominated by micro-void coalescence. In contrast, the same zone in bainite mainly consists of quasi cleavage features, indicating lower fracture toughness for bainite.

Another possibility that has been investigated in this thesis is the potential development of a heat treatment involving rapid heating followed by quenching. In this way, the carbon concentration remains locally inhomogeneous, which can trigger

different phase transformations during cooling. Thus, a multi-phase microstructure can be eventually obtained in a single step, without intermediate quenching or holding steps. To investigate this possibility, we have performed a comparative study on the microstructural changes after conventional (20 $^{o}C/s$) and ultrafast (300 $^{o}C/s$) heating on a medium carbon steel in the soft annealed condition. Continuous-heating dilatometry experiments have been carried out and the volume phase fraction of austenite has been determined. The microstructure was observed via Optical (OM), Scanning (SEM) and Transmission Electron Microscopy (TEM). The effect of heating rate on the kinetics of cementite dissolution and austenite formation has been rationalized. The experimental results have been compared with Dictra calculations, and the possible effects on the kinetics of diffusion-controlled austenite formation are discussed.

Although this thesis has shown a positive outlook, our study has shown that the alloy composition of 51CrV4 is not optimal for producing springs in bainitic condition. A new alloying strategy, tailored for the isothermal bainitic treatment using cost efficient alloying concepts would be required to benefit fully from the austempering treatment. Finally, certain challenges are foreseen that would need to be addressed for successful industrial implementation. These topics will be further discussed in the following sections.

7.1. Scaling up to industrial production

7.1.1. Preliminary industrial trial results

VDL Weweler at the new production facility in Apeldoorn, The Netherlands, has performed initial industrial trials based on the results and the suggestions from this research. For the heat treatment of the hot-formed trailing arms, austenitisation was performed in a controlled atmosphere gas furnace followed by quenching in series of salt baths. Shot peening was subsequently carried out in a hanger type shot blasting machine similar to the one used in Chapter 4, using cut wire shot and the process conditions used for the conventional Q&T trailing arms. The results have shown that the fatigue lives obtained after isothermal bainitic treatment at 300^{o}C for 1 h are comparable to the ones obtained after quenching and tempering at 480^{o}C. The energy consumption was monitored during both treatments. The energy consumption during the bainitic treatment was less than in the Q&T treatment, resulting in cost decrease of 16 Euro per metric ton of produced trailing arms. The results are encouraging, but the expected significant improvement in fatigue performance, as found on the lab scale, could not yet be verified. Such verification is important, because the improved properties of the bainitic material can be taken into consid-

eration in the design of the trailing arms in order to lead to weight reduction.

7.1.2. Discrepancies between laboratory scale results and industrial scale results

There are several factors explaining the apparent discrepancies between the results of lab scale experiments and industrial scale trials:

1. As-received material. The material used for this study has a nominal composition according to standard, but possible variation of the chemical composition or the significant difference in the reduction ratio in the wire production as compared with the plate production, (50 x 95 mm^2 for VDL Weweler's material vs a diameter of 16 mm used in the mechanical properties and fatigue study). The different reduction ratio has an influence on the alloying element segregation wavelength. This means that a product resulting from a rolling process of higher reduction ratio will have a chemical composition distribution that resembles less to the one of the as-cast slab.

2. The sample geometry. The cylindrical geometry employed in the laboratory experiments is ideal. This factor can be determining, as a component with rectangular or complex geometry will exhibit local stress concentrations affecting the results.

3. The surface condition. The condition of the surface in the laboratory experiments is ground or even polished before the fatigue tests. This means that the roughness present in the industrial conditions is not a factor considered on the lab scale.

4. The occurrence of decarburisation. In industrially produced components, a decarburised layer is present at the surface. Decarburisation has multiple effects, as it alters the surface chemical composition and the hardenability. As a consequence of the decarburisation, the surface of the component remains soft, which results in high roughness after shot peening. Additionally, decarburized components are expected to exhibit low fatigue life and reduced tensile properties, due to the presence of soft ferrite at the surface.

5. The shot peening parameters are not optimised for the new treatment. Findings of Chapter 4 as well as unpublished rotating bending fatigue results show that a non-optimised shot peening treatment would not improve the fatigue performance of the components.

6. The fatigue loading conditions and the testing method. Tests in industry were performed using a custom machine on final parts, with imposed mean stress. The laboratory bending fatigue tests employed different stress conditions, with a zero-imposed mean stress.

7.1.3. Shot peening considerations

The effect of the shot peening treatment will certainly be influenced if a bainitic treatment is adopted, according to the research performed in Chapter 4. Based on this study's findings, it would be beneficial to adopt a longer shot peening time, which will allow the coverage to be complete. Additionally, as it was found that the resulting roughness of the bainitic components was higher than the one for tempered martensite, it would be sensible to investigate the effects of different shot types that can produce a smoother surface. The reported experiments were carried out using cut-wire rounded shots, which are more resistant to wear and breaking. On the other hand, they are often reported to cause increased roughness after shot peening when compared to their casted equivalents [1]. There is no well-defined procedure to follow in order to find the right shot peening parameters and the experience of the current project shows that the Almen intensity cannot by itself be the criterion of a well-designed shot peening treatment. The surface needs to be inspected closely for incomplete coverage and roughness.

7.1.4. Decarburisation

Decarburisation is a serious problem in spring production. It has also been shown to be critical for benefiting from improved material properties, as in the case of the bainitic treatment. A decarburised layer was found to be present already in the as received material for this study. The issue of decarburisation would need to be tackled either by grinding or by imposing stricter specifications regarding presence of a decarburised layer to the supplying steelmakers. During heat treatment, it is possible to reduce decarburisation by better control of the atmosphere in the austenitising furnace. Reducing the austenitisation temperature and time can be beneficial for limiting oxidation, decarburisation and prior austenite grain growth.

7.2. Suggestions for future research

7.2.1. New alloy design concept based on the results and the experience of this project

51CrV4 is a common medium carbon, low alloy spring steel designed to be used in quenched and tempered condition. Alloying elements such as C, Si, Cr and V are added to steels for increasing strength by solid solution and precipitation hardening [2-6]. The high value of C content and with the addition of Cr increase the hardenability. Micro-alloying with V results in precipitation of vanadium carbides during tempering, which increases the hardness. During an isothermal bainitic treatment (austempering), this alloying concept does not perform optimally, because the formation mechanism of bainite is affected differently by the alloying elements than the microstructural processes during quenching and tempering. Increase of the C and Cr content retards the bainite formation, and Cr and V do not form carbides during this process. In the formation of lower bainite, which is the desired microstructure, carbides precipitate with diffusion of carbon only, and therefore only para-equilibrium cementite can form. No significant Cr partitioning was detected in bainitic carbides forming during an isothermal treatment at 300^{o}C and no vanadium carbides precipitated because the isothermal treatment temperature is too low.

An increased carbon content increases the hardenability and delays the isothermal bainite formation. Therefore, the carbon content can be reduced in order to accelerate the bainitic reaction. This can also be proven beneficial for increasing corrosion fatigue life [7]. Chromium was found to exhibit strong segregation during casting. It reduces the driving force for the γ to α transformation and retards the bainite formation kinetics at the locations of high segregation. Therefore, it is suggested that the C and Cr content can be reduced while, for compensating the hardenability loss, increasing the Mn content.

Silicon is not used in typical 51CrV4 steel as a major alloying element. Silicon is added in spring steels up to a content of 2.2 wt.% [8] because it strengthens the matrix while remaining in solid solution, which increases the material's sag resistance. The sag resistance of springs is defined, as the resistance to plastic deformation during dynamic and static loading in service.

On the other hand, silicon is a key addition to a relatively new class of bainitic steels, the so-called nano-bainitic grades. A significant number of studies were devoted to the development of bainitic steels with high Si content (more than 1.5 wt.%). This is because high Si inhibits the formation of cementite and thus carbide-free bainite can form, which consists of bainitic ferrite with retained austenite. This microstructure is claimed to exhibit a good combination of high strength and ductility.

Si addition as an alloying element can have some drawbacks which need to be considered in the alloy design, the most important of which are: a) the retardation of bainite formation and b) the susceptibility to the formation of surface defects, internal oxidation, and decarburisation during forming. Taking the above described points into consideration, a moderate increase of Si content can be beneficial for the properties of the steel for spring applications.

Another important parameter affecting the bainite morphology and its formation kinetics is the prior austenite grain size. The current alloy design contains vanadium, which, in principle, by its carbides helps to restrict the austenite grain growth during austenitisation. In the present production route the austenitisation temperature is as high as 1200^{o}C, at which temperature the vanadium carbides are dissolved. For this purpose, it would be more appropriate to consider a minor niobium addition. Niobium is the most effective alloying element for grain refinement by conventional controlled rolling [9]. As the austenite grain becomes smaller, the transformation becomes faster. Thus, in an indirect way, niobium can enhance the bainite transformation kinetics. Hence, niobium could substitute vanadium for the bainite treatment to a great extent.

Boron can be used to increase the strength of springs without increasing the cost significantly. However, some studies have shown that boron can cause embrittlement at the prior austenite grain boundaries [5].

Minor nickel addition enhances hardenability and has been reported to retard pitting corrosion [5]. Nickel is already present in the standard alloy composition (maybe as a residue). Due to its price, no increase is recommended in the new design.

7.2.2. Suggested chemical composition and TTT diagram

In this section, a preliminary proposition for the chemical composition will be presented, based on the alloying concepts analysed in the previous section and the price of alloying elements as of February 2017. Geopolitical developments can cause variations in these prices, especially for the alloying elements controlled by few suppliers, e.g. Nb. The suggestions of this section are made from the perspective of physical metallurgy, whereas there might be additional challenges involved in secondary metallurgy for the production of the suggested grade. In this case, refining of the suggested composition should be done in consultation with the steelmaker.

For spring applications, the internal cleanliness of the steel is of vital importance in order to achieve good fatigue properties. The internal cleanliness is assessed in terms of inclusion content. The inclusions are formed during secondary metallurgy

and special attention is required at this production stage to minimise their density. Use of high quality scrap can help to limit the trump element concentration, e.g. Cu. The phosphorus and sulphur contents must be limited in the new grade, since they are detrimental for the mechanical properties. Phosphorus can cause embrittlement and sulphur will from manganese sulphide inclusions, the density of which should be minimised.

In **Table 7.1** the suggested chemical composition is shown together with the one measured for the 51CrV4 specimens used in Chapters 2-5:

Table 7.1: Suggested chemical composition for isothermal bainitic treatment, in comparison with the standard composition of 51CrV4.

Element	51CrV4 measured (wt.%)	Suggested bainitic grade (wt.%)
C	0.5100	0.400
Mn	1.0200	1.400
Cr	1.1500	0.700
Si	0.3300	0.700
Al	0.0080	0.008
V	0.1200	0.080
Nb	-	0.020
Ti	-	0.030
B	-	0.002
N	0.0114	0.0114
S	0.0100	0.008
P	0.0120	0.008
Cu	0.1600	0.160
Ni	0.1100	0.110

In order to estimate the behaviour of the new alloy with the suggested composition in comparison with the standard 51CrV4, the TTT diagrams were calculated with the software provided online at the website of ref. [10]. **Figure 7.1a** and **Figure 7.1b** show the TTT diagrams of the 51CrV4 and the suggested bainitic grade:

It is evident that reduction of the C and Cr content is compensated by the increase of the Mn content. The finishing times of the bainitic transformation are shorter for the new grade, as expected to result from the reduction of the Cr content.

x

7.2.3. Thermodynamics, kinetics and microstructure of the new grade

There are two primary objectives to be fulfilled before a new grade can be tested for industrial components. The first one is the accurate design of the optimal chemical composition of the steel grade and the second is the selection of the most appropriate heat treatment. Thermodynamic calculations are required to refine the concepts

described in the previous section. With the aid of thermodynamics, the composition and the stability of the precipitates can be established for the desired temperatures. Furthermore, since 51CrV4 has a composition that is close to the eutectoid composition, local gradients in alloy concentration can have important influence on the transformation products and kinetics. The new design should lead to a grade remaining that is always in the hypo-eutectoid range, also considering the expected degree of segregation.

Once the new material has been cast, kinetic studies with dilatometry can be carried out to evaluate the isothermal bainite formation kinetics and accurately design the optimal heat treatment. The results obtained from the current thesis can be used as benchmark for evaluating the potential of the new grade. The microstructure created in the dilatometer will further need to be characterised in similar way as described in Chapter 2 and Chapter 3, although TEM and APT might not be required for the application assessment.

7.2.4. Mechanical testing of the new grade

51CrV4 was chosen for the present investigation because it is a standard steel grade used for spring making. By designing a new alloy composition, the mechanical properties would need to be investigated, which can be time consuming. The results of the present study can be used as benchmark for the mechanical properties assessment of the new grade. Standard tensile tests to determine the monotonic material properties before and after heat treatment, in combination with fatigue tests in the finite life region (10^4-10^6 cycles), can form a picture of the performance of the material. The sag resistance is considered to be an important parameter of spring steel performance, which can be evaluated according to the method proposed in ref [11].

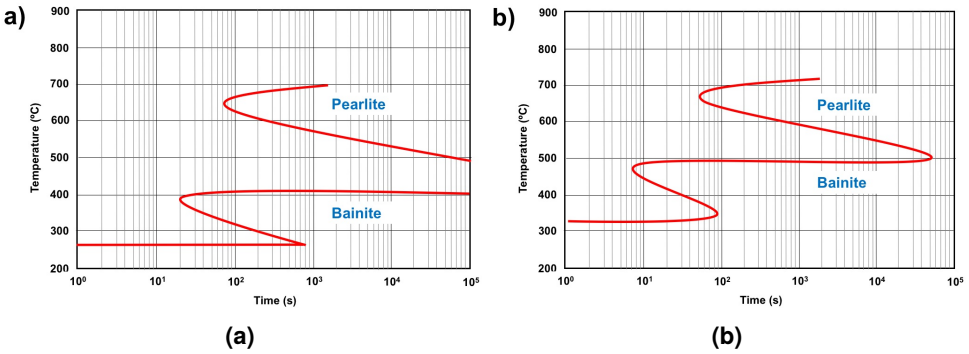

Figure 7.1: a) Calculated TTT diagram of 51CrV4. b) Calculated TTT diagram of the suggested bainitic grade.

References

1. Influence of the shot type on residual stresses of trailing arm, ASCOMETAL internal report, 2011.
2. T. Iikubo and Y. Ito, Denki Seiko (Electr. Furn. Steel), 57 (1986) p 33.
3. W.J. Nam and H.C. Choi, Wire J. Int. 29 (1996) p 94.
4. W.E. Heitmann, T.G. Oakwood and H.J. Dziemballa, Proc. Of Microalloying 1995, Pittsburgh, PA, The Iron and Steel Society, Warrendale, PA, p 395.
5. N. Ridley, S. Maropoulos and J.D.H. Paul, Mater. Sci. Technol. 10 (1994) p 239.
6. T. Yamamoto, R. Kobayashi, T. Ozone and M. Kurimoto, J. Heat. Treat., 3 (1984) p 220.
7. A.A. Barabi, F. Li, P. Romano, D. Ponge and D. Raabe, Mater. Sci. Eng. 463A (2007) pp 138-146.
8. T. Nakano, T. Sakayuki, M. Wakita and A. Sugimoto, JSAE Review 22 (2001) pp 337-342.
9. W.J. Nam, C. S. Lee, D. Y. Ban, Mater. Sci. Eng. 289A, (2000) pp 8-17.
10. http://calculations.ewi.org, accessed on 16.05.2017
11. S.T Furr, J. Basic Eng. ASME 94 (1972), p. 223.

Acknowledgements

First of all, I would like to thank my promoter, Prof. dr. ir. J. Sietsma for giving me the opportunity to work on this project. This thesis would not have been realised without the contribution of Dr. M.G. Mecozzi. Pina, thank you very much for the daily supervision and the enjoyable collaboration.

I would like to thank M2i and VDL Weweler for setting up the project. Especially I would like to thank Mr. D. Aalderink for the continuous support and the industrial input to this research. I also thank Dr. V. Savran for managing the project and all M2i staff for helping me during my PhD period.

At a critical moment of the project, I had the pleasure to meet Dr. K. Findley. Kip, I would like to thank you for the support during the last part of the experiments, for organising my stay at Colorado School of Mines, revising my manuscript and the very fruitful discussion. I would also like to thank Advanced Steel Processing and Products Research Center and Dr. J. Speer for the hospitality during my stay in Colorado and for enabling me to perform the fatigue and residual stresses experiments.

During these wonderful years, I had the opportunity and the pleasure to spend a significant amount of time at Gent University. I am grateful to Prof. dr. ir. Roumen Petrov for the collaboration and the guidance through the microscopy part of the project and for revising my manuscripts. At the University of Gent, I met a wonderful colleague and scientist, Dr. F.M. Castro-Cerda, with whom I worked closely, discussed and exchanged ideas. This evolved into a lasting friendship and a considerable number of common publications, thank you Felipe!

I would also like to thank my officemate and friend Ir. A. Kumar, for the good times in and out of the office and for the collaboration on the TEM and APT experiments of Chapter 3. These experiments would have been impossible without the support of Max Planck Institute of Iron research in Düsseldorf. For this, I would like to thank Prof. D. Raabe and Dr. Michel Herbig.

Since the first day in the department, I met Ir. A. Navarro-Lopez, with whom I went together through the process of the PhD. Thank you Alfonso for all the unforgettable moments and for being a paranymph in my defence!

TEM measurements were also performed at U Gent, at TU Delft and at National Technical University of Athens. For this I would like to thank Mr. Vitaliy Bliznuk, Dr.

B.N. Kim Lee and Dr. P. Tsakiridis respectively.

In the framework of Chapter 4, we carried out a study on shot peening. This would have been impossible without the contributions of a great consortium. I would like to thank Dipl.-ing H. Steinmetz and Mr. Beloch from Wheelabrator group in Metelen, Germany for helping with the shot peening trials. Additionally, I would like to thank Ir. C. Jimenez Peña and Dr. D. Debruyne for the FEM simulations.

I would like to thank Dr.-ing. S.Papaefthymiou for inspiring me to pursue a PhD, the mentoring during the beginning of the project and the collaboration in the framework of the Ultrafast Heat Treatment project.

In 2013, Ir. Nikolas Mavrikakis, who is best friend of mine since school years, came to Delft for an internship. It was meant to be the beginning of a new stage of our friendship, not only because we became roommates, but also because he decided to pursue a PhD in the field of Metallurgy. Nikola, I am very happy that, even though we have been living in different countries since you left Delft, we have been able to stay as close as always. I really hope that we get to live closer some time in the future. Thank you for the creative help during the PhD, for designing the thesis cover and for being a paranymph in my defence.

After finishing the PhD, I joined RAMLAB. I want to thank Vincent Wegener and Dr. ir. Wei Ya (Niya) for their understanding during this year. Niya, I also want to thank you for your help with LateX.

I would like to thank, for their contributions to my work, the colleagues from the TU Delft Lab: Nico Geerlofs, for the assistance during dilatometer tests and his ideas and initiatives for the UFHT project. Richard Huizenga, for all the XRD measurements and the fruitful discussions on diffraction and residual stresses. Hans Hofman, for the support with the salt bath treatments of the mechanical property specimens. Sander van Asperen, for the support in metallography and the collaboration in teaching lab classes. Dr. ir. Ton Riemslag for the support with the mechanical tests. Kees Kwakernaak, for the support in SEM and for performing EPMA measurements.

Working daily in the department, I had the pleasure to work together with wonderful people: Tungky, Ashwath, Jun, Qin, Javi, Carola,Chrysa, Wei, Sudhi, Behnam, Konstantina, Viviam, Zaloa, Gautam, Parisa. Thanks everyone! Specifically for their contribution to this thesis, I would like to thank Casper Versteylen for translating my summary in Dutch and Zaloa Arechabaleta for helping with the dislocation model.

After leaving from my home in Athens in 2013, I moved to the Netherlands as a perfect stranger. Nevertheless, I ended up feeling at home at the places, where I stayed during the PhD. This is because I met wonderful people there. The first

place I felt and still feel home is Delft, and for this a special thanks goes to Dr. M. Rota, Dr. K. Efmorfiadis and Ir. J. Gonzalez-Perez. The second place I consider home is Gent, and this is because of Nikolas, Merce, Carlos, Felipe, Marion, and all the Erasmus friends. Thank you for making the time in Gent unforgettable! The last place I felt home is Golden, CO. I was very lucky to meet and live together with Pete, Lucas and Heather. Dear Golden house mates, thank you for introducing me to the US, and for the tips on discovering the national parks. I miss you, hope we meet again soon.

I would like to thank my professors from NTUA for intruducing me to the fascinating field of Metallurgy and the staff of ELKEME SA for teaching me all the skills necessary for working in this field.

Last but not least, I would like to thank my parents, Apostolos and Asia and my sister Christiana for the love, understanding and continuous support. Thank you for helping me pursue my dreams, even though I am far away.

Delft, January 2018

Constantinos

List of Publications

A. International Peer-Reviewed Journals

1. C. Goulas, A. Kumar, M.G. Mecozzi, F.M. Castro-Cerda, M. Herbig, D. Raabe, R.H. Petrov and J. Sietsma, Atomic-scale investigations of isothermally formed bainite microstructures in 51CrV4 spring Steel, to be submitted for publication.

2. C. Goulas, K. Findley, F.M. Castro-Cerda, M.G. Mecozzi, R.H. Petrov and J. Sietsma, Fatigue performance of 51CrV4 steel with bainitic and tempered martensitic microstructure, to be submitted to Materials Science and Engineering: A.

3. C. Goulas, C. Jiménez-Peña, F.M. Castro-Cerda, M.G. Mecozzi, D. Debruyne, R.H. Petrov and J. Sietsma, The effect of shot peening on 51CrV4 spring steel with bainitic and tempered martensitic microstructure, submitted for publication to Journal of Materials Processing Technology.

4. S. Papaefthymiou, C. Goulas, F.M. Castro Cerda, N. Geerlofs, and R.H. Petrov (2017). The effect of heating rate on the microstructure of a soft-annealed medium carbon steel, Steel Research International 87.

5. F.M. Castro Cerda, C. Goulas, I. Sabirov, L.A.I. Kestens, R.H. Petrov (2017). The effect of the pre-heating stage on the microstructure and texture of a cold rolled FeCMnAlSi steel under conventional and ultrafast heating, Materials Characterization 130 pp 188-197 DOI: 10.1016/j.matchar.2017.06.010.

6. S. Papaefthymiou, A. Vazdirvanidis, G. Pantazopoulos and C. Goulas (2017). Fatigue fracture of a high resistance structural steel component designed to sustain severe loads under service conditions, Journal of Failure Analysis and Prevention 17 pp. 79-85. DOI: 10.1007/s11668-016-0216-9

7. F.M. Castro-Cerda, I. Sabirov, C. Goulas, J. Sietsma, A. Monsalve and R.H. Petrov (2017). Austenite formation in 0.2%C and 0.45%C steel under conventional and ultrafast heating, Materials & Design 116 pp. 448-460. DOI: 10.1016/j.matdes.2016.12.009

8. F.M. Castro Cerda, C. Goulas, S. Papaefthymiou, I. Sabirov, A. Monsalve and R.H. Petrov (2016). Microstructure, texture and mechanical properties in a low carbon steel after ultrafast heating, Materials Science and Engineering: A, pp. 108-120.
DOI:10.1016/j.msea.2016.06.056

9. C. Goulas, M.G. Mecozzi and J. Sietsma (2016). Bainite Formation in Medium Carbon Low Silicon Spring Steels Accounting for Chemical Segregation, Metallurgical and Materials Transactions A: Physical Metallurgy and Materials Science 47, pp.3077-3087. DOI: 10.1007/s11661-016-3418-6

10. S. Papaefthymiou, C. Goulas and E. Gavalas (2015). Micro-Friction Stir Welding of Titan Zinc Sheets, Journal of Materials Processing Technology 216, pp. 133-139. DOI: 10.1016/j.jmatprotec.2014.08.029

11. S. Papaefthymiou, C. Goulas and V Panteleakou (2015). Study on the evolution mechanism of oxidation and copper diffusion and precipitation phenomena and their effect on the surface quality of steel plates, International Journal of Structural Integrity, 6 (2), pp. 214-224. DOI: 10.1108/IJSI-08-2013-0018

B. International Conferences with Referees

1. C. Goulas, R.H. Petrov, W. Ya, M.C.M. Hermans and I.M. Richardson, Oral presentation and abstract published in proceedings, ICOTOM 18, St. George, UT, USA, 2017.

2. C. Goulas, A. Kumar, M.G. Mecozzi, F.M. Castro-Cerda, M. Herbig, D. Raabe, R.H. Petrov and J. Sietsma, Characterisation of isothermally formed bainite microstructures in a medium carbon spring steel, Oral presentation and abstract published in proceedings, EUROMAT Congress, Thessaloniki, Greece, 2017.

3. W. Ya, C. Goulas, K. Hamilton, M.C.M. Hermans, G.R.B.E. Romer, and I.M. Richardson, Microstructure and mechanical properties of CuAl8Ni6 produced by Wire Arc Additive Manufacturing for marine applications, Oral presentation and abstract published in proceedings, EUROMAT Congress, Thessaloniki, Greece, 2017.

4. C. Goulas, C. Jimnez-Pea, F.M. Castro-Cerda, M.G. Mecozzi, R. Petrov, and J. Sietsma, Influence of Shot Peening on the Microstructure of Medium Carbon Spring Steels, Oral presentation and abstract published in proceedings. THERMEC, Graz, Austria, 2016.

5. F.M. Castro-Cerda, C. Goulas, S. Papaefthymiou, I. Sabirov, A. Monsalve, R. Petrov, Oral presentation and abstract published in proceedings. THERMEC, Graz, Austria, 2016.

6. C. Goulas, M.G. Mecozzi, and J. Sietsma: Bainite formation in a medium carbon, chemically inhomogeneous spring steel. Oral presentation at the International Conference for Solid-Solid Phase Transformations, Whistler, Canada, 2015.

7. S. Papaefthymiou, C. Goulas, J. Sietsma, F.M. Castro-Cerda, R. Petrov, Microstructural evolution during ultrafast heat treatment of medium carbon steels. Oral presentation at the International Conference for Solid-Solid Phase Transformations, Whistler, Canada 2015.

8. S. Papaefthymiou, A. Vazdirvanidis, G. Pantazopoulos, C. Goulas, Root cause analysis of an early fatigue failure of a boron flat steel component designed for heavy duty structural applications. Poster presentation and abstract published in proceedings .4^{th} International Conference for Engineering Against Failure, Skiathos, Greece, 2015.

9. C. Goulas, M.G. Mecozzi, L. Zhao, J. Sietsma, Investigation of bainite formation in Medium carbon low silicon spring steels, oral presentation at DGM MSE Congress Darmstadt, Germany, 2014.

10. S. Papaefthymiou, C. Goulas, V. Panteleakou, D.D. Papamantellou, Study on the evolution mechanism of oxidation and copper diffusion and precipitation phenomena and their effect on the surface quality of steel plates, Oral presentation and article published in proceedings at 3^{rd} International Conference for Engineering Against Failure, Kos, Greece, 2013.

About the Author

Constantinos GOULAS

I. Professional Experience

06.2017-Present	Delft University of Technology Post-Doctoral Researcher Project topic: Functionally Graded Materials Through Wire Arc Additive Manufacturing.
2013 - 2017	Stichting Materials innovation institute (M2i) PhD Researcher Project topic: Switching from Martensitic to Bainitic Microstructure in Medium Carbon Spring Steels.
03.2016- 05.2016	Colorado School of Mines Research Associate, Research topic: Fatigue properties of medium carbon spring steels.
2011 - 2012	ELKEME S.A. (Hellenic Research Centre for Metals S.A) Research Assistant, Group of Steel Physical Metallurgy.

II. Studies

2013 - 2017	Doctorate of Philosophy (PhD) Delft University of Technology (TU Delft)
2007 - 2012	Diploma of Mining and Metallurgy of National Technical University of Athens (NTUA) Diploma Thesis: "Welding of thin Twin Roll Casted ZnTiCu sheets". Diploma grade: 7,92/10 (Very Good).
1995 - 2007	Moraitis School (Apolytirion: Excellent 19,1/20)

III. Languages

- Greek: Native
- English: Excellent (Cambridge, Proficiency C2, 2005)
- German: Very Good (Goethe-Zertifikat C1, 2012)
- French: Good (Institut Francais d' Athenes, DELF II C1, 2005)
- Spanish: Intermediate (currently studying at level B1)
- Dutch: Intermediate (currently studying at level B1)